Quantitative contrast enhanced CT for the assessment of hepatic extracellular volume: optimisation and application in liver-directed cancer therapy

A thesis submitted to the University of Manchester for the degree of
Doctor of Clinical Science
in the Faculty of Biology, Medicine and Health

2021

Christopher D Baker

School of Medical Sciences

Contents

Section 1: Introduction and literature review

Section 2: Optimisation of extracellular volume measurement in equilibrium contrast enhanced CT: a phantom study

Section 3: Optimisation of equilibrium contrast enhanced CT imaging for the non-invasive assessment of extracellular volume in liver-directed cancer therapy

Section 4: Discussion and conclusions

Total thesis word count: 34,018

Abstract

Background: Equilibrium CT (EQ-CT) is a quantitative contrast enhanced CT technique that is used to measure extracellular volume (ECV). ECV measurements have been shown to correlate with fibrotic burden in a range of chronic liver conditions, however evidence in liver cancer is lacking. ECV has the potential to be related to the aggressiveness and metastatic potential of tumours and could be used to monitor response to treatment. However, in order to be a useful diagnostic and prognostic tool, the accuracy, precision and repeatability of the technique must be understood. This has not been addressed in the literature.

Aims: The main research aims of this study are to establish the optimal acquisition and reconstruction parameters for EQ-CT in the liver; to determine the accuracy and clinical reproducibility of the technique; to measure ECV in liver cancers and to establish the feasibility of ECV measurement after the administration of novel radiopaque transarterial chemoembolisation (TACE) beads to monitor response to treatment.

Materials and methods: A literature search was carried out, followed by a phantom study to investigate the effect of kVp, $CTDI_{vol}$ and slice width on simulated ECV measurements in both conventional and dual energy CT modes. Accuracy of the technique was established and precision was related to a novel imaging metric for EQ-CT: 'enhancement to noise ratio' (ENR). A clinical study of ECV measurements made in patients with liver cancer being treated with TACE followed. ECV was measured in unaffected liver and tumour lesions at successive visits, prior to and after therapy, using conventional and dual energy CT. All imaging was performed using a wide beam (16 cm) CT system.

Results: The literature search revealed there was little technical detail attributed to existing EQ-CT protocols, which were predominantly clinically focussed. The phantom study demonstrated a mean error of 0.1% (interquartile range 9.1%) associated with simulated ECV measurements. Accuracy was robust to changes in acquisition parameters and precision was maximised at low kVp values and increased with ENR. Images from 6 patients indicated dual energy iodine density mode was unsuitable for clinical ECV measurements. Accuracy at clinically obtained ENR values was approximately ±17%. Results were reproducible across two patient visits separated by up to seven days. It was not possible to establish a definitive difference between ECV measured in tumour lesions and uninvolved tissue due to low patient numbers and lack of histopathological analysis. ECV measurement was possible with TACE beads present. Image registration was highlighted as problematic.

Conclusions: EQ-CT to measure ECV in the liver is accurate and clinically reproducible. Precision is related to acquisition and reconstruction settings and dual energy iodine density mode offers no advantages over conventional CT. The technique is a potentially useful tool for the diagnosis and monitoring of patients with liver cancer.

Declaration

No portion of the work referred to in the thesis has been submitted in support of an application for another degree or qualification of this or any other university or other institute of learning.

Dedication

To Fenella, my incredible wife, I could not have done this without your support.

Preface

This thesis is presented in part fulfilment of the Doctor of Clinical Science (DClinSci) programme run by the Manchester Academy for Healthcare Scientist Education. This programme comprises of three sections:

- Section A: Leadership and professional development (120 credits)
- Section B: Specialist scientific clinical programme (150 credits)
- Section C: Research, development and innovation (270 credits)

Sections A and B have previously been completed; a summary of the modules studied, work completed and credits awarded is shown in Appendix 1. A 'doctoral research and innovation in clinical science project' carrying 70 credits has also been completed in part fulfilment of section C; the innovation proposal that was submitted and assessed is included as Appendix 2. The subject of the innovation proposal is unrelated to this thesis.

Previous academic qualifications include:

- BSc Natural Sciences (University of Birmingham)
- MSc Radiation Physics (University College London)

The thesis presented here represents the first substantial research project undertaken. It was performed whilst working as a registered clinical scientist in the Radiological Physics and Radiation Safety Group at the Royal Free London NHS Foundation Trust.

The inspiration for this research came from Dr Steven Bandula, an Interventional Oncology Consultant and Senior Lecturer in Cancer Intervention at University College London Hospitals NHS Foundation Trust and University College London.

Thesis format

This thesis is submitted in journal format. It is structured in four sections:

- an introduction and literature review;
- a phantom study journal article;
- a clinical study journal article;
- a discussion and conclusion.

The two journal articles are written to be submitted for publication in the 'Journal of Applied Clinical Medical Physics', an open access journal published by the American Association of Physicists in Medicine. The referencing in these articles follows the American Medical Association referencing system required by this journal. The referencing in the opening and closing sections follows the 'Harvard Manchester' style required by the University of Manchester.

Whilst the phantom study was performed in isolation with no significant input from other individuals, the clinical study utilises data from an existing clinical trial. This required collaboration with the trial chief investigator, Professor Ricky Sharma, and radiologists working on the trial, Dr Laura Beaton and Dr Steven Bandula. These individuals are named as authors on the clinical study due to their involvement in collecting the clinical images, reviewing the manuscript and in the case of Dr Steven Bandula, assisting in the positioning of regions of interest for image analysis (as described in the clinical study). They did not directly contribute to any other areas of data processing, data analysis or writing of the article. These articles will be submitted for publication in the near future.

It is hoped this thesis reads as a coherent body of work in which the research questions are formed and subsequently addressed in complimentary phantom and clinical studies. This is followed by a discussion and recommendations for further work.

Section 1

Introduction and literature review

1 Introduction

Hepatic fibrosis is a process associated with most chronic liver diseases (Friedman, 2003). It is characterised by an increase in collagen extracellular matrix deposits leading to an expansion of the extracellular volume (ECV), disrupting the normal architecture and function of the liver (Afdhal and Nunes, 2004). Cirrhosis is a state of severe fibrosis and is associated with an increased risk of hepatocellular carcinoma (HCC) (Chiou et al., 2015; Kondo et al., 2016). Localised ECV will be further affected in liver cancers due to high intratumoural cell density leading to a decrease in ECV, which is potentially counteracted by further fibrotic changes often associated with cancers (Conrad et al., 2013).

Being able to accurately measure the degree of hepatic fibrosis is a useful prognostic tool for the assessment and staging of many liver diseases (Martínez et al., 2011; Ito et al., 2020). The assessment of ECV in liver cancer could provide a similar tool for characterising and staging of disease and potentially for monitoring response to treatment, although this is yet to be established. A technique that could measure ECV in the liver that is accurate, quick, practical, easily accessible and cheap is therefore of clinical interest.

This study will be focussed on developing and optimising a tool for measuring ECV in a cohort of patients being treated with liver-directed cancer therapy. Patients with resectable HCC or metastatic colorectal cancer (mCRC) are being recruited to the VEROnA trial: *'*a window of opportunity study of vandetanib-eluting radiopaque beads (BTG-002814) in patients with resectable liver malignancies*'* (Beaton et al., 2019). This is a phase 0 trial of a novel radiopaque drug eluting embolic bead used for transarterial chemoembolization (TACE) treatment. The primary objectives of the trial are to establish the safety of the treatment and to assess the effectiveness of delivering the drug to the target site. Secondary and exploratory objectives include assessing the distribution of the beads on computed tomography (CT) imaging. For this, CT imaging is being performed both prior to and after bead administration. In this study the data and images obtained will be used alongside a phantom study to investigate and optimise CT imaging for the non-invasive measurement of ECV using an equilibrium CT (EQ-CT) technique. This will include measurements prior to and after TACE therapy. As far as the author is aware, there are no previous studies investigating the optimisation, accuracy or precision of EQ-CT to measure ECV in the liver and no studies in which the ECV has been investigated specifically in liver cancer.

2 Assessment of ECV

The majority of the literature linked to the measurement of ECV in the liver is focussed on the correlation of ECV results to other measures of fibrosis, commonly histologic analysis (considered to be the gold standard for fibrosis assessment) and serum biomarkers. However, quantitative imaging techniques are increasing in prevalence, driven by the difficulties and shortcomings associated with histologic analysis.

2.1 Histologic analysis

Histologic analysis requires a liver biopsy. Tissue samples are qualitatively assessed by a pathologist and assigned a fibrosis score on a discrete scale based on the architectural structure of the tissue. Commonly used systems include the Ishak and METAVIR scores, which both start with a score of F0 for 'no fibrosis' and end with F6 or F4 (respectively) for 'cirrhosis', but neither method gives a quantitative measure of ECV.

Biopsy is seen as advantageous as it can provide information on the aetiology of the ECV changes which would be particularly useful in the setting of cancer, however there are many documented drawbacks and risks associated with the technique (Horowitz et al., 2017). The invasive nature of the procedure results in it being expensive, poorly tolerated by patients and there is a small but not insignificant risk of complication (Afdhal and Nunes, 2004). These factors prevent biopsy being a viable method for long term monitoring of a condition or in assessing response to treatment.

Another major drawback of biopsy is the small tissue sample size obtained during biopsy means there are inherent sampling errors associated with the technique: the typical sample size is approximately 1/50,000 of the total liver parenchyma and therefore any spatial variations in fibrosis or a geographical miss of a target lesion could easily lead to incorrect measurement and classification. In fact, Regev et al. (2002) found a 33% discrepancy rate in reported fibrosis stage due to sampling error. It has also been reported that inter-observer variability using discrete fibrosis scoring systems such as the Ishank score is high (Pavlides et al., 2017). In addition, this type of scoring does not inform the clinician of any subtle changes in ECV, which may be of particular importance for monitoring response to treatment.

Measurement of collagen proportionate area using quantitative digital imaging has shown promise for assessment of fibrosis (Tsochatzis et al., 2014; Pavlides et al., 2017). However, the issues surrounding obtaining the biopsy sample still remain.

2.2 Serum biomarkers

Serum biomarker tests that detect the synthesis and/or degradation of collagen associated with fibrosis or changes in hepatic function, are minimally invasive and widely available.

However, they suffer from being non-specific with a high level of equivocal results and are unable to give a measure of ECV or differentiate between different stages of fibrosis (Horowitz et al., 2017; Nallagangula et al., 2017). The enhanced liver fibrosis test is a combination of three serum biomarkers which measure extracellular matrix metabolism, which has shown to be successful for predicting moderate fibrosis and cirrhosis (Lichtinghagen et al., 2013). However, they cannot be used for subtle differentiation of small changes in fibrotic burden or ECV which may be important in monitoring liver cancers. Additionally, they provide no visual representation of the extent or regional distribution of ECV and it is not possible to perform targeted measurements in a particular segment or target lesion (Varenika et al., 2013).

2.3 Qualitative Imaging

Assessment of fibrosis using imaging has traditionally been limited to morphologic changes to the liver which can be performed with CT, magnetic resonance imaging (MRI) and ultrasound. Qualitative imaging is widely used in cancer diagnostics and its advantages are it is simple, non-invasive, generally widely available and can provide information on a large volume of the liver. Imaging is a non-specific diagnostic tool so it may provide additional information on the patient's condition that would not be available from biopsy or specific serum biomarkers. However, qualitative imaging can be subjective and by its nature it cannot provide a quantitative assessment of fibrosis stage or ECV and therefore it is not sensitive to diagnosis of early and intermediate stages of fibrosis (Lubner and Pickhardt, 2018). Qualitative imaging is not considered useful in isolation for diagnosis or monitoring of fibrosis or changes in ECV (Petitclerc et al., 2017; Lubner and Pickhardt, 2018), however, as imaging modalities and their applications become more advanced there are an ever-increasing number of quantitative imaging techniques which show promise.

2.4 Quantitative imaging

Quantitative analysis enables additional information to be extracted from otherwise qualitative images which can be used to detect microscopic tissue changes that are not macroscopically visible or to obtain quantitative information without the need for invasive clinical procedures.

2.4.1 Transient elastography

Transient elastography is a technique used to measure liver 'stiffness': a physical property of the liver that changes with fibrosis. It can be performed using either ultrasound or MRI. Both techniques have been shown to be able to differentiate between absent/mild fibrosis and severe fibrosis/cirrhosis with MRI being more successful at differentiating between earlier stages of fibrosis (Bonekamp et al., 2009; Dietrich et al., 2017). Liver stiffness has also been shown to be a predictor of outcomes in patients with a range of chronic liver diseases including cancer (Singh et al., 2013).

Unfortunately ultrasound techniques suffer from being highly operator dependent and measurements are limited to those areas of the liver that can be visualised which results in the technique being contraindicated in obese patients (Venkatesh et al., 2013). In contrast, magnetic resonance (MR) elastography is not affected by obesity, it is independent of operator skill, has a low rate of technical failure and can be used to image the whole liver (Venkatesh et al., 2013). Unfortunately, MR is not as widely available as ultrasound and it is contraindicated in many patients with non-MR compatible devices and those who suffer from claustrophobia. Additionally, transient elastography results can be influenced by many factors independent of liver fibrosis state such as inflammation and amyloidosis (Venkatesh et al., 2013).

2.4.2 CT Perfusion imaging

CT perfusion involves repeated image acquisitions of a volume of tissue following the administration of a contrast agent. After post-processing of images, it is possible to obtain quantitative parameters such as fractional flow rates and mean transit times of iodinated contrast, as well as the extracellular extravascular volume fraction (different to ECV due to the exclusion of the intravascular space), that can provide useful prognostic information for the diagnosis and monitoring in a range of clinical scenarios. However, results can be acquisition and processing software dependent, the technique typically requires high doses of ionising radiation or very limited scan ranges, particularly for abdominal organs, and significant organ motion during the relatively long examination times creates image registration issues for repeated images (Cuenod and Balvay, 2013; Kim et al., 2014; Ronot et al., 2020). CT perfusion has been demonstrated to provide useful parametric imaging biomarkers in the assessment of liver cancer (Kim et al., 2014), however its use has not been widely applied to assessment of hepatic fibrosis.

2.4.3 Equilibrium imaging

Equilibrium imaging is a technique that has shown promise for the clinical measurement of ECV in the liver and other organs, with correlation to fibrosis stage using histopathology as the gold standard reported in the literature, for example (Bandula et al., 2013b; Bandula et al., 2015; Fukukura et al., 2020). It can be performed with contrast enhanced CT or MRI, known as EQ-CT and equilibrium MRI (EQ-MR) respectively. EQ-CT and EQ-MR techniques have all the advantages of imaging-based methods as discussed above with the additional advantage of quantitative measurement that is relatively simple to achieve and in the case of EQ-CT, at a modest radiation dose.

This body of work will aim to investigate EQ-CT in order to optimise the technique for the measurement of ECV in the liver. The details of the technique, a consideration of the

technical factors associated with CT that could influence clinical ECV measurements and a summary of available literature on the subject are given in the following sections.

3 Equilibrium imaging to measure ECV

3.1 Theory

The concept of equilibrium imaging works on the principle that the total space occupied by a soft tissue can be thought of as being comprised of three compartments: intracellular space (ICS), intravascular space (IVS) and extracellular, extravascular space (ECEVS) (Equation ***1***). As the IVS and ECEVS combined represent all the space that is not contained in the ICS it is known as the extracellular space (ECS) (Equation 2). The volume occupied by the ECS is the ECV and is comprised of interstitial fluid and blood plasma.

$$\text{Total volume} = \text{ICS} + \text{IVS} + \text{ECEVS}$$

Equation 1

$$\text{ECS} = \text{Total volume} - \text{ICS} = \text{IVS} + \text{ECEVS}$$

Equation 2

The low-molecular weight iodine and gadolinium based contrast agents ubiquitously used in CT and MRI are able to pass freely between the IVS and ECEVS but they do not enter living cells (Varenika et al., 2013). They can therefore be thought of as exclusively extracellular. The volume of distribution of the contrast agent within a tissue is therefore equal to the ECV.

Dean et al. (1978b) first published the theory of using CT along with the pharmacologic concept of 'volume of distribution' as a method for the non-invasive measurement of the volume of distribution of contrast material within tissue, which is equivalent to the ECV. This can be done relatively simply by measuring contrast concentration in that tissue compared to the concentration in blood plasma (Equation 3). Instead of being given as an absolute value the volume is given as fraction of the total volume of the tissue: a fractional extracellular volume (fECV).

$$Fractional\ distribution\ volume\ in\ tissue = \frac{tissue\ contrast\ agent\ concentration}{plasma\ contrast\ agent\ concentration}$$

Equation 3

It is essential to note that for Equation 3 to be valid the system being measured must be in equilibrium; the concentration of the contrast agent must be the same in the IVS and the ECEVS. This requirement gives the technique its name as well as having important practical consequences for fECV measurement which are discussed in detail in section 4.

Without invasive means it is not possible to measure the true concentrations of contrast agent concentrations in either the liver or the plasma. However, when using CT, CT

numbers, specifically Hounsfield units (HU), scale linearly with contrast agent concentration (Seeram, 2018). It is therefore possible to use contrast enhancement as a surrogate for contrast agent concentration where contrast enhancement is the change in measured HU between an unenhanced image and an enhanced (in this case equilibrium phase) image. MRI can also be used to measure contrast enhancement based on T1 relaxation times pre- and post-contrast administration, although this is more technically challenging. Equation 3 now becomes:

$$fECV_{liver} = \frac{\Delta HU_{liver}}{\Delta HU_{plasma}}$$

Equation 4

Where $\Delta HU = HU_{equilibrium} - HU_{unenhanced}$

It is not possible to measure the concentration of plasma on CT or MRI images as it is unavoidably mixed with the haematocrit. However, by considering the blood as a different tissue (Equation 5) and dividing Equation 4 by the result, the plasma contrast agent concentration cancels out. Equation 6 is also known as the partition coefficient.

$$fECV_{blood} = \frac{\Delta HU_{blood}}{\Delta HU_{plasma}}$$

Equation 5

$$\frac{fECV_{liver}}{fECV_{blood}} = \frac{\Delta HU_{liver}}{\Delta HU_{blood}}$$

Equation 6

As the contrast agent is known not to enter cells (including red blood cells), the $fECV_{blood}$ is simply the fraction of blood that is not haematocrit. Haematocrit can be measured with a blood sample and is given as a fraction of total blood volume, therefore $fECV_{blood}$ becomes 1 minus the haematocrit. Equation 6 now becomes:

$$fECV_{liver} = \frac{\Delta HU_{tissue}}{\Delta HU_{blood}} \times (1 - haematocrit)$$

Equation 7

Equation 7 provides a method for measuring the fECV of the liver, or any other tissue, simply using contrast enhancement measured in CT or MRI images alongside a haematocrit measurement. Blood measurements can be taken from any location where there is a volume of blood large enough to be measured without interference from other tissues. The aorta is commonly used, but the inferior vena cava and the left atrium are also possible locations.

Due to the requirement to acquire the enhanced images during the equilibrium phase when the concentration of contrast is the equal in the IVS and ECEVS, this technique is known as equilibrium imaging: equilibrium CT (EQ-CT) or equilibrium MRI (EQ-MR).

3.2 First applications of equilibrium imaging

The concept of measuring ECV using non-invasive methods was proven by Dean et al. (1978b) in rats approximately 40 years ago, however, the first example of equilibrium imaging being used in humans was published almost 30 years later by Flett et al. (2010). They used EQ-MR techniques to measure fECV in diffuse myocardial fibrosis. They were successful in measuring fECV using gadolinium enhancement by measuring T1 relaxation times on T1 weighted images. As mentioned above, EQ-MR is more technically challenging than EQ-CT as, unlike in CT where the relationship between HU values and contrast agent concentration is linear, the relationship between T1 relaxation times and gadolinium concentration is not simple. T1 signals can also be altered by the presence of excess iron in tissue introducing an additional source of error (Banerjee et al., 2014).

Notwithstanding these difficulties, Bandula et al. (2013a) subsequently successfully used EQ-MR to measure fECV in the liver, however, the technique was described as “complicated, time consuming and prone to error” (Bandula et al., 2013a, p. 863). Additionally, there are many contraindications to MRI including claustrophobia and the presence of ferrous metal in the body. In fact, Sadigh et al. (2017) found that 16.7% of approximately 34,500 routine MRI examinations had ‘unexpected events’ leading to difficulties or failure of the examination. Of these, 10.5% were non-contrast patient related events such as patient motion, discomfort or claustrophobia, 1.5% were technical acquisition issues and 0.5% were foreign bodies such as unanticipated metal within the patient.

For these reasons it is believed that EQ-CT fECV measurement would be a more useful application of the technique. CT is now a ubiquitous, quick, non-invasive and relatively cheap imaging modality, although it must be acknowledged that CT does involve exposing the patient to ionising radiation which requires justification on an individual patient basis (Ionising Radiation (Medical Exposure) Regulations 2017).

Nacif et al. (2012) performed the first trials of EQ-CT fECV measurement in humans. This, again, was performed in the myocardium. They found that fECV correlated well with similar measurements from EQ-MR. Notably the time it took for the CT and MRI measurements was 13 and 47 mins respectively, which could have a significant impact on how readily the technique could get adopted into routine clinical use. The technique was further validated in the myocardium by correlating EQ-CT fECV measurements with collagen volume fraction from biopsy specimens (Bandula et al., 2013b). Zissen et al. (2013) published the first study of the EQ-CT technique being successfully applied to measuring fECV in the liver.

One of the aims of this body of work is to investigate and optimise the use of EQ-CT to measure fECV in the liver. Based on the theory presented in section 3.1, fECV values will depend on:

- ensuring a state of contrast agent equilibrium has been achieved;
- measured attenuation (HU) values;
- measured haematocrit values.

Haematocrit values are measured from a blood sample taken prior to EQ-CT acquisition that has been processed in a haematology lab. The measurement is therefore completely independent of the CT acquisition. Whilst a detailed analysis of the accuracy and precision of the haematocrit results is beyond the scope of this body of work, values quoted in the literature for 'state of the art' haematology analysers are 1.8% (accuracy) and 1.2% (precision) (Vis and Huisman, 2016). The significance of these figures will have to be considered in the context of the accuracy of measured contrast enhancement values to establish the potential influence on the uncertainty associated with fECV results. Interestingly, the accuracy or precision of haematocrit values is not considered by any authors of the current literature surrounding EQ-CT fECV measurement, as summarised in the proceeding sections.

The remaining two factors are discussed further in the following sections and will be the subject of a detailed literature search presented in section 7.

4 Time of equilibrium

The importance of acquiring the EQ-CT at the right time point was first highlighted by Dean et al. (1978a). In a proof of concept study, they found that the time elapsed after administration of iodine significantly affected the calculated volume of distribution in 13 different tissues in rats and stated “The time elapsed after contrast medium injection appears to be of pivotal importance” (Dean et al., 1978a, p. 314). Although this was based on uptake of radioactive iodine in tissues which was empirically converted into HU, this confirms the importance of selecting the right time point to ensure reliable fECV measurements.

Of relevance to hepatic EQ-CT in humans, Dawson and Morgan (1999) produced a mathematical model to define and predict the equilibrium phase in the liver using iodinated contrast material. When contrast is introduced intravenously, the contrast concentration is high in the IVS. It therefore diffuses into the ECEVS until the concentration in both compartments is equal i.e. in equilibrium. As contrast is removed from the plasma via glomerular filtration, the concentration in the IVS will begin to drop and the concentration in the ECEVS will follow in almost equilibrium: not total equilibrium as the plasma concentration will always be slightly lower to allow for diffusion back into the IVS and subsequent excretion. This therefore leads to a ‘dynamic equilibrium phase’ where the concentrations in both compartments can be considered to be very similar and decreasing at the same rate over time.

This is demonstrated in Figure 1, which shows the theoretical ratio of ΔHU_{liver} and ΔHU_{blood} which, over time, becomes asymptotic to the line determined by the IVS and ECEVS in the liver and the patient’s haematocrit (Dawson and Morgan, 1999). The time points when the two lines converge is the start of the equilibrium phase. The time of equilibrium will be patient specific, however using typical values for the relevant factors Dawson and Morgan (1999) show the equilibrium phase is expected to be reached approximately 120 seconds after the contrast bolus. Therefore, as long as the imaging is performed after this time point, and the liver and blood (aorta) are imaged at the same time, the system can be assumed to be in equilibrium and HU measurements used to calculate the fECV.

The disadvantage of using very long delays will be a loss of signal from a globally reduced iodine concentration due glomerular filtration. A further consideration for long time delays is the possibility for patient movement between the pre-contrast and delayed image acquisitions, which would make measuring iodine concentrations in exactly the same position on both acquisitions challenging. Therefore, for clinical applications of EQ-CT there will be a fine balance between leaving enough time to ensure the equilibrium phase has been reached versus a reduced iodine signal and potential for patient movement.

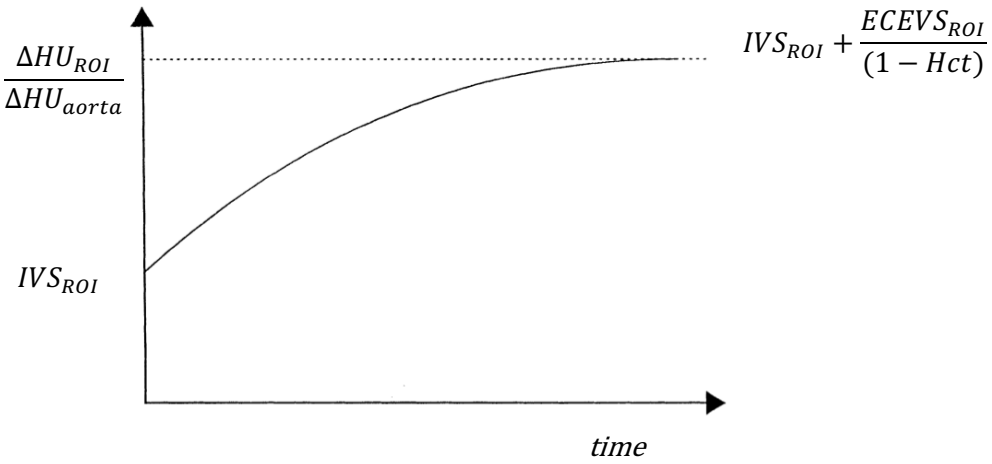

Figure 1 *The theoretical ratio of measured HU enhancement values of a region of interest in the liver and aorta over time assuming a rapid bolus administration of iodine, adapted from (Dawson and Morgan, 1999); ΔHU = Hounsfield unit enhancement following administration of iodine, ROI = region of interest drawn in the liver away from major blood vessels, IVS_{ROI} = intravascular space of the region of interest, $ECEVS_{ROI}$ = extracellular extravascular space of the region of interest, Hct = haematocrit.*

Recognising the criticality of acquiring images in the equilibrium phase, in the first prospective study of fECV measurement in the liver, Bandula et al. (2015) used a bolus contrast administration followed by a slow contrast infusion. This had previously been shown to create a steady-state of plasma iodine concentration as the slow infusion replaced the contrast removed from the body by glomerular filtration to allow a state of contrast equilibrium between the IVS and ECEVS to develop (Bandula et al., 2013b). However, due to the long examination time and high contrast dose associated with the technique it was recognised it was not practical for widespread implementation of EQ-CT. Clearly a quicker bolus only method that could facilitate imaging during the equilibrium phase would be preferable. Work by Schelbert et al. (2011) and White et al. (2013) had previously validated moving from an infusion to a bolus only technique, although these were MRI studies using gadolinium contrast agents in the myocardium where contrast dynamics are likely to be different. Therefore, the time of onset of the equilibrium phase and optimal timing of EQ-CT image acquisitions for measurement of fECV in the liver with a bolus only contrast administration will be areas of interest in the literature search.

5 CT number

Accurate HU measurement is clearly central to the EQ-CT technique. The HU is a measure of the linear attenuation coefficient (μ) of a material relative to water, on a scale where the linear attenuation coefficients of water and air are defined as 0 and -1000 respectively (Equation 8), assuming air has a linear attenuation of 0 (Seeram, 2018).

$$HU = \frac{\mu_{material} - \mu_{water}}{\mu_{water}} \times 1000$$

Equation 8

The linear attenuation coefficient depends on physical properties of that material, namely the atomic number and electron density, as well as the energy spectrum of the x-ray beam. Every voxel of a CT image is assigned an HU value based on the sum of the attenuation of all the materials that voxel contains which will also depend on the energy of the x-ray photons incident upon it. As HU values for each voxel (or pixel in the case of 2D images) are mapped to different greyscale levels for qualitative image interpretation, differences in attenuation manifest as different greyscale levels. The difference in greyscale values between two materials is known as image contrast. Improving the contrast between materials will make them more clearly visible to the image reader.

Quantitative measurements can be made of pixel values with user defined regions of interest (ROIs) which are commonly given as a mean of all the voxels contained within the specified ROI alongside a standard deviation. The standard deviation describes how much variation there is in pixel values around the mean and is commonly known as ‘noise’. Nosie is unavoidable in imaging modalities such as CT where pixel values are influenced by Poisson statistics; however, lower noise in an image means there is less variation in the greyscale levels attributed to voxels/pixels which have the same underlying attenuation properties. Images with lower noise look less ‘mottled’ and it can be easier to see different structures. However, as previously mentioned, the visibility of a structure will also depend on the contrast between adjacent materials. Therefore, contrast and noise are frequently coupled together as an image quality metric: the contrast to noise ratio (CNR) (Equation 9).

$$CNR = \frac{contrast}{noise}$$

Equation 9

In the context of fECV measurement, the contrast of interest is given by the difference between the pre-contrast and equilibrium phase images within either the liver or the aorta. In order to achieve the least statistical uncertainty in this value and therefore the most accurate fECV, the contrast between the pre-contrast and delayed images would be as large as

possible whilst keeping the image noise as low as possible therefore maximising the CNR. A discussion on how to improve contrast will be followed by one on how to reduce image noise.

5.1 Contrast

Image contrast is dependent on both the materials being imaged and the energy of the x-ray photons used to create the image. At x-ray energies encountered in CT imaging, the total linear attenuation coefficient is a result of the combination of both Compton scattering and the photoelectric effect (Smith, 2006). The probability of Compton scattering is dependent almost exclusively on the density of the attenuating material (Equation 10). As the majority of soft tissues in the body have similar densities, there is not much difference in attenuation between soft tissue due to this phenomenon. However, the photoelectric effect has a strong dependence on atomic number and photon energy, as well as density of the attenuating material (Equation 11) (Smith, 2006). Therefore, a small difference in atomic number between two tissues manifests as relatively large differences in attenuation. It follows that by artificially adding a material with a relatively high atomic number to a volume of tissue, that volume becomes more attenuating than the surrounding tissue, generating improved image contrast. So called contrast agents used in CT are typically iodine based as iodine has a relatively high atomic number compared to most tissues within the body.

$$\mu_{compton} \propto \rho$$

Equation 10

$$\mu_{PE} \propto \rho \frac{Z^3}{E^3}$$

Equation 11

Where $\mu_{compton}$ and μ_{PE} are the Compton and photoelectric effect components of the total linear attenuation coefficient respectively for photon energies in the diagnostic radiology range, ρ is the density of the attenuating material, Z is the atomic number of the attenuating material and E is the energy of the incident photon. Note the cube relationships stated for Z and E are approximate, with large discontinuities in linear attenuation near the binding energies of the inner shell electrons of the attenuating material.

In order to exploit the benefits of iodine contrast agents further, it is important to consider that the photoelectric effect is also inversely proportional to approximately the cube of the incident photon energy (Equation 11). This means attenuation is increased and contrast is improved at lower kVps: iodine is twice as attenuating with an 80 kVp x-ray spectrum compared to 140 kVp (Michalak et al., 2016). It is vital to note that as HU values describe attenuation relative to that of air and water for a specific photon spectrum, imaging the same

material at a different kVp will produce a different HU value. Additionally, imaging the same material on different models of CT scanner may also produce different HU values due to variations in hardware and software between manufacturers (Cropp et al., 2013; Lamba et al., 2014).

Reducing the kVp therefore seems a logical choice to increase iodine signal and therefore potentially reduce the uncertainty of fECV measurement using EQ-CT. Historically 120 kVp has been the default x-ray tube voltage setting in CT imaging, however, modern technology has allowed reduced kVp imaging to become a viable option thanks to automatic kVp and tube current selection. It is therefore suggested here that exploration of reduced kVp acquisition should be investigated for measurement of fECV. In order to achieve this, it will be essential to characterise the relationship between HU values and kVp for the concentrations of iodine likely to be encountered in clinical EQ-CT imaging.

It is also important to consider that reduced kVp imaging also carries with it the risk of reduced image quality in terms of increased noise, beam hardening artefacts and inadequate photon penetration. Automatic tube current modulation can help compensate for a potential increase in noise associated with reduced kVps; however, beam hardening and inadequate penetration may be unavoidable. Beam hardening is a physical phenomenon that manifests as the mean energy of the x-ray spectrum increases as it is attenuated in the patient (Seeram, 2018). As a consequence, tissues close to highly attenuating objects can appear to be less attenuating than they actually are. This would manifest as lower HU values and therefore could result in erroneous fECV measurements. Inadequate penetration describes the situation where a large proportion of the x-ray photons do not have enough energy to travel through the entire thickness of the patient and reach the detector. If an insufficient number of photons reach the detector this can lead to particularly noisy images with a high degree of inaccuracy in the HU value. This can potentially be seen in large patients, in areas close to large volumes of highly attenuating materials within the patient or in cases where an inadequately low initial x-ray spectrum has been selected.

Both beam hardening and inadequate penetration are exacerbated at lower kVp selection. Caution must therefore be taken when selecting the optimum x-ray spectrum as a compromise between the potential for increased contrast versus the potential for degradation in CT number accuracy and increased noise.

5.2 Noise

Image noise can be influenced by many factors. The two main sources of noise in CT are electronic noise and quantum noise (Seeram, 2018). Electronic noise is a property of the scanner hardware (mainly the detectors and associated data acquisition systems) and under normal operation will usually result in an insignificant contribution to the total noise in an

image, although will be scanner model specific (Duan et al., 2013). Quantum noise is therefore the main source of noise in CT imaging.

Quantum noise is a function of the number of photons that are detected and used in image reconstruction, which is governed by Poission statistics (Equation 12). Quantum noise is therefore influence by factors including acquisition parameters and patient size (Seeram, 2018). Increasing the number of photons in the CT acquisition (for example increased mA, reduced rotation time, reduced pitch, increased kVp) is an obvious way to reduce the noise. However, the disadvantage of this is an increase in radiation dose to the patient. All commercially available CT scanners now come with an automatic exposure control system that automatically modulates the tube current in order to achieve a certain image noise level that can be selected depending on the balance between desired image quality and acceptable dose level. Again, quantum noise has been shown to be dependent on scanner make and model (Ohno et al., 2019).

$$Noise \propto \frac{1}{\sqrt{N}}$$

Equation 12

Where N is the number of photons detected during image acquisition.

Aside from acquisition factors, image reconstruction parameters can influence noise in CT images. Increased reconstructed slice thickness, smoother reconstruction algorithms and iterative reconstruction can all reduce noise, although each one of these will also have potential downfalls, for example partial volume effects or reduced resolution. Patient anatomy and radiographer scan technique must also be considered- large patients and those with areas of highly attenuating materials can result in higher noise levels, and mispositioning of the patient by the radiographers can result in increased noise in certain parts of the patient images (Szczykutowicz et al., 2017). The underlying variation in some anatomical structures can also act as a source of image noise if it interferes with the clinical interpretation of the image.

It is clear that HU values and image CNR are the function of many different factors which need to be understood and investigated to ensure the accuracy and precision of fECV measurements derived from EQ-CT. As the EQ-CT technique was first developed and implemented, clinical CT imaging was almost universally performed as a ‘single energy’ (SE) acquisition; images were acquired and reconstructed with one fixed x-ray spectrum. However, relatively recent developments in CT scanner technology have resulted in ‘dual energy’ (DE) CT scanners where data is acquired at with two different x-ray spectra. These have now become widely available and have introduced the possibility of many additional

processing and quantification opportunities. These are considered below in the context of application to fECV measurements.

6 Dual energy CT

DE-CT can be used to identify the physical properties of materials based on their attenuation properties at two different energies, a technique first described by Alvarez and Macovski (1976). In summary, the total attenuation, μ, measured using energy, E, at any point in the projection or image data can be described by the sum of the mass attenuation coefficients (μ/ρ) of two known materials, known as the basis pair (Equation 13). Any materials can be selected as the basis pairs, as long as the mass attenuation coefficients are known for the energies at which the CT scanner will acquire the dual energy data. Common basis pairs in contrast enhanced CT are water and iodine.

$$\mu_{unknown\ material}(\mathrm{E}) = \left(\frac{\mu}{\rho}\right)_{water}(E).\rho_{water} + \left(\frac{\mu}{\rho}\right)_{iodine}(E).\rho_{iodine}$$

Equation 13

Where ρ = the mass density of each material (Patino et al., 2016)

Acquiring dual energy data can be done in different ways, as demonstrated by the fact that all major manufacturers of CT equipment have developed different techniques (Johnson, 2012; Goo and Goo, 2017). These include: sequentially scanning the same volume of tissue using two different kVps; using an x-ray tube with a rapidly switching kVp as it rotates around the patient; using two x-ray tubes mounted orthogonally to each other that rotate around the patient at the same time; using filtration at the x-ray tube head to 'divide' the beam into two energies and using a dual layered detector to provide a separation in energies after the photons have passed through the patient. All DE-CT imaging methods will produce a 'high' and 'low' kVp image and all manufacturers have a processing algorithm to produce an image at an intermediate kVp, typically 120 kVp, to simulate a typical SE-CT acquisition (Yu et al., 2009). Additionally all manufacturers have attempted to make their DE-CT acquisitions dose neutral when compared to traditional SE-CT (Leng et al., 2015).

Whilst the techniques will have their technical differences (including processing and reconstruction software) DE-CT enables new possibilities for CT image processing and presentation some of which will have potential applications for fECV measurement with EQ-CT: material maps, virtual non contrast images and monoenergetic reconstructions.

6.1 Material maps

Measuring the μ of a material at two known energies creates two equations which can be solved to establish the values of density ρ for each material. This process is carried out using data from either the projection domain or the image domain (depending on the technology specific to the scanner hardware), which can subsequently be reconstructed to produce a 'mass density' image for each basis material (Patino et al., 2016). In practice, an

iodine mass density image would map densities of iodine and regions of interest could be used to measure the concentration of iodine, as first demonstrated in the human abdomen by Johnson et al. (2007). ROI measurements can either be given directly as iodine concentrations (typically mgI/mL) or an HU value of just the iodine component of the image. If these measurements were proven to be accurate, they could potentially be used to directly measure iodine density on fECV images, negating the need to measure kVp dependent HU values.

6.2 Virtual non-contrast imaging

An additional advantage of DE-CT systems that can produce material maps is that once the distribution and concentration of the material of interest is known, it is possible to subtract this from the original SE-CT dataset. This has powerful consequences as it enables the creation of virtual non contrast (VNC) images, giving the user an image that is theoretically the same as a conventional SE-CT true non contrast image, without the need to perform the initial pre-contrast acquisition (Johnson et al., 2007). Theoretically this could half the radiation dose to the patient which would be a major advantage for the technique.

6.3 Monoenergetic reconstructions

A further application of DE-CT is the reconstruction of monoenergetic or monochromatic images at a user defined keV, as opposed to traditional CT images which are formed of a spectrum of energies defined by the acquisition kVp. This is possible as once the mass density of a basis pair is known, Equation 13 can be 'reversed' to enable the attenuation of the material to be calculated at any monochromatic energy, as long as the mass attenuation coefficients at that particular energy are known (Yu et al., 2011). Depending on the technology implemented, this can be done in the projection or image domain. This process theoretically allows for the reconstruction of images at any monochromatic energy, the major advantages of this being improved contrast at lower keVs and the theoretical elimination of beam hardening artefacts (Mileto et al., 2014). Elimination of beam hardening has the potential to avoid errors in HU values due to this phenomenon as previously discussed. A combination of energies can also be used to recreate a virtual 120 kVp image so the user can compare this to a conventional CT acquisition and obtain 'traditional' HU values. However, it remains true that either type of reconstruction will require careful characterisation and validation of the HU values prior to being used for fECV calculation.

The evidence presented above demonstrates there are a huge number of technical factors and new opportunities that need to be considered when optimising the fECV measurement technique using EQ-CT. In order to establish current practice for this technique and therefore to identify areas where further investigation is required or new technologies could be applied, a literature search on this subject was carried out.

7 Literature review of current practice

In order to establish the current evidence for EQ-CT as a tool for measuring hepatic fECV a literature search was performed using the PubMed database. Search terms included: 'ECV liver', 'ECV liver CT', 'hepatic extracellular volume CT', 'Extracellular volume CT liver' and 'Equilibrium CT liver'. Note the search term 'EQ-CT' returned no results. The literature search process is shown in Figure 2 and the relevant papers found are summarised in Table *1*.

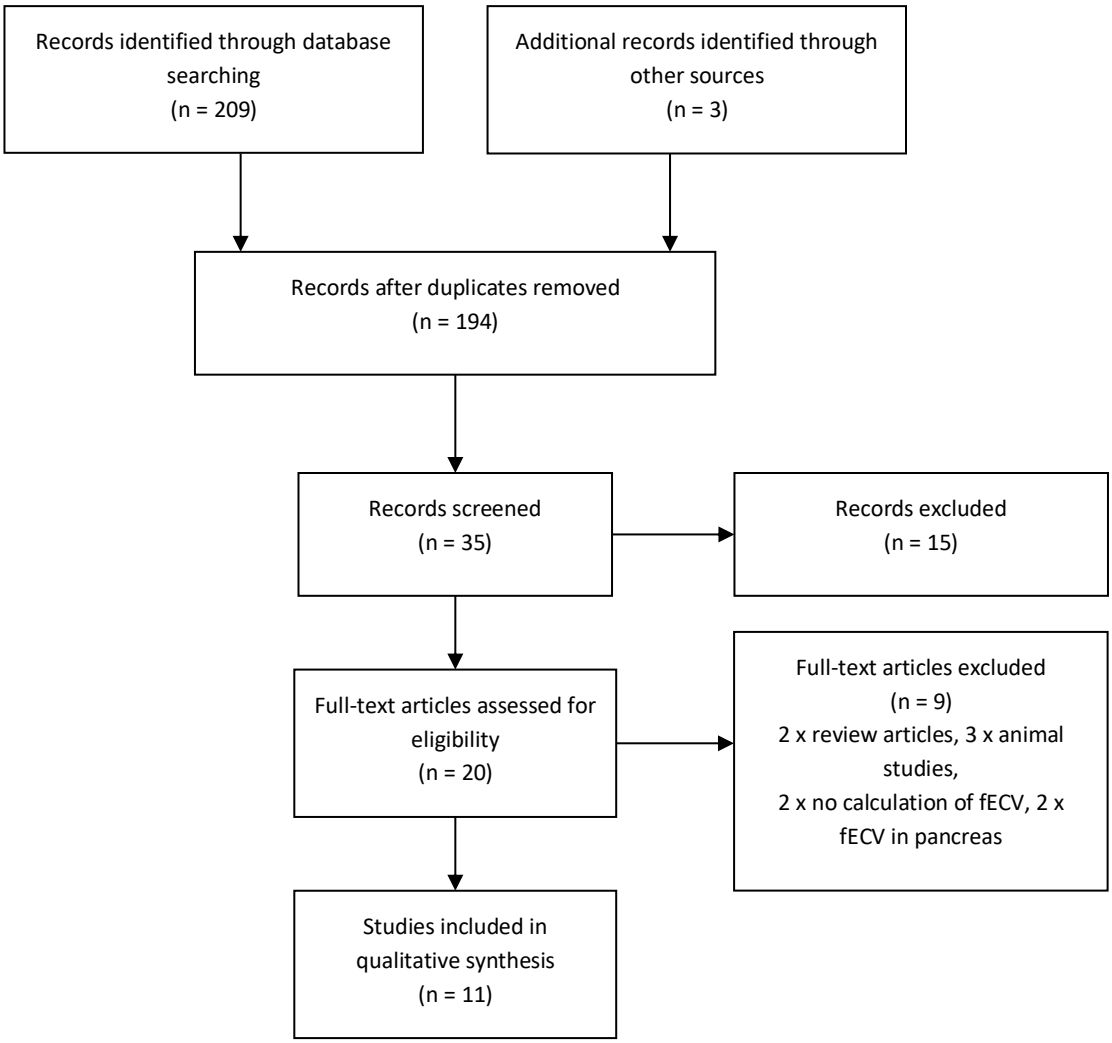

Figure 2 *Literature search process, based on the PRISMA method (PRISMA, 2015).*

Table 1 *Summary of relevant literature search results*

Author	Prospective/ retrospective; N; aetiology	CT manufacturer; kVp; slice width; time of acquisition	Contrast iodine concentration; dose; administration	Image ROI location (size)	Comparison	Results summary	ROC analysis: fECV cut off for fibrosis stage [sensitivity, specificity]	Comments/limitations
Varenika et al. (2013)	Prospective; N =21; Induced fibrosis in rats	Siemens Inveon microCAT II (micro-CT); 80 kVp; 5 mins	300 mgI/mL; 600 mgI/kg; bolus	Liver: 2 in each lobe (0.25 cm2). Inferior vena cava (0.35 cm2)	Histopathology (Ishak); morphometric measurements	Strong correlation between fECV and both Ishak and morphometric scores	-	No cirrhosis- only early and intermediate fibrosis
Zissen et al. (2013)	Retrospective; N = 106; HVC (11), ALD (6), HBV (3), AIH (3), others (12), control (70)	GE; 140 and 120 kVp; 1.25 mm; 10 mins	350 mgI/mL; 150 mL; 3 mL/s	Liver: 2 in each lobe (1 cm2). Aorta (1 cm2).	MELD score; clinical diagnosis	ECV was significantly higher in patients with cirrhosis; significant correlation between ECV and MELD score.	30% for cirrhosis [92%, 83%]	Only cirrhosis vs non cirrhosis (no intermediate fibrosis); portal venous scan not useful for ECV measurement; different kV for pre- and post-scans; no gold standard to quantify degree of fibrosis

Author	Prospective/ retrospective; N; aetiology	CT manufacturer; kVp; slice width; time of acquisition	Contrast iodine concentration; dose; administration	Image ROI location (size)	Comparison	Results summary	ROC analysis: fECV cut off for fibrosis stage [sensitivity, specificity]	Comments/limitations
Bandula et al. (2015)	Prospective; N = 33; HVC (23), HBV (10)	Siemens; 120 kVp; 10 mm; 30 minutes into infusion.	Bolus (300mgI/m; 1 mL/kg; 3 mL/s) followed by infusion (300 mgI/mL; 1.88 mL/kg/hour for 30 mins)	Liver segment VII (34.5 cm2). Aorta (1.6 cm2)	Histopathology (Ishak); CPA; ELF	ECV and ELF correlated with CPA. All 3 can distinguish S0-S1 (low) versus S5-S6 (severe) and S2-S4 (moderate) vs. S5-S6. ECV and ELF together were better predictors of CPA than either in isolation.	-	Most patients had mild fibrosis; no control for other things that might affect ECV (inflammation, steatosis, venous congestion)
Yoon et al. (2015)	Retrospective; N = 135; HCC or liver failure due to HBV (102), HVC (11), ALD (9), NBNC (8), PBC (2), mCRC (2), others (7)	Siemens; 120 kV; 3 mm; 180 s	370 mgI/mL; 1.5 mL/kg; 2-4 mL/s	Liver: at site of surgery (8.6 cm2). Subtraction and non-rigid registration images used. Aorta (0.6 cm2) and portal vein (0.9 cm2)	Histopathology (Korean Study Group classification)	fECV show significant correlation with histology; significant difference between F0-F1 and F2-F4 but not between F0 and F1 or among F2, F3 or F4.	28.76% for significant fibrosis [87.5%, 71%]. 31% for cirrhosis [73.3 %, 62.7%].	Compared the enhancement of aorta and portal vein to establish if equilibrium had been reached; histology looks at the worst bit of fibrosis, fECV looks at all the liver

Author	Prospective/ retrospective; N; aetiology	CT manufacturer; kVp; slice width; time of acquisition	Contrast iodine concentration; dose; administration	Image ROI location (size)	Comparison	Results summary	ROC analysis: fECV cut off for fibrosis stage [sensitivity, specificity]	Comments/limitations
Yoshimitsu et al. (2016)	Retrospective; N = 32; HBC (15), HBV (6), AIH (1), other (10)	GE; dual energy; 1.3 mm: 240 s	350 mgI/mL; 600 mgI/kg; 30 s	Liver; portal vein (no further details given)	Histopathology (METAVIR); MR elastography; Child-Pugh score.	EQ-CT measured ECV with iodine map and 40 and 65 keV reconstructions correlated with MR and Child-Pugh score. Only iodine maps showed significant correlation with histopathology.	n/a	Poster presentation
Guo et al. (2017)	Retrospective; N= 60; HBV (40), AH (3), HVC (3), PBC (2), AIH (2)	Siemens; [not provided]; [not provided]; 180 s	300 mgI/mL; 1.5 mL/kg; 3 mL/s	Liver: one in each segment (1 cm2). Aorta (‘as large as possible’)	Histopathology (METAVIR)	fECV correlates with stage of fibrosis; difference between F0/F4, F1/F4 and F2/F4 significant; Cannot distinguish lower stages of fibrosis.	31.95% for advanced fibrosis [76%, 68%]; 32.74% for cirrhosis [89%, 63%]	180 s for equilibrium images was ‘a guess’; site of biopsy and ROI were not the same.

Author	Prospective/ retrospective; N; aetiology	CT manufacturer; kVp; slice width; time of acquisition	Contrast iodine concentration; dose; administration	Image ROI location (size)	Comparison	Results summary	ROC analysis: fECV cut off for fibrosis stage [sensitivity, specificity]	Comments/limitations
Yeung et al. (2017)	Prospective; N = 23; Systemic amyloid light-chain amyloidosis	Toshiba and Siemens. 120 kVp; 0.5 mm; 5 mins	300 mgI/mL; 1 mL/kg; 3 mL/s	Liver: right lobe (35.6 cm2). Spleen (11.1 cm2). Aorta (average over 15 slices to account for beam hardening)	Serum amyloid P scintigraphy; biopsy	ECV significantly elevated in amyloid; correlation between ECV and SAP grade.	-	'short' equilibrium time might not be enough due to large ECV in advanced disease
Shinagawa et al. (2018)	Retrospective; N = 40; HBV (7), HVC (16), NBNC (7), ALD (1), controls (8), AIH (1), PBC (1)	Toshiba (Canon); 120 kV; 2 mm; 240 s	370 mgI/mL; 1.6 mL/kg; 30 s	Liver: voxel by voxel. Non-rigid image registration images used.	MR elastography; histopathology (METAVIR)	fECV showed significant correlation with MR elastography and histology grade.	29.1% advanced stage fibrosis [100%, 100%]	Quality of subtraction algorithm affects ECV results; no patients had aorta >10 HU from portal vein

Author	Prospective/ retrospective; N; aetiology	CT manufacturer; kVp; slice width; time of acquisition	Contrast iodine concentration; dose; administration	Image ROI location (size)	Comparison	Results summary	ROC analysis: fECV cut off for fibrosis stage [sensitivity, specificity]	Comments/limitations
Sofue et al. (2018)	Prospective; N = 47; HVC (28), HBV (9), AH (2), PBC (2), CC (6)	GE; dual energy; 5 mm; 180 s	300 mgI/mL; 2 mL/kg; 30 s	Liver: segment V-VIII (at site of biopsy, 100 mm^2). Aorta (100 mm^2).	Histopathology (METAVIR)	fECV showed good correlation with METAVIR score.	27.0% F1 [71.4%, 100%]; 27.4% F2 [79.4%, 76.9%]; 28.6% [76%, 81.8%]; 29.9% [90%, 73%].	Used iodine density values as opposed to HU values. Normalisation to aorta still required. Patient body weight found to effect fECV (due to beam hardening).
Ito et al. (2020)	Retrospective; N = 52; HBV (11), HVC (24), ALD (1), no liver disease (11), other (6)	GE; dual energy; 240 s; 5 mm	370 mgI/mL; 600 mgI/kg; 30 s	Liver: right lobe (avoiding pathology, vessels, artifacts). Aorta and inferior vena cava	Histopathology (METAVIR); Liver MR elastography	fECV showed significant correlation with liver stiffness (kPa) and pathology fibrosis grade	26.4% for advanced stages (F3-4) [78%, 90%].	IVC and blood gave best correlation

Author	Prospective/ retrospective; N; aetiology	CT manufacturer; kVp; slice width; time of acquisition	Contrast iodine concentration; dose; administration	Image ROI location (size)	Comparison	Results summary	ROC analysis: fECV cut off for fibrosis stage [sensitivity, specificity]	Comments/limitations
Bak et al. (2020)	Retrospective; N = 305; HBV (86), HVC (81), ALD (1), AIH (9), unknown (116), antiviral treatment (10)	Siemens; 120 kV and dual energy; 1.5 mm; 180 s	370 mgI/mL; 1.5 mL/kg; 3 mL/s	Liver: to margins of liver, excluding focal lesions and major vascular branches. Aorta: average of ROIs at origins of coeliac trunk, superior mesentery artery and renal arteries.	Serum markers; MELD	fECV increased linearly with stage of fibrosis.	n/a	Conclusion that fECV can be used as a predictor of liver related events in patients with cirrhosis (at different stages); fECV superior to MELD for this use. Patients with decompensated cirrhosis had significantly higher ECV than those with compensated disease.

HBV = viral hepatitis B; HVC = viral hepatitis C; ALD = alcoholic liver disease; AH = alcoholic hepatitis; PBC = primary biliary cirrhosis; AIH = autoimmune hepatitis; DH = drug induced hepatitis; CPA= collagen-proportionate area; ELF = enhanced liver fibrosis serum biomarkers; MELD = model for end stage liver disease; CC = cryptogenic cirrhosis; MR = magnetic resonance; mCRC = metastatic colorectal cancer

7.1 Literature summary

Varenika et al. (2013) identified that there was no previous evaluation of EQ-CT to measure fECV in the liver. They performed a pre-clinical study in which an EQ-CT method was performed following the induction of hepatic fibrosis in rats. They found a correlation between measured fECV and fibrosis score following histopathologic analysis.

This was quickly followed by the first study of hepatic EQ-CT in humans (Zissen et al., 2013). Patients with cirrhosis, as well as a control group with no fibrosis, who had undergone clinically indicated CT urography through the abdomen were used as the study cohort. This CT examination was selected due to the inclusion of a 10 minute delayed acquisition phase which acted as the equilibrium phase. They found that measured fECV was significantly higher in patients with cirrhosis and there was a significant correlation between measured fECV and the 'Model of End-Stage Liver Disease' (MELD) score. The fact that this study was retrospectively performed only highlights how simple it would be to incorporate EQ-CT into the clinical workflow: no additional image acquisitions and minimal image analysis was required. However, the absence of a gold standard for cirrhosis diagnosis (biopsy) and the fact that no intermediate stages of fibrosis were included were both recognised as limitations to this study (Zissen et al., 2013). The use of different kVp for the pre-contrast and equilibrium phase CT acquisitions also raises questions over the accuracy of the calculated fECVs due to the known change of HU with kVp.

Bandula et al. (2015) were the first to perform a prospective trial in humans to assess the use of EQ-CT to measure hepatic fECV, using histopathologic analysis as a gold standard. They recognised the vital requirement of ensuring a state of contrast agent equilibrium was achieved so opted to use a contrast bolus followed by a continuous infusion. This technique had previously been proven to achieve a steady-state of equilibrium and was chosen to avoid any uncertainties associated with the timing used for the equilibrium phase (Bandula et al., 2013b). They found that measured fECV correlated with Ishak scores and CPA measured using the biopsy specimen as well as the serum biomarker ELF test. These finding were the first to demonstrate that fECV may be able to help in the grading of fibrosis, unlike Zissen et al. (2013) who only considered states of no fibrosis vs cirrhosis.

Almost simultaneously Yoon et al. (2015) published another much larger retrospective hepatic EQ-CT study. Notably this study included a large proportion of patients with HCC, however, fECV measurements were made specifically avoiding cancerous lesions. Key differences between this study and Zissen et al. (2013) were the use of histopathologic analysis as a gold standard, the use of non-rigid image registration between unenhanced and equilibrium images to improve ROI positioning accuracy and a much reduced time delay of 180 seconds for equilibrium phase imaging. The reduced time delay was seen as a more practical implementation of the EQ-CT technique as it was a standard delay in liver imaging

at the local centre and led to overall reduced examination times. Notably different from Bandula et al. (2015), a bolus only technique was used which again, was seen as a more practical application of the technique. However, still recognising the importance of achieving contrast equilibrium, they compared equilibrium phase HU values for the aorta and portal vein. In a state of equilibrium these should be equal. Yoon et al. (2015) applied a +/- 10 HU tolerance for the difference between these two ROIs: if they were outside this range they were considered not to be in equilibrium and were excluded from the study. This was the case in 6 out of 141 patients: a 4% failure rate. Nonetheless the group concluded that EQ-CT derived fECV would be a useful tool for the estimation of hepatic fibrosis.

Yoshimitsu et al. (2016) were the first to present fECV measurements calculated from DE-CT data sets using both iodine maps and virtual monochromatic energy data sets at 40 and 65 keV. The equilibrium phase was acquired at 240 seconds and MR elastography, the Child-Pugh score and pathological results were used as comparators. For the iodine map calculations, they did not use the unenhanced scan to subtract the underlying iodine density of the liver and blood from the equilibrium phase iodine density, probably assuming the iodine density of unenhanced scans would be zero. The results presented show a significant correlation for both DE-CT methods with Child-Pugh score and MR elastography, however only the iodine density technique showed statistically significant correlation with pathology (p = 0.005), with 40 keV showing a marginal correlation (p = 0.05) and 65 keV showing no significant correlation.

These results provide the first evidence that iodine maps may be useful for fECV measurements, however the relatively small study population and limited details in this poster presentation mean further evidence would be required for confident clinical implementation. The difference in results for different monoenergetic reconstructions also indicate further research and validation is required in order to establish the accuracy and possible optimisation of this technique.

Guo et al. (2017) used SE EQ-CT with a 180 second delay to demonstrate the technique could be applied to routine clinical contrast enhanced liver CT, which provided very similar results to Yoon et al. (2015). They both concluded EQ-CT could be used to distinguish absent/mild fibrosis from severe fibrosis and cirrhosis however, it could not differentiate between early stages of fibrosis. Receiver operator characteristic analysis from Yoon et al. (2015) and Guo et al. (2017) respectively produced fECV thresholds (with sensitivities and specificities) of 28.8% (88%, 71%) and 32.0% (76%, 68%) for diagnosis of significant/advanced fibrosis and fECV of 31.0% (73%, 63%) and 32.8% (89%, 63%) for cirrhosis. Whilst it is encouraging, they had thresholds in a similar range of fECVs, the overlap in the ranges for the two studies indicates the absolute threshold may be dependent on study methods or patient populations (see Table 1 for details). Notably CT number

accuracy is not something that has been discussed by either author but would also have the potential to greatly influence the results. The overlap in values as well as the fact the difference in fECV between significant/advanced fibrosis and cirrhosis are very small (an average of only 1% difference in measured fECV) highlight how important accuracy and precision would be in any technique being used for diagnosis or long term monitoring.

Shinagawa et al. (2018) used EQ-CT with an advanced image registration algorithm in a retrospective study that enabled a voxel-by-voxel measurement of fECV throughout the whole liver. They used a 240 second time delay for the equilibrium phase which, using the quality control test in a similar fashion to Yoon et al. (2015), had a 100% technical success rate of imaging at equilibrium. This perhaps indicates a 240 second delay is preferable to a 180 second delay. They found that the improved image registration algorithm gave fECV values that correlated more strongly with histopathology and MR elastography measurements compared to the conventional image registration. This highlights the importance of accurate image registration and indirectly the requirement to minimise patient movement between the pre-contrast and delayed images as far as possible. However, similarly to previously discussed studies, they could not use fECV to distinguish between intermediate stages of fibrosis although they found a cut off fECV value of 29.1% had 100% sensitivity and 100% specificity for diagnosis of advanced fibrosis.

Yeung et al. (2017) were the first group to apply hepatic EQ-CT to patients with systemic amyloid light-chain amyloidosis which followed on from a previous study using MRI (Bandula et al., 2013a). In amyloidosis there is extracellular deposition of amyloid proteins leading with an associated increase in the fECV. Measurement of fECV using EQ-CT was shown to be able to differentiate healthy tissue from those with amyloid with a correlation between fECV and amyloid burden, based on the gold standard of serum amyloid P scintigraphy (Yeung et al., 2017). These findings indicate EQ-CT could be a useful diagnostic tool in conditions other than fibrosis, although the author points out it is important to note that expansion of the fECV is a non-specific process that could be related to other processes such as inflammation and venous congestion. It is therefore a tool that should not be used in isolation.

In the study from Sofue et al. (2018) they used DE-CT with material decomposition with water and iodine as basis pairs to create iodine maps of the equilibrium phase of a contrast enhanced scan in patients with chronic liver disease. The equilibrium phase was acquired at 180 seconds post contrast administration. They considered using the iodine densities as measured in the equilibrium phase in isolation to calculate fECV with the hope of not requiring an unenhanced scan, however, they concluded that this was not possible as they observed that the iodine concentration in both the liver and aorta on the unenhanced scan was not zero. The unenhanced scan is therefore still required to give a measure of relative

iodine enhancement rather than an absolute iodine concentration. This is in contradiction to the method from Yoshimitsu et al. (2016) who did not subtract the unenhanced iodine concentrations.

Sofue et al. (2018) successfully measured fECV using iodine density in 47 patients which correlated with METAVIR fibrosis score and provided fECV cut-off values corresponding with the four METAVIR fibrosis scores with quoted accuracies ranging between 74.5%-78.7% (Sofue et al., 2018). This is clearly promising, however, using multivariate linear regression analysis they found that patient weight had a significant effect on fECV measurement. It was concluded that this was due to beam hardening associated with large patients. They concluded that the non-contrast scan is necessary to achieve meaningful fECV measurements, however they did not consider the use of virtual monochromatic imaging to mitigate the effects of beam hardening that was cited as an issue.

Similarly to Sofue et al. (2018), Ito et al. (2020) measured fECV in the liver with a DE-CT acquisition in a cohort of patients with chronic liver disease who underwent otherwise clinically indicated CT examinations. This group appear to be the first to investigate different CT reconstruction parameters and measurement techniques to improve accuracy of the technique. This is considered to be an important step for future researchers to build upon. They investigated different parameters for the iodine map reconstruction as well as different positions for the aorta ROI due to concerns regarding image artefacts caused by the adjacent highly attenuating vertebral bodies. Ito et al. (2020) concluded fECV calculated based on measurements from iodine attenuation maps with particular reconstruction parameters and the ROI to measure blood enhancement positioned in the inferior vena cava gave the best correlation to MR elastography and pathological fibrosis grade. These results can hopefully be directly translated into future studies.

Bak et al. (2020) also used DE-CT to measure fECV, but unlike any of the previous studies, they were not aiming to confirm the accuracy of the measurement: they appear to use it as a validated technique that does not require independent verification. This is the first example of this to be found in this literature search of fECV measurement in the liver and could represent the start of this technique becoming more widely accepted into the research base, as well as routine clinical use. The group used iodine concentrations measured on a 180 second delayed image. They used dual energy data with the associated iodine quantification to avoid the need for data subtraction between pre-contrast and delayed images, however this is given very limited attention by the authors and is in conflict with the finding from Sofue et al. (2018) discussed above. They successfully demonstrated different fECV results in patients with decompensated and compensated cirrhosis, and further between the aetiology of disease within the decompensated group (but not the compensated group). They demonstrated fECV performed better than the MELD score in predicting

cirrhosis stage and fECV could be used as an independent predictor of 'liver-related events'. This is clearly encouraging for the technique; however, the authors acknowledge the technical complexity of DE-CT and associated iodine quantification could mean these results would only be valid on the CT model used in the study.

There is clearly evidence in the literature that the EQ-CT is a potentially useful technique for the non-invasive measurement of hepatic fibrosis with all studies successfully demonstrating correlations with other measures of fibrosis. However, there is no evidence that EQ-CT has been directly applied to the measurement of fECV in liver cancer tumours. It is also unfortunate that most of the publications listed in Table 1 are retrospective studies that have simply used a pre-existing clinical CT protocol with little (or no) optimisation of the technical scanning parameters that could influence the measured fECV. There has also notably been no evidence presented to establish if fECV measurements are accurate or reproducible.

7.2 Additional literature

It should be acknowledged that during this literature search many publications were found that related to the use of DE EQ-CT to measure fECV in organs other than the liver (predominantly based on the myocardium). Although these were not included in the above literature search, some of these have been reviewed below as it is thought they could provide some transferrable information that could be applied to the liver.

Fukukura et al. (2020) measured fECV in the pancreas using iodine maps acquired with DE-CT. Results from DE-CT were compared to SE-CT results, although it is noted a SE 120 kVp acquisition was performed for the pre-contrast acquisition, but a DE 120 kVp 'equivalent' image was used for the SE delayed image. Any uncertainty in the accuracy of HU values between a true SE and a SE 'equivalent' image could be a potential source of error in these results. A strong correlation was found between fECV results from these and SE measurements and equilibrium phase only iodine maps; however there was a bias of -3.4% towards lower fECV values with DE-CT. It is suggested that this difference may be the result of a lack of subtraction of pre-contrast iodine concentrations.

Interestingly the Fukukura et al. (2020) group is the only one that was found to use a 'wide detector' CT technology which can perform a 16 cm axial acquisition to image entire organs in one rotation, reducing problems associated with intra-phase patient movement. The group used a previously implemented scan protocol to measure fECV, acquiring the equilibrium phase at 180 seconds and image analysis was performed by two independent observers to investigate interobserver agreement. Interobserver agreement was found to be excellent: an encouraging result for the technique.

A study by van Assen et al. (2019) to measure fECV in fibrosis in the myocardium is also reliant on delayed equilibrium images that were ‘SE equivalent’ images produced from DE data sets. It is interesting to note that van Assen et al. (2019) also generated iodine maps but these were used purely for the purpose of positioning the ROIs in the myocardium and left ventricle and not for measuring iodine concentrations, pointing to the utility of additional information obtained with DE-CT that is not present with SE-CT acquisition. Lee et al. (2016) provided evidence that this technique improved intra-observer agreement with fECV measurement in the myocardium. It is recognised that this is likely to be more of an issue when trying to differentiate between the myocardium and ventricular blood pool rather than making measurements in liver, although it could help the user avoid large blood vessels or hyper/hypo attenuating lesions that could distort fECV values.

Away from the technical aspects of the EQ-CT technique, of important clinical significance the findings from Fukukura et al. (2020) showed that fECV measured with iodine maps was an independent predictor of progression free survival in patients with pancreatic adenocarcinoma. This builds on previous evidence from Wong et al. (2012) demonstrating EQ-MR measured fECV in the myocardium being a predictor of short term mortality. These studies provide evidence that fECV measurement has important clinical applications that warrant further investigation and optimisation to enable widespread confident clinical implementation.

8 Conclusions and indications for further work

The theory and literature presented above show that the use of EQ-CT to measure fECV in the liver is a feasible and practical technique that has demonstrated correlation with established measures of fibrosis. There is, however, no evidence of EQ-CT derived measures of fECV in the clinical context of liver cancer, or as a tool for measuring response to liver-directed cancer therapies. EQ-CT has the advantage of being a relatively simple technique that uses technology that is widely available, has few contra-indications, is well tolerated by patients and has been shown to be operator independent and easily integrated into existing clinical pathways and imaging protocols. However, as with any quantitative clinical measurement, there are many technical factors that require careful consideration to ensure an accurate result is obtained, particularly with a modality that utilises ionising radiation.

With this in mind, and in the absence of any existing published literature on the subject, this body of work will focus first on establishing the accuracy and optimising the precision of the EQ-CT technique for fECV measurement in the liver in a phantom study, followed by the application of those findings in a clinical study. The clinical study will also aim to establish if and how the fECV changes between unaffected areas of the liver and tumour lesions, and if it is possible to measure fECV in the presences of TACE beads as a potential tool for monitoring response to liver-directed cancer therapy. The following research aims will be addressed:

- What is the expected accuracy of EQ-CT derived fECV measurements in the liver?
- What are the optimum acquisition and reconstruction settings for EQ-CT to measure fECV in the liver, using conventional and dual energy CT?
- Are clinical EQ-CT derived fECV measurements reproducible?
- Are the fECV values measured in liver tumour lesions different to apparently unaffected liver tissue in the same patient?
- Is fECV measurement possible in the presence of TACE therapy beads?

9 References

Afdhal, N. H. and Nunes, D. (2004) 'Evaluation of Liver Fibrosis: A Concise Review.' *The American Journal of Gastroenterology*, 99(6) pp. 1160–1174.

Alvarez, R. E. and Macovski, A. (1976) 'Energy-selective reconstructions in X-ray computerised tomography.' *Physics in Medicine and Biology*, 21(5) pp. 733–744.

van Assen, M., De Cecco, C. N., Sahbaee, P., Eid, M. H., Griffith, L. P., Bauer, M. J., Savage, R. H., Varga-Szemes, A., Oudkerk, M., Vliegenthart, R. and Schoepf, U. J. (2019) 'Feasibility of extracellular volume quantification using dual-energy CT.' *Journal of Cardiovascular Computed Tomography*, 13 pp. 81–84.

Bak, S., Kim, J. E., Bae, K., Cho, J. M., Choi, H. C., Park, M. J., Choi, H. Y., Shin, H. S., Lee, S. M. and Kim, H. O. (2020) 'Quantification of liver extracellular volume using dual-energy CT: utility for prediction of liver-related events in cirrhosis.' *European Radiology*, 30(10) pp. 5317–5326.

Bandula, S., Banypersad, S. M., Sado, D., Flett, A. S., Punwani, S., Taylor, S. A., Hawkins, P. N. and Moon, J. C. (2013a) 'Measurement of Tissue interstitial volume in healthy patients and those with amyloidosis with equilibrium contrast-enhanced MR imaging.' *Radiology*, 268(3) pp. 858–864.

Bandula, S., White, S. K., Flett, A. S., Lawrence, D., Pugliese, F., Ashworth, M. T., Punwani, S., Taylor, S. A. and Moon, J. C. (2013b) 'Measurement of Myocardial Extracellular Volume Fraction by Using Equilibrium Contrast-enhanced CT: Validation against Histologic Findings.' *Radiology*, 269(2) pp. 396–403.

Bandula, S., Punwani, S., Rosenberg, W. M., Jalan, R., Hall, A. R., Dhillon, A., Moon, J. C. and Taylor, S. A. (2015) 'Equilibrium Contrast-enhanced CT Imaging to Evaluate Hepatic Fibrosis: Initial Validation by Comparison with Histopathologic Sampling.' *Radiology*, 275(1) pp. 136–143.

Banerjee, R., Pavlides, M., Tunnicliffe, E. M., Piechnik, S. K., Sarania, N., Philips, R., Collier, J. D., Booth, J. C., Schneider, J. E., Wang, L. M., Delaney, D. W., Fleming, K. A., Robson, M. D., Barnes, E. and Neubauer, S. (2014) 'Multiparametric magnetic resonance for the non-invasive diagnosis of liver disease.' *Journal of Hepatology*, 60(1) pp. 69–77.

Beaton, L., Tregidgo, H. F. J., Znati, S. A., Forsyth, S., Clarkson, M. J., Bandula, S., Chouhan, M., Lowe, H. L., Zaw Thin, M., Hague, J., Sharma, D., Pollok, J.-M., Davidson, B. R., Raja, J., Munneke, G., Stuckey, D. J., Bascal, Z. A., Wilde, P. E., Cooper, S., Ryan, S., Czuczman, P., Boucher, E., Hartley, J. A., Lewis, A. L., Jansen, M., Meyer, T. and Sharma, R. A. (2019) 'VEROnA Protocol: A Pilot, Open-Label, Single-Arm, Phase 0, Window-of-Opportunity Study of Vandetanib-Eluting Radiopaque Embolic Beads (BTG-002814) in Patients With Resectable Liver Malignancies.' *JMIR Research Protocols*, 8(10).

Bonekamp, S., Kamel, I., Solga, S. and Clark, J. (2009) 'Can imaging modalities diagnose and stage hepatic fibrosis and cirrhosis accurately?' *Journal of Hepatology*, 50(1) pp. 17–35.

Chiou, W.-Y., Chang, C.-M., Tseng, K.-C., Hung, S.-K., Lin, H.-Y., Chen, Y.-C., Su, Y.-C., Tseng, C.-W., Tsai, S.-J., Lee, M.-S. and Li, C.-Y. (2015) 'Effect of liver cirrhosis on metastasis in colorectal cancer patients: a nationwide population-based cohort study.' Japanese Journal of Clinical Oncology, 45(2) pp. 160–168.

Conrad, R., Castelino-Prabhu, S., Cobb, C. and Raza, A. (2013) 'Cytopathologic diagnosis of liver mass lesions.' Journal of Gastrointestinal Oncology, 4(1) pp. 53–61.

Cropp, R. J., Seslija, P., Tso, D. and Thakur, Y. (2013) 'Scanner and kVp dependence of measured CT numbers in the ACR CT phantom.' *Journal of Applied Clinical Medical Physics*, 14(6) pp. 338–349.

Cuenod, C. A. and Balvay, D. (2013) 'Perfusion and vascular permeability: basic concepts and measurement in DCE-CT and DCE-MRI.' *Diagnostic and Interventional Imaging*, 94(12) pp. 1187–1204.

Dawson, P. and Morgan, J. (1999) 'The meaning and significance of the equilibrium phase in enhanced computed tomography of the liver.' *The British Journal of Radiology*, 72(857) pp. 438–442.

Dean, P. B., Kivisaari, L. and Kormano, M. (1978a) 'Contrast Enhancement: Diagnostic Significance from a Statistical Viewpoint.' *Journal of Computer Assisted Tomography*, 2(3) p. 314.

Dean, P. B., Kivisaari, L. and Kormano, M. (1978b) 'The Diagnostic Potential of Contrast Enhancement Pharmacokinetics.' *Investigative Radiology*, 13(6) p. 533.

Dietrich, C. F., Bamber, J., Berzigotti, A., Bota, S., Cantisani, V., Castera, L., Cosgrove, D., Ferraioli, G., Friedrich-Rust, M., Gilja, O. H., Goertz, R. S., Karlas, T., de Knegt, R., de Ledinghen, V., Piscaglia, F., Procopet, B., Saftoiu, A., Sidhu, P. S., Sporea, I. and Thiele, M. (2017) 'EFSUMB Guidelines and Recommendations on the Clinical Use of Liver Ultrasound Elastography, Update 2017 (Long Version).' *Ultraschall in Der Medizin (Stuttgart, Germany: 1980)*, 38(4) pp. e16–e47.

Duan, X., Wang, J., Leng, S., Schmidt, B., Allmendinger, T., Grant, K., Flohr, T. and McCollough, C. H. (2013) 'Electronic Noise in CT Detectors: Impact on Image Noise and Artifacts.' *American Journal of Roentgenology*, 201(4) pp. W626–W632.

Flett, A. S., Hayward, M. P., Ashworth, M. T., Hansen, M. S., Taylor, A. M., Elliott, P. M., McGregor, C. and Moon, J. C. (2010) 'Equilibrium contrast cardiovascular magnetic resonance for the measurement of diffuse myocardial fibrosis: preliminary validation in humans.' *Circulation*, 122(2) pp. 138–144.

Friedman, S. L. (2003) 'Liver fibrosis – from bench to bedside.' *Journal of Hepatology*. (Therapy in Liver Diseases 2003), 38, January, pp. 38–53.

Fukukura, Y., Kumagae, Y., Higashi, R., Hakamada, H., Nakajo, M., Maemura, K., Arima, S. and Yoshiura, T. (2020) 'Extracellular volume fraction determined by equilibrium contrast-enhanced dual-energy CT as a prognostic factor in patients with stage IV pancreatic ductal adenocarcinoma.' *European Radiology*, 30(3) pp. 1679–1689.

Goo, H. W. and Goo, J. M. (2017) 'Dual-Energy CT: New Horizon in Medical Imaging.' *Korean Journal of Radiology*, 18(4) pp. 555–569.

Guo, S. L., Su, L. N., Zhai, Y. N., Chirume, W. M., Lei, J. Q., Zhang, H., Yang, L., Shen, X. P., Wen, X. X. and Guo, Y. M. (2017) 'The clinical value of hepatic extracellular volume fraction using routine multiphasic contrast-enhanced liver CT for staging liver fibrosis.' *Clinical Radiology*, 72(3) pp. 242–246.

Horowitz, J. M., Venkatesh, S. K., Ehman, R. L., Jhaveri, K., Kamath, P., Ohliger, M. A., Samir, A. E., Silva, A. C., Taouli, B., Torbenson, M. S., Wells, M. L., Yeh, B. and Miller, F. H. (2017) 'Evaluation of hepatic fibrosis: a review from the society of abdominal radiology disease focus panel.' *Abdominal Radiology*, 42(8) pp. 2037–2053.

Ionising Radiation (Medical Exposure) Regulations 2017. Available at: https://www.legislation.gov.uk/uksi/2017/1322/pdfs/uksi_20171322_en.pdf (Accessed: 29 April 2019).

Ito, E., Sato, K., Yamamoto, R., Sakamoto, K., Urakawa, H. and Yoshimitsu, K. (2020) 'Usefulness of iodine-blood material density images in estimating degree of liver fibrosis by calculating extracellular volume fraction obtained from routine dual-energy liver CT protocol equilibrium phase data: preliminary experience.' *Japanese Journal of Radiology*, 38(4) pp. 365–373.

Johnson, T. R. C. (2012) 'Dual-Energy CT: General Principles.' *American Journal of Roentgenology*, 199(5_supplement) pp. S3–S8.

Johnson, T. R. C., Krauß, B., Sedlmair, M., Grasruck, M., Bruder, H., Morhard, D., Fink, C., Weckbach, S., Lenhard, M., Schmidt, B., Flohr, T., Reiser, M. F. and Becker, C. R. (2007) 'Material differentiation by dual energy CT: initial experience.' *European Radiology*, 17(6) pp. 1510–1517.

Kim, S. H., Kamaya, A. and Willmann, J. K. (2014) 'CT Perfusion of the Liver: Principles and Applications in Oncology.' *Radiology*. Radiological Society of North America, 272(2) pp. 322–344.

Kondo, T., Okabayashi, K., Hasegawa, H., Tsuruta, M., Shigeta, K. and Kitagawa, Y. (2016) 'The impact of hepatic fibrosis on the incidence of liver metastasis from colorectal cancer.' *British Journal of Cancer*, 115(1) pp. 34–39.

Lamba, R., McGahan, J. P., Corwin, M. T., Li, C.-S., Tran, T., Seibert, J. A. and Boone, J. M. (2014) 'CT Hounsfield Numbers of Soft Tissues on Unenhanced Abdominal CT Scans: Variability Between Two Different Manufacturers' MDCT Scanners.' *AJR. American journal of roentgenology*, 203(5) pp. 1013–1020.

Lee, H.-J., Im, D. J., Youn, J.-C., Chang, S., Suh, Y. J., Hong, Y. J., Kim, Y. J., Hur, J. and Choi, B. W. (2016) 'Myocardial extracellular volume fraction with dual-energy equilibrium contrast-enhanced cardiac CT in nonischemic cardiomyopathy: a prospective comparison with cardiac MR imaging.' *Radiology*, 280(1) pp. 49–57.

Leng, S., Yu, L., Fletcher, J. G. and McCollough, C. H. (2015) 'Maximizing iodine contrast-to-noise ratios in abdominal CT imaging through use of energy domain noise reduction and virtual monoenergetic dual-energy CT.' *Radiology*, 276(2) pp. 562–570.

Lichtinghagen, R., Pietsch, D., Bantel, H., Manns, M. P., Brand, K. and Bahr, M. J. (2013) 'The Enhanced Liver Fibrosis (ELF) score: normal values, influence factors and proposed cut-off values.' *Journal of Hepatology*, 59(2) pp. 236–242.

Lubner, M. G. and Pickhardt, P. J. (2018) 'Multidetector Computed Tomography for retrospective, noninvasive staging of liver fibrosis.' *Gastroenterology Clinics of North America*. (Radiologic Gastrointestinal Imaging), 47(3) pp. 569–584.

Martínez, S. M., Crespo, G., Navasa, M. and Forns, X. (2011) 'Noninvasive assessment of liver fibrosis.' *Hepatology*, 53(1) pp. 325–335.

Michalak, G., Grimes, J., Fletcher, J., Halaweish, A., Yu, L., Leng, S. and McCollough, C. (2016) 'Technical Note: Improved CT number stability across patient size using dual-energy CT virtual monoenergetic imaging.' *Medical Physics*, 43(1) p. 513.

Mileto, A., Nelson, R. C., Samei, E., Choudhury, K. R., Jaffe, T. A., Wilson, J. M. and Marin, D. (2014) 'Dual-energy MDCT in hypervascular liver tumors: effect of body size on selection of the optimal monochromatic energy level.' *American Journal of Roentgenology*, 203(6) pp. 1257–1264.

Nacif, M. S., Kawel, N., Lee, J. J., Chen, X., Yao, J., Zavodni, A., Sibley, C. T., Lima, J. A. C., Liu, S. and Bluemke, D. A. (2012) 'Interstitial myocardial fibrosis assessed as extracellular volume fraction with low-radiation-dose cardiac CT.' *Radiology*, 264(3) pp. 876–883.

Nallagangula, K. S., Nagaraj, S. K., Venkataswamy, L. and Chandrappa, M. (2017) 'Liver fibrosis: a compilation on the biomarkers status and their significance during disease progression.' *Future Science OA*, 4(1).

Ohno, Y., Fujisawa, Y., Fujii, K., Sugihara, N., Kishida, Y., Seki, S. and Yoshikawa, T. (2019) 'Effects of acquisition method and reconstruction algorithm for CT number measurement on standard-dose CT and reduced-dose CT: a QIBA phantom study.' *Japanese Journal of Radiology*, 37(5) pp. 399–411.

Patino, M., Prochowski, A., Agrawal, M. D., Simeone, F. J., Gupta, R., Hahn, P. F. and Sahani, D. V. (2016) 'Material Separation Using Dual-Energy CT: Current and Emerging Applications.' *RadioGraphics*, 36(4) pp. 1087–1105.

Pavlides, M., Birks, J., Fryer, E., Delaney, D., Sarania, N., Banerjee, R., Neubauer, S., Barnes, E., Fleming, K. A. and Wang, L. M. (2017) 'Interobserver Variability in Histologic Evaluation of Liver Fibrosis Using Categorical and Quantitative Scores.' *American Journal of Clinical Pathology*, 147(4) pp. 364–369.

Petitclerc, L., Sebastiani, G., Gilbert, G., Cloutier, G. and Tang, A. (2017) 'Liver fibrosis: Review of current imaging and MRI quantification techniques.' *Journal of Magnetic Resonance Imaging*, 45(5) pp. 1276–1295.

PRISMA (2015) *PRISMA*. [Online]. Available at: http://www.prisma-statement.org/ (Accessed: 17 September 2017).

Regev, A., Berho, M., Jeffers, L., Milikowski, C., Molina, E., Pyrsopoulos, N., Feng, Z.-Z., Reddy, R. and Schiff, E. (2002) 'Sampling Error and Intraobserver Variation in Liver Biopsy in Patients With Chronic Hcv Infection.' *American Journal of Gastroenterology*, 97(10) pp. 2614–2618.

Ronot, M., Leporq, B., Van Beers, B. E. and Vilgrain, V. (2020) 'CT and MR perfusion techniques to assess diffuse liver disease.' *Abdominal Radiology*, 45(11) pp. 3496–3506.

Sadigh, G., Applegate, K. E. and Saindane, A. M. (2017) 'Prevalence of Unanticipated Events Associated With MRI Examinations: A Benchmark for MRI Quality, Safety, and Patient Experience.' *Journal of the American College of Radiology*, 14(6) pp. 765–772.

Schelbert, E. B., Testa, S. M., Meier, C. G., Ceyrolles, W. J., Levenson, J. E., Blair, A. J., Kellman, P., Jones, B. L., Ludwig, D. R., Schwartzman, D., Shroff, S. G. and Wong, T. C. (2011) 'Myocardial extravascular extracellular volume fraction measurement by gadolinium cardiovascular magnetic resonance in humans: slow infusion versus bolus.' *Journal of Cardiovascular Magnetic Resonance*, 13:16.

Seeram, E. (2018) 'Computed Tomography: A Technical Review.' *Radiologic Technology*, 89(3) pp. 279CT-302CT.

Shinagawa, Y., Sakamoto, K., Sato, K., Ito, E., Urakawa, H. and Yoshimitsu, K. (2018) 'Usefulness of new subtraction algorithm in estimating degree of liver fibrosis by calculating extracellular volume fraction obtained from routine liver CT protocol equilibrium phase data: Preliminary experience.' *European Journal of Radiology*, 103, June, pp. 99–104.

Singh, S., Fujii, L. L., Murad, M. H., Wang, Z., Asrani, S. K., Ehman, R. L., Kamath, P. S. and Talwalkar, J. A. (2013) 'Liver stiffness is associated with risk of decompensation, liver cancer, and death in patients with chronic liver diseases: a systematic review and meta-analysis.' *Clinical Gastroenterology and Hepatology: The Official Clinical Practice Journal of the American Gastroenterological Association*, 11(12) pp. 1573-1584.e1–2.

Smith, F. A. (2006) *A Primer in Applied Radiation Physics*. Singapore: World Scientific.

Sofue, K., Tsurusaki, M., Mileto, A., Hyodo, T., Sasaki, K., Nishii, T., Chikugo, T., Yada, N., Kudo, M., Sugimura, K. and Murakami, T. (2018) 'Dual-energy computed tomography for non-invasive staging of liver fibrosis: Accuracy of iodine density measurements from contrast-enhanced data.' *Hepatology Research*, 0(0).

Szczykutowicz, T. P., DuPlissis, A. and Pickhardt, P. J. (2017) 'Variation in CT Number and Image Noise Uniformity According to Patient Positioning in MDCT.' *American Journal of Roentgenology*. American Roentgen Ray Society, 208(5) pp. 1064–1072.

Tsochatzis, E., Bruno, S., Isgro, G., Hall, A., Theocharidou, E., Manousou, P., Dhillon, A. P., Burroughs, A. K. and Luong, T. V. (2014) 'Collagen proportionate area is superior to other histological methods for sub-classifying cirrhosis and determining prognosis.' *Journal of Hepatology*, 60(5) pp. 948–954.

Varenika, V., Fu, Y., Maher, J. J., Gao, D., Kakar, S., Cabarrus, M. C. and Yeh, B. M. (2013) 'Hepatic Fibrosis: Evaluation with Semiquantitative Contrast-enhanced CT.' *Radiology*, 266(1) p. 151.

Venkatesh, S. K., Yin, M. and Ehman, R. L. (2013) 'Magnetic Resonance Elastography of Liver: Technique, Analysis and Clinical Applications.' *Journal of magnetic resonance imaging : JMRI*, 37(3) pp. 544–555.

Vis, J. Y. and Huisman, A. (2016) 'Verification and quality control of routine hematology analyzers.' *International Journal of Laboratory Hematology*, 38(S1) pp. 100–109.

White, S. K., Sado, D. M., Fontana, M., Banypersad, S. M., Maestrini, V., Flett, A. S., Piechnik, S. K., Robson, M. D., Hausenloy, D. J., Sheikh, A. M., Hawkins, P. N. and Moon, J. C. (2013) 'T1 mapping for myocardial extracellular volume measurement by CMR: bolus only versus primed infusion technique.' *JACC. Cardiovascular imaging*, 6(9) pp. 955–962.

Wong, T. C., Piehler, K., Meier, C. G., Testa, S. M., Klock, A. M., Aneizi, A. A., Shakesprere, J., Kellman, P., Shroff, S. G., Schwartzman, D. S., Mulukutla, S. R., Simon, M. A. and Schelbert, E. B. (2012) 'Association between extracellular matrix expansion quantified by cardiovascular magnetic resonance and short-term mortality.' *Circulation*, 126(10) pp. 1206-1216.

Yeung, J., Sivarajan, S., Treibel, T. A., Rosmini, S., Fontana, M., Gillmore, J. D., Hawkins, P. N., Punwani, S., Moon, J. C., Taylor, S. A. and Bandula, S. (2017) 'Measurement of liver and spleen interstitial volume in patients with systemic amyloid light-chain amyloidosis using equilibrium contrast CT.' *Abdominal Radiology*, 42(11) pp. 2646–2651.

Yoon, J. H., Lee, J. M., Klotz, E., Jeon, J. H., Lee, K., Han, J. K. and Choi, B. I. (2015) 'Estimation of Hepatic Extracellular Volume Fraction Using Multiphasic Liver Computed Tomography for Hepatic Fibrosis Grading.' *Investigative Radiology*, 50(4) pp. 290–296.

Yoshimitsu, K., Shinagawa, Y., Morita, A., Urakawa, H., Sakamoto, K. and Fujimitsu, R. (2016) *Comparison of extracellular volume fraction calculated from the three data sets of the equilibrium phase of dual-energy CT as surrogate markers for liver fibrosis: preliminary report*. ECR 2016 EPOS. European Congress of Radiology - ECR 2016. [Online]. Available at: https://epos.myesr.org/poster/esr/ecr2016/C-0874 (Accessed: 7 December 2020).

Yu, L., Christner, J. A., Leng, S., Wang, J., Fletcher, J. G. and McCollough, C. H. (2011) 'Virtual monochromatic imaging in dual-source dual-energy CT: Radiation dose and image quality.' *Medical Physics*, 38(12) pp. 6371–6379.

Yu, L., Primak, A. N., Liu, X. and McCollough, C. H. (2009) 'Image quality optimization and evaluation of linearly mixed images in dual-source, dual-energy CT.' *Medical Physics*, 36(3) pp. 1019–1024.

Zissen, M. H., Wang, Z. J., Yee, J., Aslam, R., Monto, A. and Yeh, B. M. (2013) 'Contrast-enhanced CT quantification of the hepatic fractional extracellular space: correlation with diffuse liver disease severity.' *American Journal of Roentgenology*, 201(6) pp. 1204–1210.

Section 2

Optimisation of extracellular volume measurement in equilibrium contrast enhanced CT: a phantom study

Chris Baker[1,2]

[1]School of Medical Sciences, University of Manchester, Manchester, United Kingdom
[2]Radiological Physics and Radiation Safety Group, Royal Free London NHS Foundation Trust, London, United Kingdom

Abstract

Purpose

To investigate the effect of acquisition and reconstruction parameters for equilibrium CT (EQ-CT) for the measurement of hepatic fractional extracellular volume (fECV) and establish the accuracy of the technique.

Materials and methods

A phantom with interchangeable iodine inserts was used to simulate EQ-CT imaging at a range of fECV values. Repeat image acquisitions using a range of $CTDI_{vol}$ values (5.0 – 21.6 mGy) and the full range of kVp (80 – 135 kVp) and dual energy settings were performed. Images were reconstructed with slice widths ranging between 1 and 10 mm. The limits of detection and quantification for iodine for the scanner technology were established. Hounsfield unit values taken in the iodine inserts were used to simulate a range of clinical fECV measurements for all acquisition and reconstruction parameters tested. The error with each measurement calculated based on the known iodine concentrations as a measure of accuracy of the technique. A multiple linear regression model was used to establish the effect of kVp (including dual energy mode), $CTDI_{vol}$, slice width, relative slice location and absolute fECV value on fECV calculated error and the Brown-Forsythe equality of variance test was used to investigate how the imaging parameters affected the spread of fECV results as a simple measure of precision. Accuracy and precision were correlated to a novel imaging metric: enhancement to noise ratio (ENR).

Results

The limit of detection and quantification of iodine were found to be low enough to facilitate simulated fECV measurements with the study phantom, with the exclusion of 1 mm slice widths and low dose ($CTDI_{vol}$ < 10.8 mGy) dual energy derived iodine density images. The median accuracy across all settings was 0.1% (interquartile range 9.1%). The multiple linear regression model demonstrated fECV accuracy was robust to changes in all the acquisition and reconstruction settings tested as well as absolute fECV value ($p > 0.05$), with the exception of the use of dual energy mode ($p < 0.001$). Variance in fECV measurements was lowest for 80 and 100 kVp settings and decreased with increasing $CTDI_{vol}$ and slice width. Measurement precision increased with ENR and 95% limits of agreement for fECV results were established for different ENR values.

Conclusion

The absolute accuracy of fECV measurements using phantom simulated EQ-CT is robust to changes in acquisition and reconstruction parameters, with the exception of the use of dual energy iodine quantification mode. fECV measurement precision is increased when ENR is maximised. These findings should be useful for optimisation of clinical EQ-CT in the liver.

1. Introduction

Qualitative interpretation of computed tomography (CT) images plays an essential role in the diagnosis and management of patients in the modern healthcare environment. Quantitative analysis enables additional information to be extracted from images which can be used to refine clinical decision making.[1–3] Such information can be used to detect microscopic tissue changes that can occur prior to becoming macroscopically visible on imaging or to obtain quantitative information without the need for invasive clinical procedures.

Equilibrium CT (EQ-CT) is a quantitative CT technique that has been used to measure fractional extracellular volume (fECV), principally in the myocardium and liver.[4–7] fECV is a fundamental property of tissue which describes the fraction of that tissue occupied by interstitial fluid and blood plasma. The fECV is known to increase in the presence of fibrosis, and determining the extent and degree of fibrosis is a useful diagnostic and prognostic tool in the assessment and staging of many liver diseases.[8] It follows that a measurement of the fECV could act as an indicator of fibrotic burden. The current gold standard for evaluation of fibrosis in the liver is histologic assessment following tissue biopsy, however, this is an invasive and expensive technique which is poorly tolerated by patients and suffers from interobserver variability and significant sampling errors due to the small tissue volumes that can be analysed.[8,9] EQ-CT as a non-invasive quantitative imaging technique has the potential to overcome many of these difficulties.

EQ-CT in the liver is a simple procedure that involves imaging the liver before and after the administration of intravascular iodinated contrast.[7] Such contrast agents that are ubiquitously used in CT are exclusively extracellular and their volume of distribution can be used to measure fECV as described by Equation 1.

$$fECV = \frac{\Delta HU_{liver}}{\Delta HU_{blood}} \times (1 - heamatocrit)$$

Equation 1

Where fECV is the fractional extracellular volume and $\Delta HU = HU_{equilibrium\ phase} - HU_{pre\text{-}contrast}$ or measured Hounsfield unit (HU) enhancement between the equilibrium phase (with iodine contrast present) and pre-contrast phase (with no iodine contrast present) for a region of interest (ROI) drawn in the liver and blood respectively. ΔHU_{blood} is typically measured in the aorta. The haematocrit factor accounts for the volume of blood which is not plasma and therefore does not contain iodine contrast. It must be noted that Equation 1 is only valid when the concentration of iodine contrast is equal between the interstitial fluid and the blood plasma, known as the state of equilibrium, and is where the technique gets its name. This typically involves a time delay of 3 to 10 minutes between contrast administration and the

acquisition of the equilibrium phase, although there is no consensus on the optimal time delay for EQ-CT imaging.[6,10–12]

EQ-CT can be worked into existing routine clinical CT examinations, it is widely available, minimally invasive, quick, cheap, well tolerated by patients and can facilitate measurements at any position in the liver to account for fibrotic inhomogeneity.[5,6] fECV measurements with EQ-CT have been validated against biopsy in the liver by several authors[5,7,10–14] proving its potential as a diagnostic tool. However, the existing literature is exclusively clinically focussed with little evidence of any evaluation or optimisation of the technique from a technical viewpoint. For confident and widespread clinical adoption, it is vital to ensure that EQ-CT for fECV measurement is as accurate as possible, where accuracy is defined as the percentage error in the measurement result when compared to the true value (Equation 2) and precision is defined as the closeness of agreement between repeated measurements.[15]

$$Accuracy = \frac{Measured\ value - True\ value}{True\ Value} \times 100\%$$

Equation 2

Accuracy of the fECV calculation will be primarily dependent on the accuracy of HU measurements made to calculate iodine enhancement. An accurate fECV calculation therefore requires the measured enhancement to be a true representation of the additional attenuation provided by the presence of the iodinated contrast in equilibrium phase images. Conveniently, HU values scale linearly with iodine concentration which contributes to the simplicity of this technique.[16] This, however, is dependent on the imaging system operating above the limit of detection (LOD) and limit of quantification (LOQ) for the concentrations of iodine associated with clinical EQ-CT imaging.

The LOD is defined as the lowest concentration of iodine that can be detected and differentiated from a measurement of a sample with no iodine present (a ‘blank sample’). The LOQ is the lowest amount of iodine that can be not only detected, but measured and quantified to an acceptable level of precision.[17] By definition, the LOQ will always be equal to or higher than the LOD.[18] It is considered to be vital to establish the LOQ for iodine to ensure reliable HU measurements can be made to calculate the fECV. The LOD and LOQ for iodine is likely to be CT scanner make and model dependent.[19]

The accuracy and precision of individual fECV measurements will also be influenced by the statistical uncertainty in HU measurements, which will depend on image noise. Image noise in CT describes the variations in HU values between image voxels with the same underlying attenuation and is a combination of quantum and electronic noise. Quantum noise is an unavoidable consequence of photon-based imaging and is the dominant source of noise in CT images.[16] Image noise for a specified ROI is conventionally reported as the standard

deviation of measured HU values from each pixel within that ROI and, for a quantum limited system, this will be inversely proportional to the square root of the number of photons detected and used in image reconstruction (Equation 3). A lower image noise will result in less uncertainty in the mean HU value for a specified region of interest, and therefore reducing noise should improve fECV measurement accuracy. Reducing image noise can be achieved using acquisition exposure factors that result in more photons being detected, however, this will result in a higher radiation dose to the patient. Image noise will also be influenced by reconstruction techniques such as the selected reconstruction kernels or image slice width, although reductions in noise using this approach will typically be associated with a reduction in spatial resolution.

$$Image\ noise \propto \frac{1}{\sqrt{N}}$$

Equation 3

Where N is the number of photons detected and used in image reconstruction.

Uncertainty in HU measurements can be further reduced by maximising the difference in HU values between pre-contrast and equilibrium phase images, known here as iodine enhancement. These two factors can be combined into a proposed novel image quality metric: enhancement to noise ratio (ENR, Equation 4).

$$ENR = \frac{Iodine\ enhancement}{Image\ noise}$$

Equation 4

In order to maximise iodine enhancement without changing either the volume or strength of administered contrast material (a relative contra-indication in many patients)[20,21] or reducing the time delay between the two scan phases (and risk missing the true equilibrium phase), it is proposed the image acquisition parameters could be adjusted. Due to an increase in the cross-section of the photoelectric effect, attenuation of iodine increases as x-ray photon energies decrease.[16] Therefore, using an x-ray spectrum with a lower peak kilo-voltage (kVp) than the conventionally used 120 kVp will result in improved iodine signal in the equilibrium phase, increasing enhancement and therefore ENR and potentially fECV precision. However, a lower kVp risks the prevalence of image artefacts such as beam hardening and photon starvation which can adversely affect absolute HU value accuracy as well as image noise. Changing the kVp will also change the absolute HU value for the same concentration of iodine and underlying tissue.[16]

Relatively recent advances in CT technology have led to new opportunities in quantitative CT imaging and dual energy (DE) CT has become commercially available. DE scanning

entails acquiring attenuation data of the same volume with two different x-ray spectra, as opposed to conventional imaging, referred to here as single energy (SE) that uses a single, constant x-ray spectrum. DE CT and associated software is able to generate material density maps, where image pixels represent the concentration of user defined materials, commonly iodine.[22,23] This facilitates the measurement of iodine density in contrast enhanced images as an alternative to conventional HU, potentially avoiding interference from underlying, non-iodine based tissues and negating the need for a pre-contrast acquisition. The application of DE CT to the EQ-CT technique to measure fECV in the liver has been investigated by several authors, although again, there appears to be no study on the accuracy of the technique or consensus on the optimal acquisition or reconstruction settings.[12,24,25] As with SE CT, accuracy of fECV measurements will rely on the accuracy of the measured iodine densities. There are many examples in the literature of the validation of the accuracy of phantom based iodine density measurements in DE CT, however, there is a common finding that accuracy is CT scanner make and model specific.[23,26–28]

Locally available CT technology is dominated by the Canon Aquilion ONE (Canon Medical Systems, Ōtawara, Tochigi, Japan) DE enabled CT scanner. This features a wide 320 detector array, which when used in 'volume' mode can deliver 160 mm craniocaudal image coverage enabling entire organs to be imaged with one rotation. DE CT is achieved using two axial acquisitions in rapid succession at different kVp settings. Reconstruction software can generate iodine specific material maps which can be used to visualise and measure the distribution of iodine throughout the imaged volumes. The iodine maps displayed are HU maps, where each pixel represents the HU of materials identified as iodine. Unfortunately there is little evidence in the literature of the study of quantitative accuracy of iodine in DE mode with such scanner technology and therefore local validation is required.[29] Additionally, none of the studies identified above investigating the LOD or LOQ of iodine or EQ-CT to measure fECV in the liver utilised this scanner technology in either SE or DE modes.

The need to quantify the accuracy of fECV measurements in EQ-CT is an important step in the technique achieving widespread clinical confidence in the technique. There are potential opportunities to optimise EQ-CT with the aim of improving ENR with the aim of enhancing precision whilst keeping the radiation dose and resolution at acceptable levels and avoiding image artefacts. To the best of the author's knowledge, this has not been established in previously published studies.

The aims of this phantom study using a 320-detector array CT scanner in volume mode are threefold: 1) to establish the LOD and LOQ for iodine concentration for SE and DE modes to ensure they are low enough to enable fECV measurements with EQ-CT; 2) to ascertain which (if any) acquisition and reconstruction settings affect the accuracy of simulated fECV

measurements; 3) to investigate the effect of acquisition and reconstruction settings on the precision of fECV measurements and relate this to measured ENR values.

2. Materials and Methods

2A Phantom

A phantom study was performed using a CelT phantom (Medical Physics, Betsi Cadwaladr University Health Board, Wales, United Kingdom) and locally produced cylindrical iodine inserts with a diameter of 23 mm and length of 100 mm. Three inserts of 0.42, 0.88 and 1.14 mgI/mL were made using Omnipaque 350 mgI/mL intravenous solution (GE Healthcare, Chicago, IL, USA) mixed with water. These concentrations were chosen to be broadly representative of typical iodine concentrations found in a previously published EQ-CT study.[24] A fourth insert contained only water. The inserts were placed interchangeably into the 200 x 350 x 110 mm elliptical section of the phantom (Figure 1). Imaging was carried out with a DE enabled Canon Aquilion ONE CT scanner.

2B Image acquisition and reconstruction

Conventional SE mode images were acquired with all available kVp values (80, 100, 120 and 135 kVp) at set $CTDI_{vol}$ values of 5, 10 and 20 mGy to represent the range of doses expected during clinical imaging of the abdomen in the UK.[30] DE mode images were acquired with sequential acquisitions at 80 and 135 kVp and $CTDI_{vol}$ values that were as close as possible to those used for SE imaging: 5.3, 10.8 and 21.6 mGy. All images were acquired in volume mode: 320 x 0.5 mm collimation and 'M' field of view. Images were reconstructed with the coneXact reconstruction algorithm using the FC18 (SE) and FC17 (DE) filters with SureIQ enabled. 8 repeat acquisitions were performed for every kVp and $CTDI_{vol}$ combination in both SE and DE modes. 1, 2, 5 and 10 mm slice widths were reconstructed with no overlap between slices. Iodine density images were generated from the DE data sets using the manufacturer recommended default parameters (material formula object 1: -136 and -106 and object 2: 67 and 63; slope of contrast media: 0.55) for the same set of slice widths and slice locations as the SE data.

Reconstructed images were downloaded from the scanner and analysed using open-source software (OsiriX Lite v11.0.4; OsiriX Foundation, Geneva, Switzerland). A 1 cm^2 circular region of interest was drawn within the iodine inserts and the mean HU and associated standard deviation were extracted from every image. This led to a data set consisting of HU values and standard deviations for every insert for all permutations of acquisition (kVp, to include all SE kVp settings and DE mode, $CTDI_{vol}$) and reconstruction (slice width, slice location) parameters. Images slices from 10 mm sections at either end of the phantom were excluded from further analysis to avoid any partial volume effects associated with the edge of the phantom.

2C Limit of Detection and Limit of Quantification

The LOD was established in line with the method presented by the Clinical and Laboratory Standards Institute (CLSI).[17] The LOD in terms of HU, LOD_{HU}, was calculated for a specific combination of kVp (or DE mode), $CTDI_{vol}$ and slice width using Equation 5.[17]

$$LOD_{HU} = \mu_B + 1.645\sigma_B + 1.645\sigma_S$$

Equation 5

Where μ_B is the mean HU from repeat measurements of the insert containing only water (the 'blank sample') and σ_B and σ_S are the standard deviations of repeat HU measurements of the blank sample and low-level samples (in this case the 0.42 and 0.86 mgI/ml inserts) respectively. This assumes a Gaussian distribution of data, which was verified with a visual assessment of the histogram of HU measurement results and a quantile-quantile (Q-Q) plot. In line with CLSI guidelines, measurements from 60 different slices were used to calculate the mean and standard deviations for both the blank sample and the low-level samples to establish the LOD_{HU}.

In order to convert the LOD_{HU} into an LOD in terms of iodine concentration (LOD_{iodine}) knowledge of the system calibration curve between HU value and known iodine concentration was required. This is known to depend on kVp and the mean HU value at each iodine concentration for all SE kVp values and DE mode was plotted against known iodine concentration. A least squares fit regression was performed to establish the slope, y-intercept and Pearson correlation coefficient of the calibration curves.

The LOD_{HU} was converted into LOD_{iodine} using Equation 6.[19]

$$LOD_{iodine} = \frac{LOD_{HU} - y\text{-}intercept}{gradient}$$

Equation 6

Where the y-intercept and gradient are the values corresponding to the calibration curve for the kVp setting (or DE mode) used to establish the LOD_{HU}.

The LOQ is defined as the lowest iodine concentration that can be measured to an acceptable level of precision.[18] In this study, acceptable precision for iodine quantification was defined as a coefficient of variation (CV) of 20% or lower for repeat measurements of the same insert, in line with published guidance and previous studies of this type.[18,19] Therefore, to establish the LOQ for a particular permutation of acquisition/reconstruction parameters, the CV from the 60 repeat HU measurements of each iodine insert was calculated. The relationship between CV and iodine concentration was then established

using a logarithmic trendline, which best represented the data. That relationship was used to extrapolate the data to obtain the iodine concentration that corresponded to a CV of 20%. This iodine concentration was compared to the LOD_{iodine} calculated previously: if it was higher than LOD_{iodine}, it was used as the LOQ; however, where it was lower than the LOD_{iodine}, the LOD_{iodine} was used as the LOQ.[18]

This process was repeated to establish the LOD_{iodine} and LOQ for all possible combinations of kVp (or DE mode), $CTDI_{vol}$ and slice width. Any combination of kVp, $CTDI_{vol}$ and slice width that resulted in a LOQ lower than the lowest concentration of iodine insert used were excluded from further data analysis.

2D fECV measurements

fECV measurements were simulated using the HU values obtained from the phantom inserts. Two of the possible four inserts were selected: the lower concentration insert of the two was assigned as the pre-contrast insert and the higher concentration insert was assigned as the equilibrium phase insert. The measured HU values of the pre-contrast insert was subtracted from the equilibrium phase insert resulting in a simulated enhancement value. This process was repeated using a different combination of two of the possible four phantom inserts. This resulted in two different enhancement values which were designated as simulated ‘liver’ and ‘blood’ enhancement values respectively. Note all HU values were taken from images with the same combination of acquisition/reconstruction parameters (kVp or DE mode, $CTDI_{vol}$, slice width and slice location) and as the iodine content of the insert containing only water was known to be zero the signal from the corresponding DE iodine density images was also set as zero.

The simulated enhancement values were inserted into Equation 1, with an arbitrary haematocrit value of 0.5, to calculate a measured fECV ($fECV_m$) for that particular combination of phantom inserts and acquisition/reconstruction parameters. The measurement was repeated for five slice locations, where the centre of each slice was the same for all slice thicknesses, the slice locations were 10 mm apart to ensure no overlap between the 10 mm slices and the central slice was located at the centre of the phantom in the craniocaudal direction, resulting in five $fECV_m$ results for that combination of kVp (or DE mode), $CTDI_{vol}$ and slice width.

The above process was repeated for the same combination of phantom inserts at the same five slice positions for every permutation of kVp (or DE mode), $CTDI_{vol}$ and slice width settings.

As the iodine concentration of each insert was known, the calculation was repeated with the iodine concentration substituted for the HU value measurements in Equation 1. This resulted

in a 'true' fECV ($fECV_t$) to which the $fECV_m$ could be compared. Note, as every measurement described above was made with the same combination of phantom inserts, this resulted in the same $fECV_t$ for every $fECV_m$ up to this point. The error, in terms of percentage difference between every $fECV_m$ and the $fECV_t$, was calculated using Equation 7 as a measure of accuracy of each measurement.

$$Error = \frac{fECV_m - fECV_t}{fECV_t} \times 100\%$$

Equation 7

Finally, a mean of the five repeat $fECV_m$ measurements for every kVp (or DE mode), $CTDI_{vol}$ and slice width combination was taken and designated as $fECV_{avg}$. The error between $fECV_{avg}$ and the corresponding $fECV_t$ was calculated using Equation 7 where $fECV_t$ was substituted for $fECV_{avg}$ and the result designated as $Error_{avg}$.

Assigning the phantom inserts as the pre-contrast and equilibrium phases for the liver and blood in different combinations, it was possible to generate a range of new $fECV_m$ results with associated new $fECV_t$ values. This process was repeated for all insert combinations. Any combination that resulted in a negative enhancement value or an $fECV_t$ greater than one were excluded due to not being clinically feasible, and a subset of six $fECV_t$ values were selected which represented an even distribution across the range of previously reported clinical hepatic fECV results.[6]

The average noise associated with each $fECV_m$ was determined using the standard deviations from every ROI used in the measurement, summed in quadrature. The mean of the 'liver' and 'blood' iodine enhancement for each $fECV_m$ was calculated and used as a single enhancement value. The ENR was calculated for every $fECV_m$ using Equation 2. ENR and associated error results were binned into groups of unit increments in ENR value.

2E Statistical analysis

All statistical analysis was performed in R version 4.0.1 (R Foundation for Statistical Computing, Vienna, Austria). Following a visual evaluation of the error data using histograms and Q-Q plots to assess for normality, non-parametric descriptive statistics and statistical tests were selected where appropriate. A *p*-value of less than 0.05 was used to test for significance.

In order to establish which, if any, of the factors had a significant effect on the calculated error associated with each $fECV_m$ result, a multiple linear regression model was constructed. The dependent variable was the calculated error and the independent variables were acquisition kVp (including DE mode), $CTDI_{vol}$, slice width, slice location and $fECV_t$ (note the

$CTDI_{vol}$ values for the DE data were rounded to match those of the SE data for the purposes of the model). All independent variables, with the exception of $fECV_t$, were treated as categorical data as they represent discrete acquisition/reconstruction settings. $fECV_t$ was treated as a continuous variable as the values defined by the experimental design were only a sample of all possible values.

The median error, interquartile range (IQR) and range (minimum and maximum) of error results was established separately for each acquisition/reconstruction setting using all available $fECV_m$ results for that setting, as well as for all $fECV_{avg}$ results combined (using $Error_{avg}$). The IQR of each set of results was used as a simple measure of measurement precision. The Brown-Forsythe test for equality of variance was used to establish if the difference in spread of error data between acquisition/reconstruction parameters was significant. The test was applied in the form of pairwise comparisons between all settings of each of the acquisition and reconstruction parameters tested. The results of the Brown-Forsythe test were used in combination with the IQR data to infer which settings of which parameters demonstrated the smallest spread of error data and therefore the highest level of precision.

Furthermore, a simple non-parametric approach to obtaining limits of agreement between $fECV_m$, $fECV_{avg}$ and $fECV_t$ values, broken down by categorical ENR bin, was used.[31] The 95% limits of agreement were taken as the 2.5 and 97.5 percentiles of the error results.

Figure 1 *A photo with the section of the CeIT phantom used, with locally produced iodine inserts*

3. Results

All phantom images were successfully acquired, reconstructed and exported for analysis. Some example phantom images are shown in Figure 2.

3A LOD/LOQ

The system calibration curves are shown in Figure 3, demonstrating a linear response between HU value and iodine concentration for all kVp settings ($r > 0.999$, $p < 0.001$) and DE mode ($r = 0.989$, $p < 0.001$).

The calculated LOD_{iodine} and LOQ for all combinations of acquisition/reconstruction parameters tested are shown in Table 1. The LOD_{iodine}, and therefore also the LOQ, was higher than 0.42 mgI/mL (the lowest concentration insert available) for 1, 2 and 5 mm slice widths at the lowest $CTDI_{vol}$ setting tested in DE mode (5.3 mGy). Additionally, the LOQ was higher than 0.42 mgI/mL for the 1 mm slice width for 80 and 135 kVp at a $CTDI_{vol}$ of 5 mGy and in DE mode at a $CTDI_{vol}$ of 10.8 mGy. 1 mm slices across all kVp settings and DE mode and all slice widths at the lowest $CTDI_{vol}$ setting in DE mode were therefore excluded from subsequent analysis.

3B fECV calculation

$fECV_t$ values of 0.11, 0.18, 0.24, 0.32, 0.41 and 0.65 were used. These are clinically representative of the values previously reported in the literature for both healthy individuals and those in diseased states.[6,10]

The results from the multiple linear regression model are shown in Table 2. They demonstrate that the only variable that had a significant effect on the calculated error was the use of the DE mode when compared to SE mode when the other independent variables are accounted for ($p < 0.001$). None of the other acquisition or reconstruction parameters, nor $fECV_t$, had a significant effect on the overall calculated error ($p > 0.05$).

The median error, interquartile range and minimum and maximum error results are presented in Table 3 and as a series of boxplots in Figure 4. The overall median error when all $fECV_m$ error results were grouped together was 0.1% (IQR 9.1%). The Brown-Forsythe test, as applied to $fECV_m$ error results for all pairwise comparisons of kVp and DE mode, demonstrated a significant difference in variance between all combinations ($p < 0.05$), with the exception of 80 vs.100 kVp ($p = 0.61$) and 120 vs.135 kVp ($p = 0.35$): the variance was largest for the DE setting and smallest for 80 and 100 kVp settings (Table 4). The differences in variance were significant between all of the $CTDI_{vol}$ and slice width settings ($p < 0.001$); variance decreased with increasing $CTDI_{vol}$ and increasing slice width. There was no significant difference in variance between any of the slice location results ($p > 0.05$

for all pairwise comparisons). The variance of error results was significantly larger for $fECV_m$ compared to $fECV_{avg}$ ($p < 0.001$).

3C ENR and Limits of agreement

Figure 5 demonstrates how error results are dependent on image noise, iodine enhancement and ENR for $fECV_m$ results, and separately for ENR and $fECV_{avg}$ results, when all acquisition and reconstruction parameters are grouped together. Calculated 95% limits of agreement for $fECV_m$ and $fECV_{avg}$ error values, binned by ENR value for all SE data and separately for DE iodine density mode data, are shown in Table 5. The limits of agreement decrease as the ENR bin increases: for SE measurements where ENR ≤ 1, 95% of all $fECV_m$ measurements lie within the accuracy range of -37% to 38%. This decreases to a range of -4% to 8% for 4 < ENR < 5.

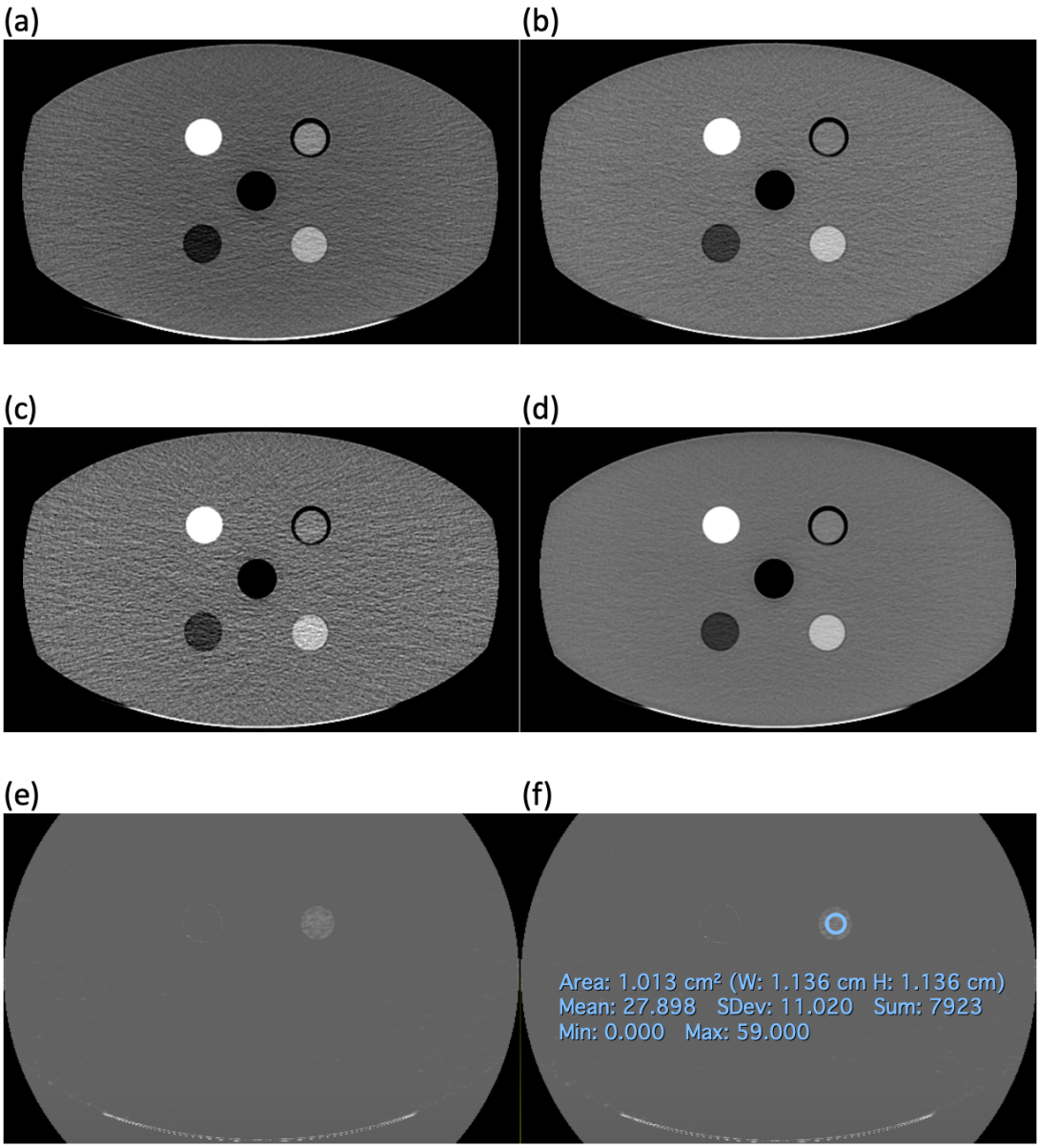

Figure 2 *Images showing the CeIT phantom with the 1.14 mgI/mL insert in the top right insert position as viewed (all other inserts are fixed), varying acquisition/reconstruction settings: (a) 80 kVp, $CTDI_{vol}$ = 10 mGy, slice width = 5 mm; (b) 135 kVp, $CTDI_{vol}$ = 10 mGy, slice width = 5 mm; (c) 120 kVp, $CTDI_{vol}$ = 5 mGy, slice width = 2 mm; (d) 120 kVp, $CTDI_{vol}$ = 20 mGy, slice width = 10 mm; (e) DE iodine map, $CTDI_{vol}$ = 10.8 mGy, slice width = 5 mm; (f) demonstration of region of interest size and placement. Default abdomen window level/width set at 40/350 for all images.*

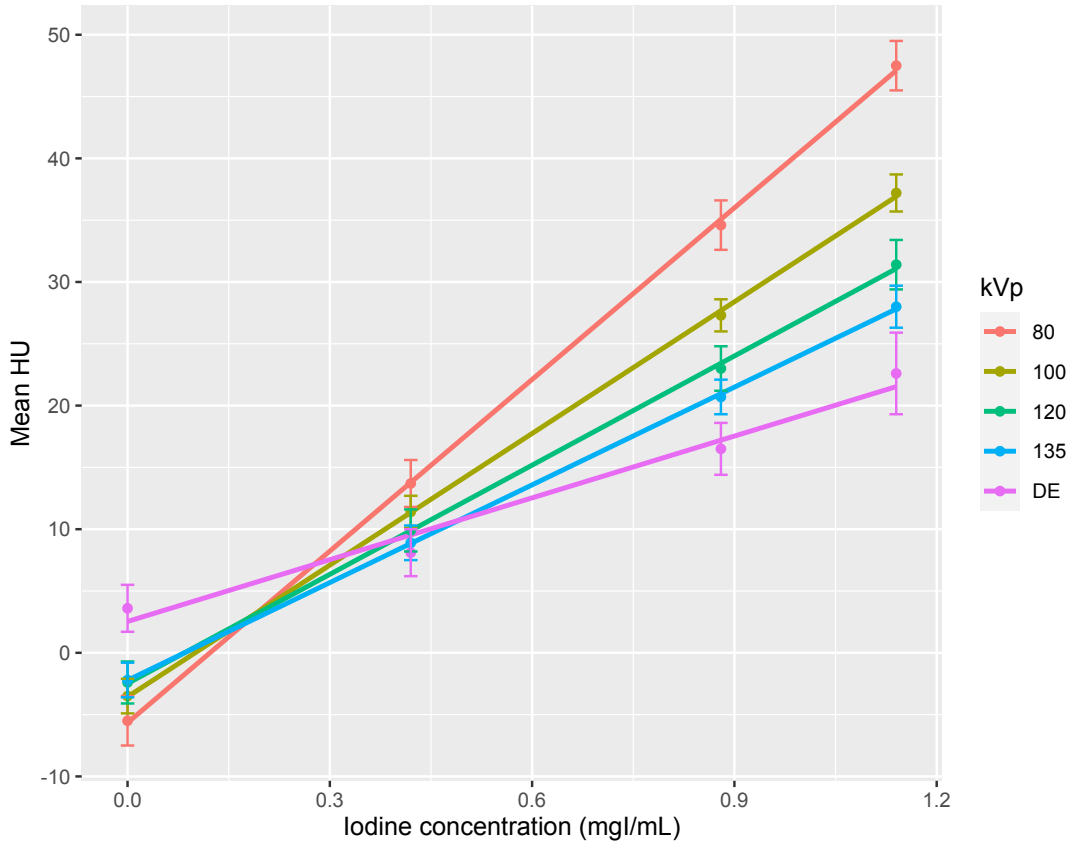

Figure 3 *System calibration curves of mean Hounsfield Unit (HU) versus concentration of iodine for all available SE kVp values and DE iodine quantification mode. Error bars represent one standard deviation from the plotted mean value.*

kVp	$CTDI_{vol}$ (mGy)	Limit of detection (LOD_{iodine}, mgI/mL)				Limit of quantification (LOQ, mgI/mL)			
		Slice width (mm)				Slice width (mm)			
		1	2	5	10	1	2	5	10
80	5	0.27	0.19	0.15	0.12	0.47	0.20	0.15	0.12
	10	0.14	0.08	0.06	0.04	0.16	0.11	0.06	0.05
	20	0.14	0.11	0.06	0.04	0.26	0.11	0.07	0.04
100	5	0.26	0.18	0.13	0.11	0.37	0.19	0.15	0.11
	10	0.17	0.10	0.06	0.04	0.20	0.10	0.06	0.05
	20	0.12	0.07	0.04	0.02	0.13	0.07	0.04	0.02
120	5	0.33	0.21	0.17	0.14	0.34	0.22	0.17	0.15
	10	0.17	0.11	0.07	0.05	0.19	0.15	0.07	0.05
	20	0.10	0.05	0.02	0.01	0.21	0.10	0.03	0.01
135	5	0.35	0.24	0.17	0.13	0.55	0.33	0.17	0.13
	10	0.20	0.13	0.07	0.04	0.31	0.13	0.07	0.05
	20	0.12	0.07	0.04	0.02	0.20	0.08	0.04	0.02
DE	5	0.64	0.54	0.46	0.40	0.65	0.55	0.46	0.41
	10	0.31	0.28	0.22	0.19	0.46	0.28	0.22	0.19
	20	0.22	0.20	0.15	0.13	0.31	0.20	0.15	0.13

Table 1 *LOD_{iodine} and LOQ for all acquisition/reconstruction parameters investigated (kVp including dual energy (DE) mode, $CTDI_{vol}$ and slice width). Values in red represent instances where the LOD_{iodine} or LOQ is higher than the lowest concentration insert used in this investigation (0.42 mgI/mL).*

Model parameter	Model base value	Categorical values for comparison to base value	Coefficient estimate	95% confidence intervals for coefficient estimate		*p*-value
				Lower limit	Upper limit	
kVp	80	100	0.015	-0.004	0.034	0.13
		120	0.007	-0.012	0.026	0.46
		135	0.011	-0.008	0.031	0.24
		DE	0.038	0.016	0.059	< 0.001*
$CTDI_{vol}$ (mGy)	5	10	0.010	-0.007	0.026	0.25
		20	-0.002	-0.018	0.014	0.81
Slice thickness (mm)	2	5	-0.004	-0.019	0.011	0.62
		10	-0.004	-0.019	0.011	0.62
Slice position	1	2	0.001	-0.018	0.021	0.89
		3	-0.001	-0.021	0.019	0.94
		4	-0.002	-0.021	0.018	0.87
		5	-0.003	-0.023	0.017	0.75
$fECV_t$	-	-	0.031	-0.005	0.066	0.09

Table 2 *Results of the multiple linear regression model where the model outcome variable is error of $fECV_m$. The lowest value for each parameter is used as the base value to which all other settings for that parameter are compared; DE = dual energy mode; * factors that are statistically significant ($p < 0.05$).*

Parameter	Parameter value	Error (%)				Median ENR
		Median	IQR	Minimum	Maximum	
kVp	80	-0.5	7.5	-38.6	18.5	2.24
	100	0.8	7.3	-30.8	27.4	1.94
	120	-1.0	8.5	-59.9	43.7	1.64
	135	0.1	8.7	-40.6	55.4	1.44
	DE	3.3	32.3	-37.2	78.0	1.73
$CTDI_{vol}$ (mGy)	5	-0.9	11.2	-59.9	55.4	1.24
	10	0.0	10.2	-37.2	78.0	1.72
	20	0.9	7.2	-29.0	53.8	2.48
Slice width (mm)	2	-0.4	13.2	-59.9	78.0	1.21
	5	0.1	8.9	-37.2	65.2	1.80
	10	0.2	6.7	-28.1	48.0	2.47
Relative slice location	1	-0.4	9.2	-37.2	78.0	1.78
	2	-0.4	9.1	-40.6	55.4	1.75
	3	-0.5	8.5	-29.3	60.6	1.76
	4	1.0	9.7	-38.6	43.7	1.77
	5	0.9	9.2	-59.9	37.1	1.77
$fECV_m$ vs $fECV_{avg}$	$fECV_m$	0.1	9.1	-59.9	78.0	1.76
	$fECV_{avg}$	0.1	4.2	-21.4	41.0	1.75

Table 3 *Median, IQR (interquartile range) and range (minimum and maximum) of error results using all available $fECV_m$ results with associated median enhancement to noise ratio (ENR) relating to the parameter value stated, with the exception $fECV_m$ vs $fECV_{avg}$ where results for all acquisition/reconstruction parameters are grouped together.*

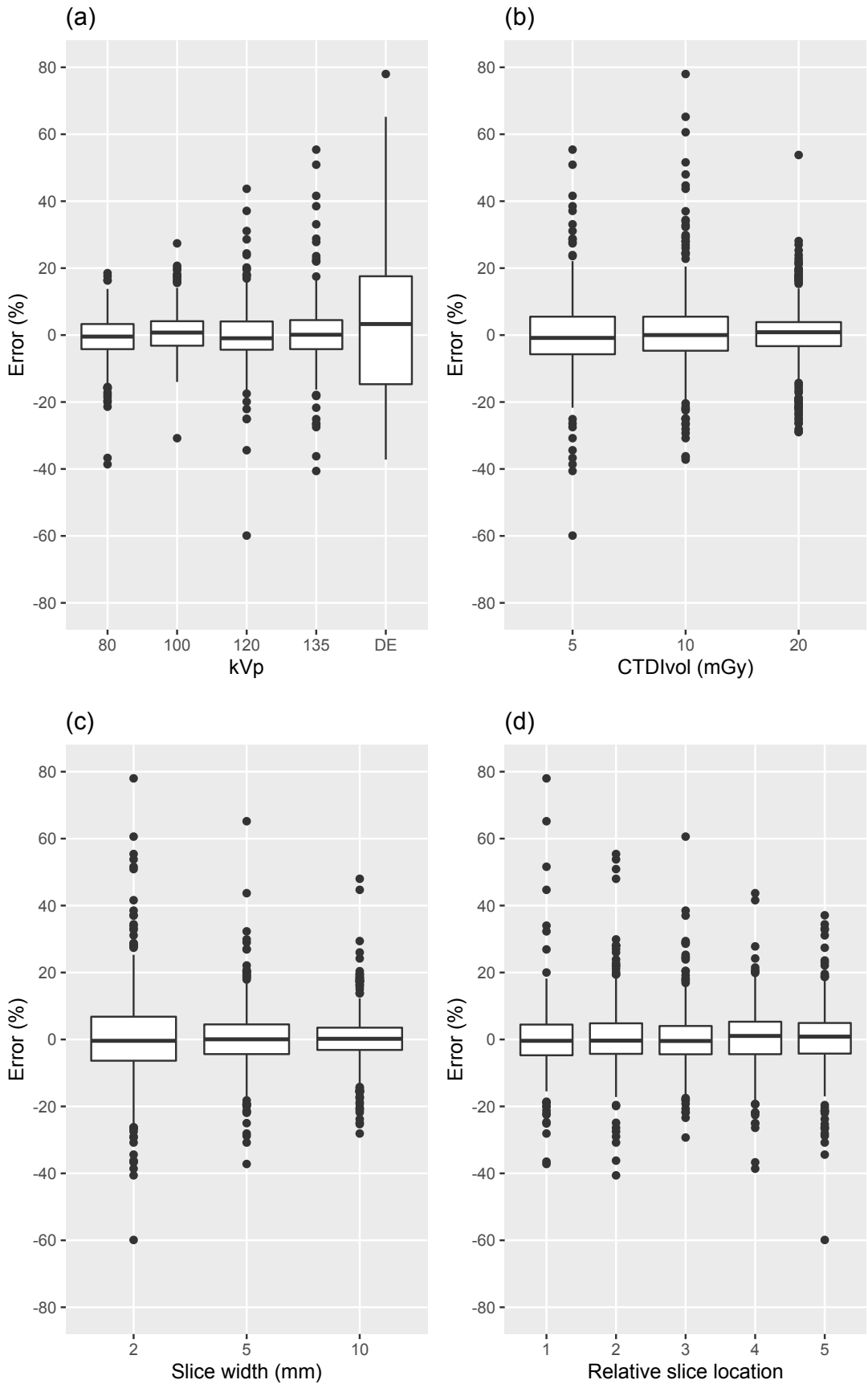

Continued overleaf

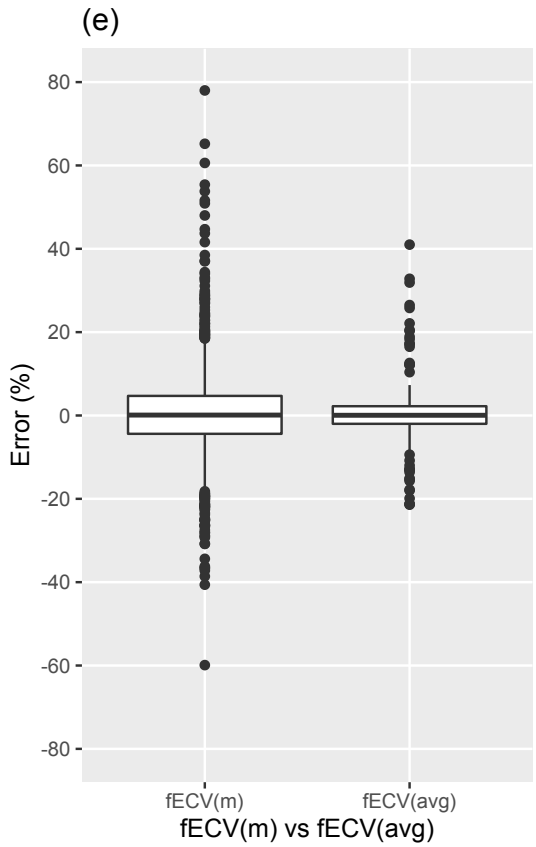

Figure 4 *Boxplots of error results for categorical acquisition/reconstruction parameters tested: (a) kVp, (b) $CTDI_{vol}$, (c) slice width, (d) relative slice position and (e) $fECV_m$ vs $fECV_{avg}$. Data for (a) to (d) represents $fECV_m$ error results. The central line represents the data median, the lower and upper limits of the box represent the interquartile range (IQR), the lines extend from the 25th percentile minus 1.5 times the IQR to the 75th percentile plus 1.5 times the IQR and the points represent outliers from this range.*

kVp	80	100	120	135	DE mode
80	-	0.61	0.01*	< 0.001*	< 0.001*
100	-	-	0.002*	< 0.001*	< 0.001*
120	-	-	-	0.35	< 0.001*
135	-	-	-	-	< 0.001*
DE mode					-

Table 4 *p-values resulting from the Brown-Forsythe test for equality of variance between all possible combinations of kVp setting (including DE mode) for all $fECV_m$ error data. * kVp pairs that demonstrate statistically different variance ($p < 0.05$).*

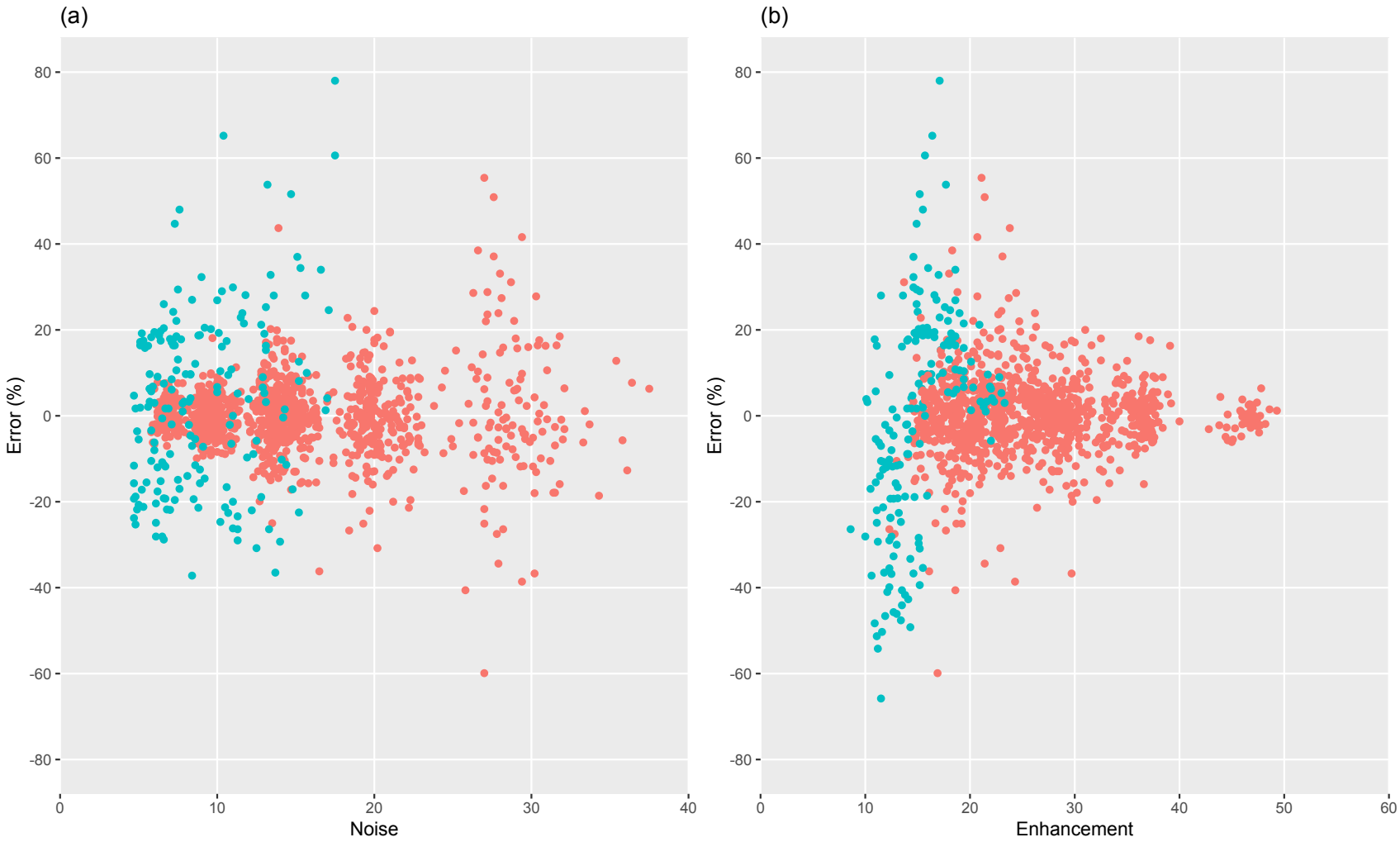

Figure 5 *[continued overleaf]*

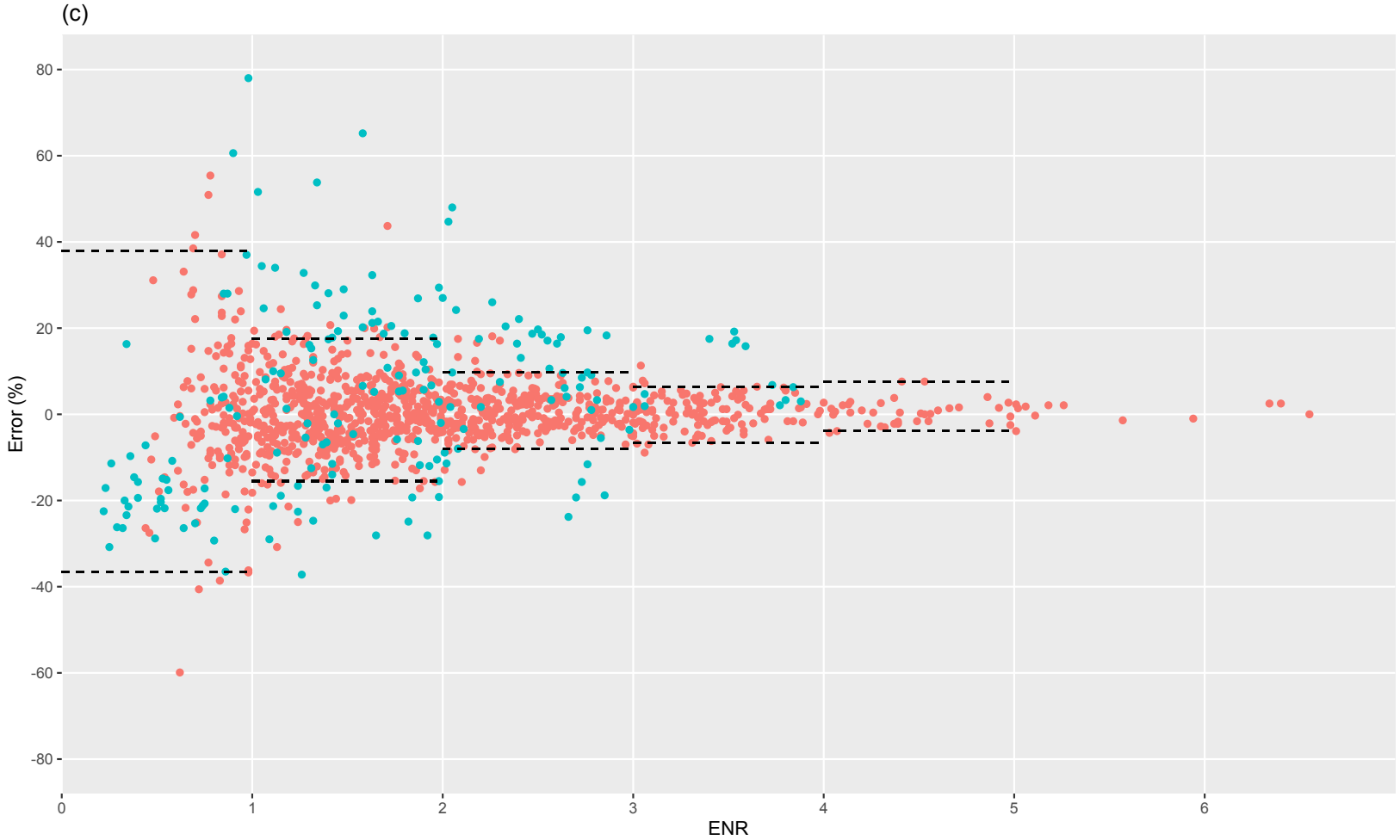

Figure 5 *[continued overleaf]*

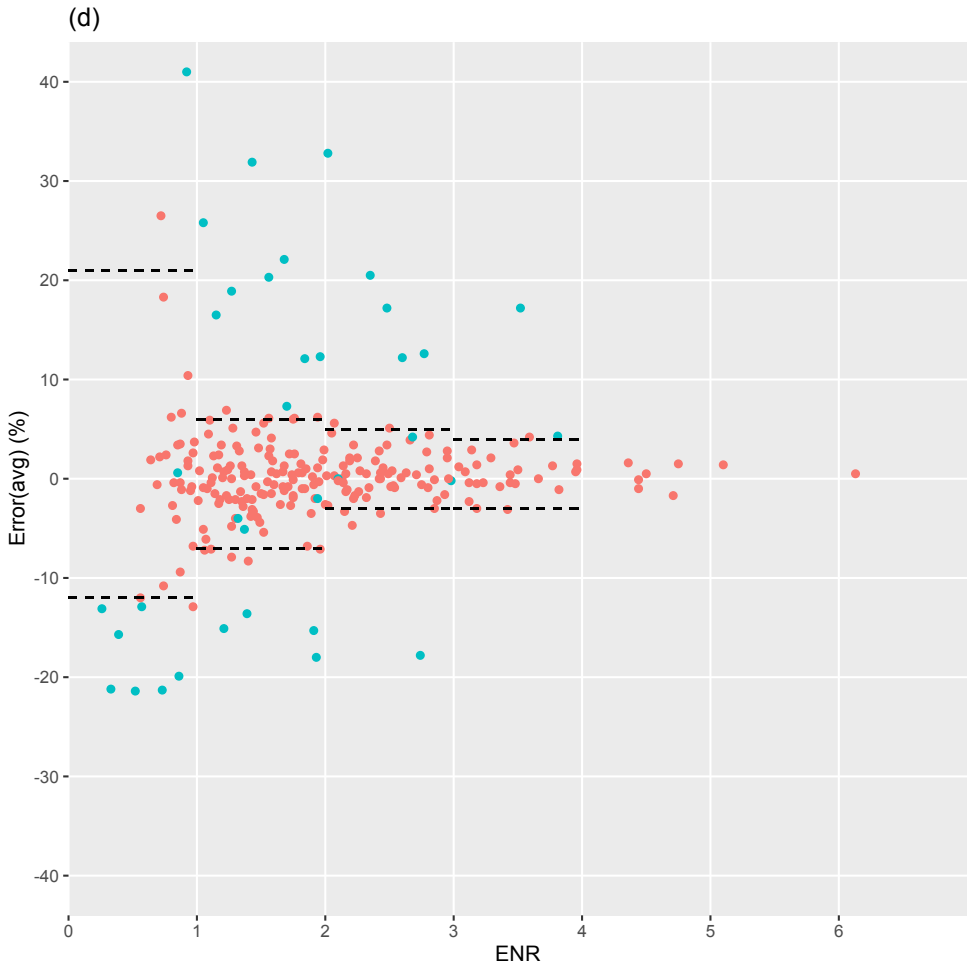

Figure 5 *Error versus (a) noise, (b) enhancement, (c) ENR for all $fECV_m$ results and (d) $Error_{avg}$ versus ENR for all $fECV_{avg}$ results; Red = SE error results, aqua = DE error results; dashed lines on (c) and (d) represent the 95% limits of agreement for $fECV_m$ and $fECV_{avg}$ error results respectively for SE only data.*

Data type	95% limits of agreement for error		All ENR bins	ENR bin				
				0-0.9	1-1.9	2-2.9	3-3.9	4-4.9
SE only	**$fECV_m$**	**Lower limit (%)**	-16	-37	-15	-8	-7	-4
		Upper limit (%)	18	38	18	10	6	8
	$fECV_{avg}$	**Lower limit (%)**	-8	-12	-7	-3	-3	-
		Upper limit (%)	6	21	6	5	4	-
DE only	**$fECV_m$**	**Lower limit (%)**	-29	-31	-28	-19	-	-
		Upper limit (%)	50	58	52	43	-	-
	$fECV_{avg}$	**Lower limit (%)**	-21	-21	-17	-	-	-
		Upper limit (%)	34	33	30	-	-	-

Table 5 *95% limits of agreement for $fECV_m$ and $fECV_{avg}$ error results for all ENR bins, broken down into SE only and DE only data; '-' indicates less than 10 data points.*

4. Discussion

This phantom study has been designed to replicate fECV measurements using an EQ-CT technique in the liver. The system calibration curves demonstrate a linear relationship between iodine concentration and HU signal for all SE and DE modes. For SE, higher signals are generated when lower kVp settings are used due to the increased attenuation as a result of the increased cross section of the photoelectric effect at lower photon energies. The DE iodine density mode resulted in a lower signal at all iodine concentrations when compared to all SE kVp settings.

The LOD_{iodine} and LOQ results demonstrate relatively low concentrations of iodine are able to be detected and quantified in both SE and DE modes with the CT technology used. Although it is recognised there will be some error associated with the described extrapolation of CV data, these results are consistent with the findings of a similar study of three other DE CT systems based on different technologies to the one used here.[19] However, markedly lower radiation doses have been used here to represent typical clinical doses and it is encouraging to see that the LOQ has been maintained. The results show improved limits of detection were seen with low kVp and high $CTDI_{vol}$ and slice width settings. This can be attributed to the higher iodine signal at lower kVp combined with reduced noise with increasing $CTDI_{vol}$ and slice width. The removal of 1 mm slice widths and the low dose setting in DE mode from this phantom study was an important outcome which could be directly applied to the clinical implementation of this fECV measurement technique to ensure accuracy. The only drawback of using slices thicker than 1 mm would be the potential introduction of partial volume effects. However, this would only become problematic in ROIs close to organ boundaries, which the EQ-CT measurement technique could easily avoid by careful ROI positioning, although it is recognised this may be more difficult in the aorta. The fact that a higher radiation dose is required to maintain the LOQ in DE mode when compared to SE is also information that would be useful for clinical implementation of the EQ-CT technique, or indeed any other technique that requires quantification of low concentrations of iodine contrast.

The multiple linear regression model demonstrated that, of all the acquisition and reconstruction parameters tested, the only factor that significantly affected the error associated with each fECV measurement was the use of DE mode over SE mode ($p > 0.001$). Table 3 shows that the median error of DE $fECV_m$ measurements was 3.3% with all other kVp values tested within ± 1%. This could potentially indicate a systematic bias in iodine HU measurements using DE mode for one or more of the inserts which was not seen in SE mode. In the context of the range of error results seen across all settings tested, this difference in median error is low, however the significance of a difference of this magnitude would require consideration and justification from the clinical team.

Aside from DE mode, absolute error was not affected by the kVp value used in SE mode, dose, slice width, slice location or $fECV_t$. As the fECV calculation is based on the relationship between HU value and iodine concentration, the linear relationship demonstrated between these two variables for a constant kVp, and the fact that dose and slice width typically should not affect absolute mean HU values provide a rational explanation for this result.[27–29] Slice location also did not affect error results. Again, HU values shouldn't be dependent on slice location therefore this is an expected and reassuring result. An important caveat from these findings is that the same kVp must be used for the pre-contrast and equilibrium phase imaging to ensure a consistent calibration curve is applied. This was not the case in some of the existing literature.[6] The result in this study showing that the error is independent of the underlying fECV value provides important evidence that the accuracy of the technique is robust to changes in clinical condition.

When considering the precision of the fECV measurements the data shows that the spread of error results in DE mode was significantly higher than any SE kVp setting ($p > 0.001$). For DE mode, the IQR of error results is almost four times that of 135 kVp, which is the SE kVp setting with the largest IQR. The large errors for DE iodine density based fECV calculations could be attributed to the lower signal generated in DE mode as demonstrated by the system calibration curves resulting in lower contrast. Conversely, the noise measured in DE images was lower than SE images for broadly equivalent dose levels (Figure 5(a)), potentially explained by the additional processing that is likely to include some noise suppression in the production of the iodine density maps.[32] The reduced contrast and reduced noise somewhat cancel each other out, resulting in broadly similar ENR values between SE and DE data (Figure 5(c)). This is in contrast to findings from a previous study which demonstrated superior ENR with SE, however, this was with different scanner technology and iodine map reconstruction algorithms.[33]

The decrease in precision could also be a result of the nature of the data available with iodine density maps. To calculate fECV with SE data, a subtraction technique is applied where the underlying signal from the pre-contrast scan is subtracted from the equilibrium phase. For this phantom study, this means the underlying measured HU from the insert containing only water was subtracted from iodine containing inserts before being used in the calculation. This normalises any non-zero signal from background attenuation in the enhancement measurement. However, this is not possible with iodine density maps which only display what the system has identified as iodine: any signal that is less than the LOQ (identified in this case as 0.42 mgI/mL) cannot be accurately quantified and is assumed to be zero. If the signal from the 'pre-contrast' phase is less than the LOQ this then doesn't allow for any subtraction of underlying iodine signal (weather real or not) and therefore systematic or random errors in iodine quantification will not be identified. This introduces the potential for greater errors in the final fECV calculation and in this study have manifested as

a larger variance in fECV accuracy results for DE images. This issue was identified in a study of clinical hepatic fECV measurements, although no attempt was made to ascertain the LOQ of iodine to take into account the accuracy of iodine quantification in pre-contrast scans.[12] Other publications have taken a similar approach to the one taken here and assumed iodine concentration to be zero in pre contras scans.[24,34] This has the additional advantage of potentially avoiding the need for the pre-contrast acquisition which could result in a halving of the radiation dose to the patient and would avoid any issues with patient motion between pre-contrast and equilibrium phase imaging. As the equilibrium time delay is up to ten minutes, patient motion could be a significant source of error.

However, based on this phantom study, the variance in accuracy associated with DE mode fECV calculations is statistically larger than SE modes and therefore SE appears to be a superior technique in terms of precision.

When considering the SE data, fECV measurement showed the smallest IQR for the 80 and 100 kVp acquisition settings. This could represent the optimal kVp selection based on improved iodine signal and associated image contrast when compared to 120 and 135 kVp, although care would be needed to avoid potential beam hardening or photon starvation artefacts that could be related to the use of a relatively low energy spectrum such as 80 kVp. Precision increased with $CTDI_{vol}$ and slice width as an increase in both these factors are associated with a decrease in noise. This presents the clinical dilemma of balancing the need of accuracy with the radiation dose to the patient which requires justification on an individual patient basis.[35] Increased radiological contrast, leading to increased enhancement, and reduced noise combine to improve ENR which, as demonstrated by Figure 5(c), has a stronger influence on technique precision that either factor in isolation.

Using ENR as a potential indicator of accuracy could be a useful tool when quoting clinical fECV results however, no previous authors have attempted to do this. From the results of this phantom study, it is suggested 95% limits of agreement based on measured ENR value could be used to define the accuracy of the fECV measurement. ENR is considered to be a convenient metric as it doesn't rely on prescribed acquisition or reconstruction settings, allowing the scan protocol to be manipulated and optimised by the user without losing the ability to calculate an associated error.

As an example of how the data presented here could be used to calculate an error associated with an fECV measurement consider a hypothetical fECV measurement of 0.27, acquired with and SE mode and an associated ENR of 2.5. Table 5 gives a 95% confidence interval of -8% to 10% for this level of ENR. Averaging this to give a confidence interval of ±9%, the clinician could be 95% confident that the true result laid between 0.25 and 0.29. Using confidence intervals based on a percentage of the fECV result will result in wider

confidence intervals for larger fECV values, however, due to the nature of the technique, as the fECV increases measured liver enhancement increases. Assuming enhancement in the blood remains the same (a valid assumption unless there is a significant change in technique or an expansion of the volume in which the iodine contrast agent is diluted) this will result in an increased ENR. The two effects therefore conveniently counteract each other. The confidence intervals have been shown to be smaller when the average of five readings are used to generate the final fECV result ($fECV_{avg}$ with associated $Error_{avg}$). This improvement comes at the cost of a five-fold increase in analysis time. The practicality of this in the clinical environment would need consideration. Additionally, this approach would only be clinically sound for a homogenous liver which may not be a valid assumption when considering patients with extensive disease.

One additional factor that could influence the accuracy of clinical fECV results that has not been considered up until now is the accuracy of the haematocrit measurement which is critical for the fECV calculation. The reported accuracy and precision of haematocrit measurements are 1.8% and 1.2% respectively,[36] which are larger than the errors presented here, particularly for lower ENR values. The error associated with haematocit measurement will therefore only make up a small portion of the overall error in clinical fECV measurement.

It must be recognised that there are several limitations associated with this study. This is a phantom based study, so results cannot necessarily be applied directly to the clinical setting. Only one size of phantom was used that was relatively homogeneous in composition. Previous studies have reported differences in HU accuracy measurements in different sized phantoms and that body weight affected fECV measurements.[12,37] Additionally, highly attenuating structures in the body (vertebral bodies) have been shown to cause beam hardening artefacts in adjacent (aortic) ROIs in clinical studies of fECV measurement.[5,10,25] Future phantom studies consisting of different phantom sizes with anthropomorphic characteristics could be considered to address these issues.

The errors associated with the concentrations of iodine in the locally made phantom inserts have not been quantified. This could result in a systematic error in fECV accuracy results, however the linear system calibration curves and the lack of a consistent bias in SE accuracy results demonstrate this source of error to be small in the context of the overall results. Additionally, the inserts used to simulate clinical concentrations of iodine were an exclusive mix of iodine contrast with water, whereas in a patient contrast will be diluted in various body fluids. The accuracy of DE iodine density measurements in a range of simulated body fluids when compared to water has been previously validated, however this was performed only for DE iodine maps in the context of higher iodine concentrations and different scanner technology than were used in this study so the findings may not be directly applicable here.[28] Similarly, it has also not been verified that the LOD and LOQ established

here would be valid with a background of hepatic tissue or blood, however this would be difficult to achieve in vivo.

Similarly, no alternative reconstruction methods such as smoother reconstruction kernels or iterative reconstruction, were used in this study. These would both produce images with less noise without increasing patient dose. According to the findings presented here, these could be an interesting avenue of investigation to increase ENR and therefore accuracy of fECV measurement without increasing dose. It would be important to verify that HU values are not affected by iterative reconstruction, particularly for the relatively low levels of absolute iodine contrast achieved with EQ-CT and that the reduction in resolution associated with a smoother reconstruction algorithm would not result in the incorrect placement of the ROI.[38]

In conclusion, this phantom study has demonstrated that EQ-CT as an application of quantitative CT can potentially accurately measure fECV on a wide detector CT system at the concentrations of iodine expected in routine clinical studies, and it is robust to changes in acquisition and reconstruction settings tested. SE modes produced more accurate and precise measurements of fECV compared to the DE mode tested, and precision increases with ENR.

References

1. Jacobsen MC, Thrower SL, Ger RB, et al. Multi-energy computed tomography and material quantification: Current barriers and opportunities for advancement. *Medical Physics*. 2020;47(8):3752-3771. doi:https://doi.org/10.1002/mp.14241
2. Parr DG. Clinical Applications of Quantitative Computed Tomography in Chronic Lung Disease. *International Journal of Pharmaceutical Medicine*. 2003;17(2):71-78. doi:10.2165/00124363-200317020-00005
3. Smith AD. Enter the Era of Quantitative Liver CT. *Radiology*. 2018;289(3):708-709. doi:10.1148/radiol.2018181847
4. Nacif MS, Kawel N, Lee JJ, et al. Interstitial Myocardial Fibrosis Assessed as Extracellular Volume Fraction with Low-Radiation-Dose Cardiac CT. *Radiology*. 2012;264(3):876-883. doi:10.1148/radiol.12112458
5. Bandula S, White SK, Flett AS, et al. Measurement of Myocardial Extracellular Volume Fraction by Using Equilibrium Contrast-enhanced CT: Validation against Histologic Findings. *Radiology*. 2013;269(2):396-403. doi:10.1148/radiol.13130130
6. Zissen MH, Wang ZJ, Yee J, Aslam R, Monto A, Yeh BM. Contrast-Enhanced CT Quantification of the Hepatic Fractional Extracellular Space: Correlation With Diffuse Liver Disease Severity. *American Journal of Roentgenology*. 2013;201(6):1204-1210. doi:10.2214/AJR.12.10039
7. Bandula S, Punwani S, Rosenberg WM, et al. Equilibrium Contrast-enhanced CT Imaging to Evaluate Hepatic Fibrosis: Initial Validation by Comparison with Histopathologic Sampling. *Radiology*. 2015;275(1):136-143. doi:10.1148/radiol.14141435
8. Afdhal NH, Nunes D. Evaluation of Liver Fibrosis: A Concise Review. *The American Journal of Gastroenterology*. 2004;99(6):1160-1174. doi:10.1111/j.1572-0241.2004.30110.x
9. Horowitz JM, Venkatesh SK, Ehman RL, et al. Evaluation of hepatic fibrosis: a review from the society of abdominal radiology disease focus panel. *Abdom Radiol*. 2017;42(8):2037-2053. doi:10.1007/s00261-017-1211-7
10. Yeung J, Sivarajan S, Treibel TA, et al. Measurement of liver and spleen interstitial volume in patients with systemic amyloid light-chain amyloidosis using equilibrium contrast CT. *Abdom Radiol*. 2017;42(11):2646-2651. doi:10.1007/s00261-017-1194-4
11. Shinagawa Y, Sakamoto K, Sato K, Ito E, Urakawa H, Yoshimitsu K. Usefulness of new subtraction algorithm in estimating degree of liver fibrosis by calculating extracellular volume fraction obtained from routine liver CT protocol equilibrium phase data: Preliminary experience. *European Journal of Radiology*. 2018;103:99-104. doi:10.1016/j.ejrad.2018.04.012
12. Sofue K, Tsurusaki M, Mileto A, et al. Dual-energy computed tomography for non-invasive staging of liver fibrosis: Accuracy of iodine density measurements from contrast-enhanced data. *Hepatology Research*. 2018;0(0). doi:10.1111/hepr.13205

13. Yoon JH, Lee JM, Klotz E, et al. Estimation of Hepatic Extracellular Volume Fraction Using Multiphasic Liver Computed Tomography for Hepatic Fibrosis Grading. *Investigative Radiology*. 2015;50(4):290-296. doi:10.1097/RLI.0000000000000123
14. Guo SL, Su LN, Zhai YN, et al. The clinical value of hepatic extracellular volume fraction using routine multiphasic contrast-enhanced liver CT for staging liver fibrosis. *Clinical Radiology*. 2017;72(3):242-246. doi:10.1016/j.crad.2016.10.003
15. British Standards Institution. *BS ISO 5725-1:1994 Accuracy (Trueness and Precision) of Measurement Methods and Results. General Principles and Definitions*. British Standards Institution; 1995. Accessed October 21, 2021. https://bsol.bsigroup.com/PdfViewer/Viewer?pid=000000000030021602
16. Seeram E. *Computed Tomography: Physical Priciples, Clinical Applications and Quality Control*. 4th ed. Saunders; 2015.
17. EP17-A Protocols for Determination of Limits of Detection and Limits of Quantitation; Approved Guideline. :52.
18. Armbruster DA, Pry T. Limit of Blank, Limit of Detection and Limit of Quantitation. *Clin Biochem Rev*. 2008;29(Suppl 1):S49-S52.
19. Jacobsen MC, Cressman ENK, Tamm EP, et al. Dual-Energy CT: Lower Limits of Iodine Detection and Quantification. *Radiology*. 2019;292(2):414-419. doi:10.1148/radiol.2019182870
20. Riley P. Does iodinated contrast medium amplify DNA damage during exposure to radiation. *BJR*. 2015;88(1055):20150474. doi:10.1259/bjr.20150474
21. The Royal Australian and New Zealand College of Radiologists. RANZCR Iodinated Contrast Guidelines. Published 2018. Accessed December 10, 2020. https://www.ranzcr.com/search/ranzcr-iodinated-contrast-guidelines
22. Alvarez RE, Macovski A. Energy-selective reconstructions in X-ray computerised tomography. *Phys Med Biol*. 1976;21(5):733-744. doi:10.1088/0031-9155/21/5/002
23. Patino M, Prochowski A, Agrawal MD, et al. Material Separation Using Dual-Energy CT: Current and Emerging Applications. *RadioGraphics*. 2016;36(4):1087-1105. doi:10.1148/rg.2016150220
24. Bak S, Kim JE, Bae K, et al. Quantification of liver extracellular volume using dual-energy CT: utility for prediction of liver-related events in cirrhosis. *Eur Radiol*. 2020;30(10):5317-5326. doi:10.1007/s00330-020-06876-9
25. Ito E, Sato K, Yamamoto R, Sakamoto K, Urakawa H, Yoshimitsu K. Usefulness of iodine-blood material density images in estimating degree of liver fibrosis by calculating extracellular volume fraction obtained from routine dual-energy liver CT protocol equilibrium phase data: preliminary experience. *Jpn J Radiol*. 2020;38(4):365-373. doi:10.1007/s11604-019-00918-z
26. Pelgrim GJ, van Hamersvelt RW, Willemink MJ, et al. Accuracy of iodine quantification using dual energy CT in latest generation dual source and dual layer CT. *Eur Radiol*. 2017;27(9):3904-3912. doi:10.1007/s00330-017-4752-9

27. Ehn S, Sellerer T, Muenzel D, et al. Assessment of quantification accuracy and image quality of a full-body dual-layer spectral CT system. *J Appl Clin Med Phys*. 2017;19(1):204-217. doi:10.1002/acm2.12243
28. Kim H, Goo J, Kang C, Chae K, Park C. Comparison of Iodine Density Measurement Among Dual-Energy Computed Tomography Scanners From 3 Vendors. *Investigative Radiology*. 2018;53(6):321-327. doi:10.1097/RLI.0000000000000446
29. Ohno Y, Fujisawa Y, Fujii K, et al. Effects of acquisition method and reconstruction algorithm for CT number measurement on standard-dose CT and reduced-dose CT: a QIBA phantom study. *Jpn J Radiol*. 2019;37(5):399-411. doi:10.1007/s11604-019-00823-5
30. Shrimpton PC, Hillier MC, Meeson S, Golding SJ. *Doses from Computed Tomography (CT) Examinations in the UK- 2011 Review*. Public Health England; 2014. Accessed November 15, 2016. https://www.gov.uk/government/uploads/system/uploads/attachment_data/file/349188/PHE_CRCE_013.pdf
31. Bland JM, Altman DG. Measuring agreement in method comparison studies. *Stat Methods Med Res*. 1999;8(2):135-160. doi:10.1177/096228029900800204
32. Kalender WA, Klotz E, Kostaridou L. An algorithm for noise suppression in dual energy CT material density images. *IEEE Trans Med Imaging*. 1988;7(3):218-224. doi:10.1109/42.7785
33. Baerends E, Oostveen LJ, Smit CT, et al. Comparing dual energy CT and subtraction CT on a phantom: which one provides the best contrast in iodine maps for sub-centimetre details? *Eur Radiol*. 2018;28(12):5051-5059. doi:10.1007/s00330-018-5496-x
34. Yoshimitsu K. Comparison of extracellular volume fraction calculated from the three data sets of the equilibrium phase of dual-energy CT as surrogate markers for liver fibrosis: preliminary report. Published March 2, 2016. Accessed April 12, 2019. https://posterng.netkey.at/esr/viewing/index.php?module=viewing_poster&task=&pi=133412
35. *Ionising Radiation (Medical Exposure) Regulations 2017*. 2017. Accessed September 26, 2021. https://www.legislation.gov.uk/uksi/2017/1322/contents/made
36. Vis JY, Huisman A. Verification and quality control of routine hematology analyzers. *International Journal of Laboratory Hematology*. 2016;38(S1):100-109. doi:https://doi.org/10.1111/ijlh.12503
37. He T, Qian X, Zhai R, Yang Z. Computed Tomography Number Measurement Consistency Under Different Beam Hardening Conditions: Comparison Between Dual-Energy Spectral Computed Tomography and Conventional Computed Tomography Imaging in Phantom Experiment. *J Comput Assist Tomogr*. 2015;39(6):981-985. doi:10.1097/RCT.0000000000000287

38. Kondo M, Hatakenaka M, Higuchi K, et al. Feasibility of low-radiation-dose CT for abdominal examinations with hybrid iterative reconstruction algorithm: low-contrast phantom study. *Radiol Phys Technol*. 2013;6(2):287-292. doi:10.1007/s12194-012-0197-7

Section 3

Optimisation of equilibrium contrast enhanced CT imaging for the non-invasive assessment of extracellular volume in liver-directed cancer therapy

Chris Baker[1,2], Laura Beaton[3], Ricky A Sharma[4], Steven Bandula[5]

[1]School of Medical Sciences, University of Manchester, Manchester, United Kingdom
[2]Radiological Physics and Radiation Safety Group, Royal Free London NHS Foundation Trust, London, United Kingdom
[3]University College London Cancer Institute, University College London, London, United Kingdom
[4]National Institute for Health Research University College London Hospitals Biomedical Centre, University College London Cancer Institute, London, United Kingdom
[5]University College London Centre for Medical Imaging, University College London, London, United Kingdom

Abstract

Purpose

Measurement of fractional extracellular volume (fECV) using equilibrium CT (EQ-CT) has the potential to be a useful non-invasive diagnostic and prognostic tool for the assessment of liver cancers. This technique involves the measurement of iodine enhancement in the liver tissue and the aorta following the intravascular administration of iodinated contrast medium. The optimum acquisition and analysis techniques and clinical repeatability of EQ-CT fECV measurements are investigated, as well as the feasibility of measuring fECV in tumour lesions prior to and post transarterial chemoembolisation (TACE) therapy.

Methods

EQ-CT imaging was performed in patients a cohort of trial patients with primary or secondary liver cancer at two time points prior to, and once after TACE therapy. Conventional CT images at 80, 120 and 135 kVp, as well as iodine density images derived from dual energy (DE) CT acquisitions, were used to calculate fECV in apparently disease-free liver tissue and tumour lesions at each trial visit. A novel method for measuring blood contrast enhancement along a section of the abdominal aorta was investigated in an effort to reduce the effects of beam hardening artefact on quantification.

Results

A high technical failure rate (77.8%) and an increased radiation dose were associated with DE CT iodine density images. fECV measurements were reproducible across two successive pre-treatment visits in apparently disease-free sections of the liver. fECV measurement results were independent of acquisition kVp (including DE CT), however, variation in results was highest with DE CT. Increased measurement precision was possible with a novel method of blood enhancement measurement, using a 10 cm section of the aorta in an effort to reduce the effect of beam hardening artefacts. fECV values were higher in tumour lesions compared to apparently disease-free sections of the liver in 3 out of 6 patients, although low patient numbers and the possibility of many conflicting intratumoural processes prevent any firm conclusions. fECV measurement was successful in the presence of TACE beads. Image registration issues and inadequate iodine enhancement provided technical challenges to the technique.

Conclusions

fECV measurement using EQ-CT is shown to be a reproducible technique, best performed with a relatively high kVp; DE CT is not recommended. fECV measurement was successful in tumour lesions prior to and after the presence of TACE beads, although it was unable to categorically distinguish between apparently healthy and diseased tissue. It is a technique that shows promise as a routine diagnostic and potentially prognostic tool in the management of patients with liver cancer.

1. Introduction

In 2018 primary liver cancer was the sixth most commonly diagnosed cancer and the fourth highest cause of cancer related death worldwide.[1] Furthermore, secondary cancer in the liver is more prevalent than primary cancers.[2] Risk of hepatocellular carcinoma (HCC) is increased in patients with cirrhosis, which is characterised by an increase in the extracellular volume (ECV) due to an excess in collagen extracellular matrix deposits.[3] In both primary and secondary cancers, the ECV in and around tumour sites is likely to be further affected. Increased cell density within tumours will lead to a decrease in ECV, however, intratumoural fibrosis and the formation of fibrotic capsules could lead to a to contrary increase in ECV.[4] It is therefore proposed that measurement of ECV within tumours could provide useful additional diagnostic information to aid in the characterisation of liver cancers to determine risk and severity of disease. As far as the authors are aware, this has not been investigated previously in the context of diagnosed liver cancer. Serial ECV measurements could also provide a useful metric for the monitoring response to treatments such as transarterial chemoembolization (TACE), a commonly used treatment in this cohort of patients.[5] For these reasons, an accurate, reproducible and practicable measure of hepatic ECV would be of widespread clinical interest.

The current gold standard for assessment of liver tissue is histopathologic analysis following biopsy. Unfortunately this is a process with many documented drawbacks and associated risks which prevent it being a viable method for long term monitoring of a condition or continued assessment of treatment response.[3,6] Conversely, fractional extracellular volume (fECV) measurement using equilibrium-CT (EQ-CT) is a non-invasive, simple quantitative technique that has been shown to correlate with histopathologic analysis and other relevant measures of fibrosis in the setting of hepatic fibrotic disease and amyloidosis in several exploratory studies.[7–16] However, little attention has been paid to absolute accuracy or reproducibility of EQ-CT fECV measurements, with all fECV results previously reported being obtained from a measurement at a single time point. There has also been no attempt in the literature to measure fECV in liver tumour lesions to establish if the technique is able to distinguish between healthy and diseased tissue, or to further characterise tumours as a possible diagnostic or prognostic tool. It should be noted that EQ-CT is considered to be preferable over similar MRI based techniques due to simpler image analysis, fewer patient contraindications, and the ability to easily incorporate EQ-CT into existing diagnostic pathways.[16–18]

fECV measurement with EQ-CT utilises measured attenuation values in the liver and blood from a pre-contrast and an equilibrium phase CT acquisition, combined with a haematocrit value (Equation 1). This is possible as the iodine based contrast agents ubiquitously used in CT are exclusively extracellular and the volume of distribution within a tissue is equal to the ratio of contrast concentration in tissue to blood plasma.[19]

$$fECV_{liver} = \frac{Liver\ enhancement}{Blood\ enhancment} \times (1 - haematocrit)$$

Equation 1

Where $fECV_{liver}$ is the fractional extracellular volume in a user specified region of interest (ROI) in the liver and liver enhancement is the measured Hounsfield unit (HU) of the equilibrium phase image subtracted from the pre-contrast HU value, both measured in the specified ROI. Blood enhancement is typically measured using an ROI in the aorta and the haematocrit value is taken from a blood test immediately prior to the EQ-CT acquisition. It must be noted that for Equation 1 to be valid the equilibrium phase image must be acquired when the concentration of iodine in the extracellular extravascular space and the intravascular space in the liver ROI is in a state of dynamic equilibrium. This is where the technique gets its name. There is no consensus for the optimum time delay between pre-contrast and equilibrium imaging, and values in the literature range from 3 to 10 minutes.[14,16]

Based on the above equation, it is clear the fECV measurement will be dependent on quantitative metrics derived from CT images, namely HU values. HU values represent the attenuation properties of the materials being imaged relative to air and water.[20] Absolute HU values are therefore dependent on the attenuating material as well as the energy of the x-ray photons used to acquire the attenuation data, notwithstanding the presence of image artefacts, such as beam hardening artefacts which have the potential to alter absolute HU values. Furthermore, uncertainty in HU values is dependent on image noise, an unavoidable consequence of photon-based imaging, which is reliant on dose and image reconstruction methods. Understanding the complex interactions between these factors should allow the user to manipulate acquisition and reconstruction settings to obtain optimised quantitative information in order to calculate the fECV. The advent of dual energy (DE) CT has also led to new opportunities for quantitative CT imaging. Of particular interest for the EQ-CT technique is ‘DE iodine density mode’ where material specific (in this case, iodine) density maps are formed in place of conventional HU values.[12–14]

Evidence from a phantom study demonstrated the overall accuracy of simulated EQ-CT fECV measurements were robust to changes in acquisition kVp and dose settings.[21] However, measurement precision was dependent on a novel image metric: enhancement to noise ratio (ENR). Enhancement was defined as the measured HU enhancement averaged over liver and blood ROIs (Equation 2), and average noise was the standard deviation (SD) associated with each HU value used in the enhancement measurements, summed in quadrature (Equation 3). ENR is simply the ratio of the average enhancement to the average image noise (Equation 4), and precision was found to increase with increasing ENR.[21]

$$Average\ enhancement = \frac{\left(HU_{liver,equ} - HU_{liver,pre}\right) + \left(HU_{blood,equ} - HU_{blood,pre}\right)}{2}$$

Equation 2

$$Average\ noise = \sqrt{SD_{liver,pre}{}^2 + SD_{liver,equ}{}^2 + SD_{blood,pre}{}^2 + SD_{blood,equ}{}^2}$$

Equation 3

$$Enhancement\ to\ noise\ ratio\ (ENR) = \frac{Average\ enhancement}{Average\ noise}$$

Equation 4

Where HU is the Hounsfield unit measurement from the pre-contrast ('pre') and equilibrium ('equ') phase images in the liver and blood respectively and SD is the standard deviation associated with each HU measurement.

In the phantom study, lower kVp settings (80 and 100 kVp) were associated with higher ENR values and improved fECV measurement precision when compared to higher kVp values (120 and 135 kVp).[21] This was attributed to increased attenuation of iodine at lower kVp values. DE CT iodine density images were shown to have significantly lower precision than any conventional kVp settings tested.[21] This would make lower kVp values a logical choice for fECV measurement using EQ-CT, however, this introduces the risk of beam hardening artefacts in clinical images. Beam hardening artefacts have been cited by several authors as problematic when measuring blood enhancement in the aorta due to adjacent highly attenuating vertebral bodies.[12,13,22] The balance between the use of low kVp values to optimise fECV measurements and the risk of beam hardening artefacts therefore requires careful consideration. The phantom study results are yet to be validated in the clinical setting and a method to mitigate the effects of beam hardening in the aorta warrants further investigation.

The aims of this study are to address some of the knowledge gaps identified above as relating to the EQ-CT technique to measure fECV in the liver in the setting of diagnosed liver cancer. These are: to investigate the effect of EQ-CT acquisition parameters (to include DE CT) and analysis techniques on clinical fECV results and ENR values; to establish the reproducibility of the EQ-CT technique to measure hepatic fECV; to ascertain if there is a difference in fECV values between tumour lesions, and to establish the feasibility of fECV measurement in the tumours treated with TACE to determine if this is an appropriate method for monitoring fECV in response to such therapies.

2. Methods

2A Imaging protocol

This study involved using images from a prospective trial of Vandetanib-eluting radiopaque embolic beads (BTG-002814) in patients with resectable HCC or hepatic metastases from colorectal cancer (mCRC) (ClinicalTrial.gov registration NCT03291379), which received all relevant local approvals (Medicines and Healthcare Products Regulatory Agency, Clinical Trials Authorisation number 2016-004164-19, and the Health Research Authority which includes ethics approval, reference 17/LO/00/11).[23] The primary aims of this phase 0 trial included establishing the safety and tolerability of the embolic beads and assessment of the concentration of Vandetanib in plasma and surgically resected liver tumours following treatment. Secondary aims included assessment of the anatomical distribution of the embolic beads, for which CT imaging was performed. A total of 8 patients were recruited onto the trial.

The trial protocol involved CT liver imaging at three timepoints: approximately 7 days prior to treatment (‘visit 1’), the day of treatment (prior to TACE administration, ‘visit 2’) and 6 - 20 days post-treatment (‘visit 3’). A blood sample was taken to measure haematocrit prior to imaging at every visit. This gives a unique opportunity to perform serial hepatic fECV measurements in the same individual in relatively quick succession (between visits 1 and 2) to test the clinical reproducibility of the technique, as well as measuring fECV both in visually unaffected sections of the liver and specifically within tumour lesions. The feasibility of performing fECV measurements in the presence of radio-opaque beads could also be investigated using images from visit 3.

2B Image acquisition and reconstruction

All image acquisition was performed on a Canon Aquilion ONE Vision (Canon Medical Systems, Ōtawara, Tochigi, Japan). This has a 160 mm wide detector bank, allowing the entire liver to be acquired in one axial rotation. EQ-CT imaging consisted of a pre-contrast acquisition followed by the intravenous administration of a bolus of 0.5 mL/kg of 300 mgI/mL iodine contrast, at a rate of no less than 5 mL/s, and 7 minute delayed (equilibrium) phase imaging. Conventional single energy (SE) and DE modes were acquired.

The DE acquisitions and reconstructions were performed with the following parameters: 320 x 0.5 mm collimation; large field of view; sequential 80 and 135 kVp rotations; 0.5 second rotation; automatic tube current selection on; reconstruction kernel FC13-H and a 5 mm reconstructed slice width. Images were reconstructed separately at 80 kVp and 135 kVp and DE iodine density images generated using iodine and water as basis pairs with the system default parameters (material formula object 1: -136 and -106 and object 2: 67 and 63; slope of contrast media: 0.55; reconstruction kernel FC07-H). DE iodine density images were presented as HU maps, where the HU value represented the HU exclusively of materials

identified as iodine. This was followed by a 120 kVp helical acquisition and reconstruction: 80 x 0.5 mm collimation; large field of view; 0.5 second rotation; pitch 0.813; automatic tube current selection on; reconstruction kernel FC07-H and 5 mm reconstructed slice width.

The same imaging parameters were used for the pre-contrast and equilibrium phase images. This generated a pre-contrast and equilibrium phase 'image pair' at 80 kVp, 120 kVp, 135 kVp and DE iodine density mode for each trial patient at each visit. The $CTDI_{vol}$ for all image acquisitions were recorded as a measure of radiation dose.

2C Image analysis

Images were downloaded and analysed using independent image analysis software (Horos v3.3.6, horosproject.org). Image analysis was performed by a clinical scientist (CB) in conjunction with a radiologist (SB). Manual, rigid image registration was performed between image pairs for matching kVp datasets for each trial patient at every visit to ensure consistency in placement of ROIs, as described below.

Taking a slice of an equilibrium phase image, three independent ROIs were drawn: ROI_{liver}, ROI_{tumour} and ROI_{blood} (Figure 1). ROI_{liver} was placed in an area of the liver that was visually unaffected by disease, avoiding the TACE therapy target area and any major blood vessels. ROI_{liver} was propagated over five consecutive slices taking care to avoid liver boundaries and any gross image artefacts such as beam hardening. These slices were assigned arbitrary slice numbers of one to five. This gave five ROI_{liver} values for each CT dataset. The five consecutive slices were combined to form a single liver volume of interest (VOI), designated as VOI_{liver}.

ROI_{tumour} was drawn to outline the largest visible tumour in the TACE therapy target area on all slices on which the lesion was visible. In some cases, due to poor visibility of lesions on CT images, MRI images were used to assist in placement of these ROIs. The series of ROI_{tumour} outlines created a volume which was equivalent to the gross tumour volume, designated as VOI_{tumour}. In the case of images from visit 3 where the highly attenuating TACE beads were unavoidably included within VOI_{tumour}, all pixel values within that VOI of 100 HU or higher were manually set to a value corresponding to the average HU taken from VOI_{liver} for that patient at that visit, in an effort to avoid the presence of the beads affecting the fECV result.

ROI_{blood} of approximately 1 cm^2 was placed in the centre of the aorta and copied to the same five slices that contained ROI_{liver}. From the central slice of these five, ROI_{blood} was propagated along the centre of the vessel by 5 cm in both the superior and inferior directions. This created VOI_{blood} which was 10 cm in length, in an effort to reduce the

influence of vertebral beam hardening artefact on blood enhancement measurement in any individual slices.

The mean HU value and SD from all ROIs and VOIs were extracted. This process was completed for the equilibrium phase images of the 80, 120 and 135 kVp datasets. Due to the low visibility of lesions on the DE iodine density images, ROIs were copied from the 80 kVp data set onto the DE iodine density images. The ROIs for the equilibrium phase images were then copied to the pre-contrast phase images of the same image pair. Manual adjustment of ROI placement was performed where necessary to account for organ motion that could not be corrected for during image registration. Again, ROIs were used to generate corresponding VOIs and mean HU and SD were extracted for pre-contrast images.

fECV values were calculated for the liver and tumour using different combinations of the ROIs and VOIs detailed above using Equation 5Equation 6 and Equation 7.

$$fECV(liver, ROI) = \frac{HU_{ROI(liver),equ} - HU_{ROI(liver),pre}}{HU_{ROI(blood),equ} - HU_{ROI(blood),pre}} \times (1 - haematocrit)$$

Equation 5

$$fECV(liver, VOI) = \frac{HU_{VOI(liver),equ} - HU_{VOI(liver),pre}}{HU_{VOI(blood),equ} - HU_{VOI(blood),pre}} \times (1 - haematocrit)$$

Equation 6

$$fECV(tumour) = \frac{HU_{VOI(tumour),equ} - HU_{VOI(tumour),pre}}{HU_{VOI(blood),equ} - HU_{VOI(blood),pre}} \times (1 - haematocrit)$$

Equation 7

Where fECV(liver,ROI) is the fECV for the liver using ROI_{liver} and ROI_{blood} from the same single image slice; fECV(liver,VOI) and fECV(tumour) are the fECV values for the liver and tumour using VOIs for the liver, tumour and blood as appropriate, and HU_{equ} and HU_{pre} are the mean HU values from the respective ROIs and VOIs from equilibrium phase and pre-contrast imaging: when subtracted this represents the enhancement of the ROI or VOI in question. The haematocrit value was taken from the blood sample obtained prior to imaging.

fECV(liver, ROI) was calculated for the five consecutive slices containing ROI_{liver} and ROI_{blood} for each image pair (80, 120 and 135 kVp and DE iodine density images) for each patient for visits 1 and 2. A single fECV(liver,VOI) was also calculated for each image pair at visits 1 and 2 for comparison to fECV(liver,ROI) results to investigate if this analysis method reduced the influence of beam hardening present in the ROI_{blood}. fECV(tumour) was

calculated for every image pair for every patient at visits 1, 2 and 3. In addition, for every fECV value calculated, a corresponding ENR value was generated using the HU and associated SD values for each ROI or VOI using Equation 2,Equation 3 and Equation 4.

Prior to statistical analysis the enhancement values associated with every fECV calculation were scrutinised. Data from previous work to establish the lowest concentration of iodine that can be measured to an acceptable level of precision (the 'limit of quantification') was used to establish that for conventional kVp modes for acquisition and reconstruction settings similar to those used here, the lowest level of iodine that can be quantified equates to an enhancement of 3 HU.[21] The equivalent figure was 4 HU for DE iodine density mode. For this reason, any fECV results calculated using enhancement values that were less than these figures for the relevant kVp or DE iodine density mode were excluded from any further analysis.

2D Statistical analysis

All statistical analysis was performed in R version 4.0.1 (R Foundation for Statistical Computing, Vienna, Austria). fECV data was checked for normality using a visual assessment of histograms and quantile-quantile plots and as a result, non-parametric summary statistics and statistical tests were used where appropriate. A *p*-value of less than 0.05 was used as a test of significance for all statistical tests.

A linear mixed effects model was constructed, presented as Equation 8 following typical notation for such models.[24] The dependent variable in the model was fECV(liver,ROI), with visit number and kVp included as fixed effects to investigate their effect on the dependent variable. A nested random effect of slice location within patient ID was included, to take into account the fact that measurements were taken at multiple slice locations within each patient. Only data from visits 1 and 2 were used: visit 3 was excluded to avoid any effects from TACE treatment even in untreated areas of the liver. Once constructed, the residuals of the model were visually assessed ensure requirement for homoscedasticity was satisfied.

$$\text{fECV(liver,ROI)} \sim \text{visit} + \text{kVp} + (1|\text{patient/slice})$$

Equation 8

To establish if there was a difference in fECV results between fECV(liver,ROI) and fECV(liver,VOI), the Wilcoxon rank sum test was used to compare all results (from all patients, kVp values and visits) from these two fECV calculation techniques.

The difference between fECV(liver,VOI) and fECV(tumour), averaged over all kVps, was calculated on individual patient basis using results from visit 1. The error associated with

these results were based on findings of a previous study, which established 95% confidence intervals for fECV measurements based on ENR magnitude.[21]

Finally, fECV(tumour) from all patients at each visit were compared using the Wilcoxon signed rank test. Pairwise comparisons between visits 1, 2 and 3 were made to establish if there was any significant difference in fECV(tumour) results between visits.

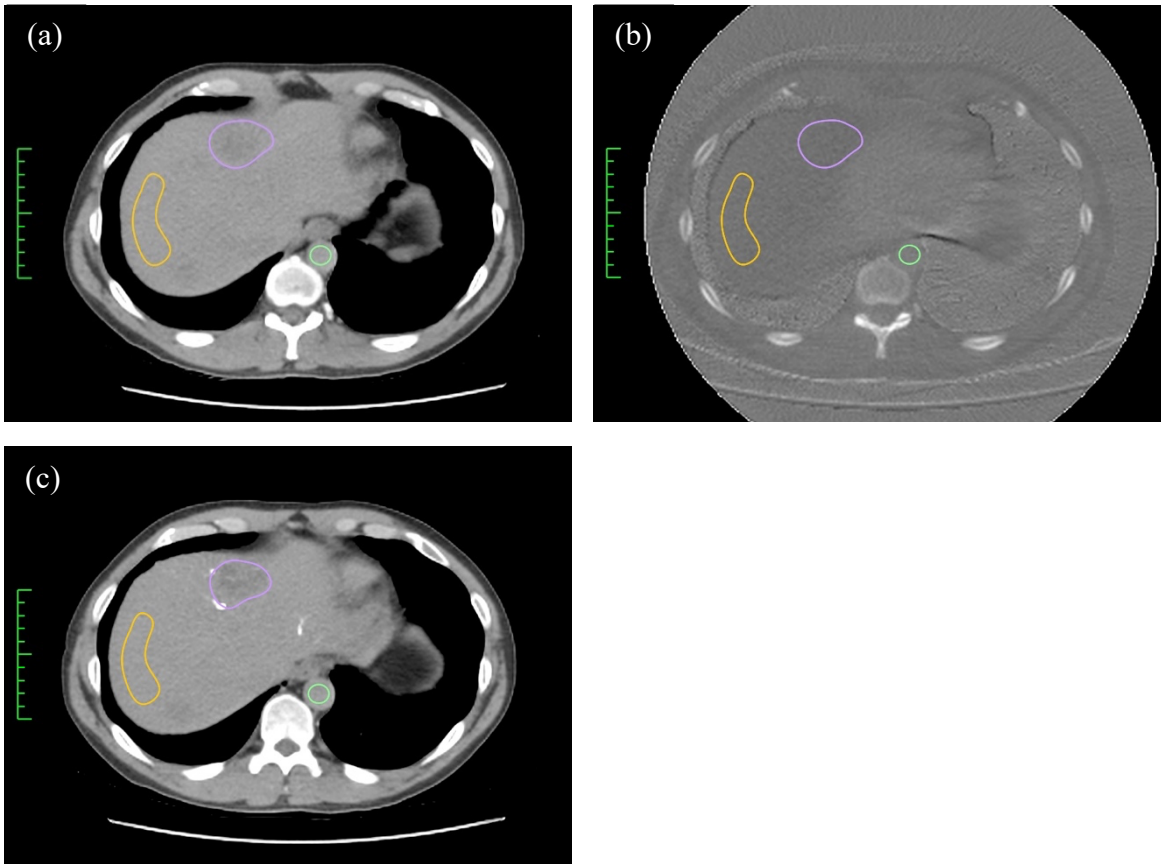

Figure 1 *Example of trial images with an indication of the placement of three regions of interest. All images shown here are of the same patient at approximately the same relative slice position: (a) 135 kVp at visit 1, (b) iodine density image at visit 1 and (c) and 135 kVp at visit 3 (note the presence of radiopaque therapy beads); orange = ROI_{liver}; purple = ROI_{tumour}; green = ROI_{blood}.*

3. Results

A full set of images were available for 6 out of 8 trial patients (1 female, mean age 60, age range 50-69). EQ-CT images were not available for 2 patients due to incomplete datasets. Mean $CTDI_{vol}$ for pre-contrast and equilibrium phase acquisitions were 7.7 mGy for 120 kVp (range 6.8 – 9.3 mGy) and 16.1 mGy for the combined 80 and 135 kVp DE acquisition (range 12.3 – 22.8 mGy). With a 16 cm scan length and a conversion factor for the abdomen of 0.024 mSv/mGycm, this results in a mean whole body effective dose of 5.9 mSv for the EQ-CT acquisition at 120 kVp, calculated using the ICRP 103 definition of effective dose in the ICRP adult reference computational phantoms (averaged for male and female).[25]

All ROI and VOI mean HU and SD values were successfully extracted for all images available and the corresponding enhancement and fECV values were calculated. Prior to statistical analysis, the threshold enhancement values of 3 HU (conventional kVp mode) and 4 HU (dual energy iodine density mode) were applied to ensure an accurate measurement of iodine enhancement, as previously described. Out of a possible total of 360 fECV values available for analysis, 74 (20.6%) were excluded from further analysis due to either the liver, tumour or blood ROI or VOI (or both) being lower that the relevant threshold enhancement. 70 out of a total of 90 (77.8%) of the data points from the DE iodine density images were excluded on this basis.

The results of the linear mixed effects model are shown in Table 1. They demonstrate that neither visit (p = 0.10) nor kVp (p = 0.94) had a significant effect on fECV(liver,ROI) results when the nested random effect of slice location and patient is accounted for. A summary of the fECV(liver,ROI) results for each patient at visits 1 and 2 are shown in Table 2 and Figure **2** (for all kVp settings combined). The fECV(liver,ROI) results broken down by kVp setting, summed for all patients, are shown in Table 3 and Figure 3.

The results of fECV(liver,ROI) versus fECV(liver,VOI), summed for all patients and kVp settings at visits 1 and 2, are shown in Figure 4. The Wilcoxon rank sum test showed no significant difference between these two groups (p = 0.97). Table 4 and Figure 4 demonstrate that the interquartile range (IQR) is lower with fewer outlying results for fECV(liver,VOI).

Table 5 and Figure 5 compare the results from fECV(liver,VOI) and fECV(tumour) for each patient at visit 1. fECV(tumour) was higher than fECV(liver,VOI) in 50% (3/6) of the patients, although the estimated errors associated with these measurements demonstrate these differences are unlikely to be significantly different in all cases. When all fECV(tumour) results were grouped for all patients for each visit (Figure 6) there was no significant difference between visits 1, 2 and 3 (Wilcoxon signed rank test: visit 1 vs visit 2, p = 0.64; visit 2 vs visit 3, p = 80; visit 1 vs visit 3, p = 0.43).

Model parameter	Model base value	Categorical value for comparison to base value	Coefficient estimate	95% CI for coefficient estimate		*p*-value
				Lower limit	Upper limit	
kVp	80	120	-0.001	-0.003	0.001	0.94
		135	-0.002	-0.007	0.002	0.86
		DE	0.016	-0.015	0.047	0.45
Visit	visit 1	visit 2	0.017	-0.017	0.051	0.10

Table 1 *Results of the linear mixed effects model where the dependent variable was fECV(liver,ROI) and a nested random effect of slice location and patient was included; DE = dual energy iodine density mode; CI = confidence interval.*

Patient	Visit number	fECV(liver,ROI)		Median ENR
		Median	Interquartile range	
A	1	0.25	0.06	1.40
	2	0.24	0.05	1.42
B	1	0.27	0.05	1.62
	2	0.25	0.09	1.94
C	1	0.22	0.04	0.94
	2	0.26	0.05	1.00
D	1	0.35	0.07	1.13
	2	0.34	0.08	1.16
E	1	0.20	0.05	1.36
	2	0.25	0.09	0.71
F	1	0.28	0.05	0.99
	2	0.28	0.09	1.25

Table 2 *fECV(liver,ROI) results (median and interquartile range) with associated median enhancement to noise ratio (ENR) for each patient at visits 1 and 2, averaged over all kVp settings.*

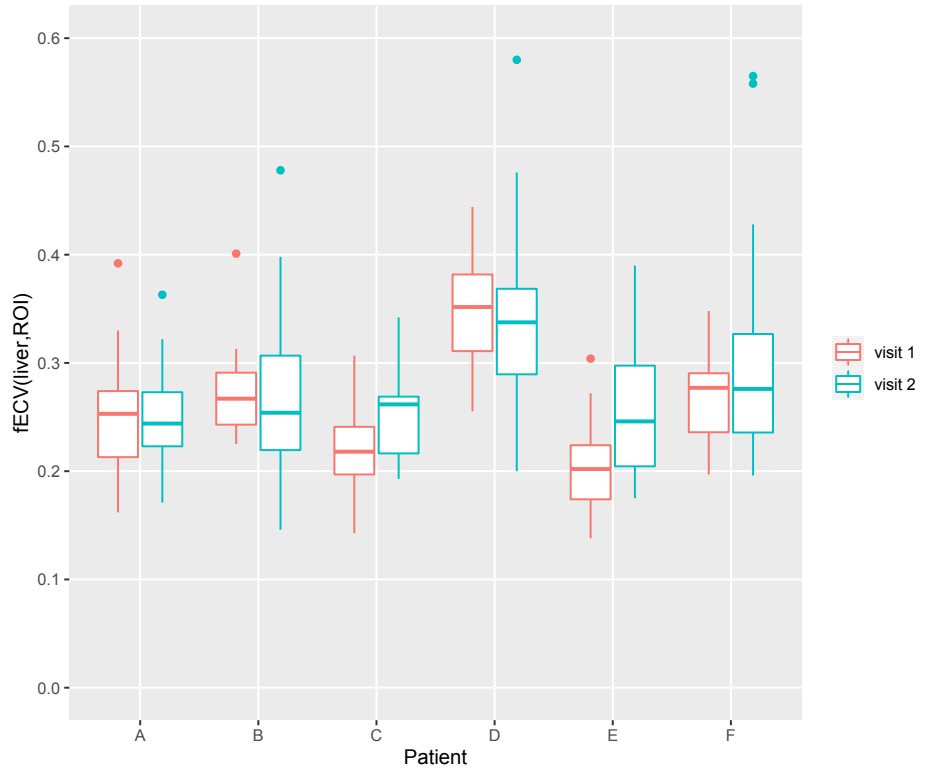

Figure 2 *A boxplot of fECV(liver,ROI) results for each patient at visits 1 and 2 (data from all kVp settings included); the central line of each box represents the data median, the lower and upper limits of the box represent the interquartile range (IQR), the lines extend from the 25th percentile minus 1.5 times the IQR to the 75th percentile plus 1.5 times the IQR and the points represent outliers from this range.*

kVp	fECV(liver,ROI)		Median ENR
	Median	Interquartile range	
80	0.26	0.06	1.39
120	0.26	0.08	1.11
135	0.26	0.08	1.29
DE	0.30	0.23	0.89

Table 3 *fECV(liver,ROI) results (median and interquartile range) with associated median enhancement to noise ratio (ENR) for each kVp setting, summed for all patients across visits 1 and 2; ENR = enhancement to noise ratio; DE = dual energy iodine density mode.*

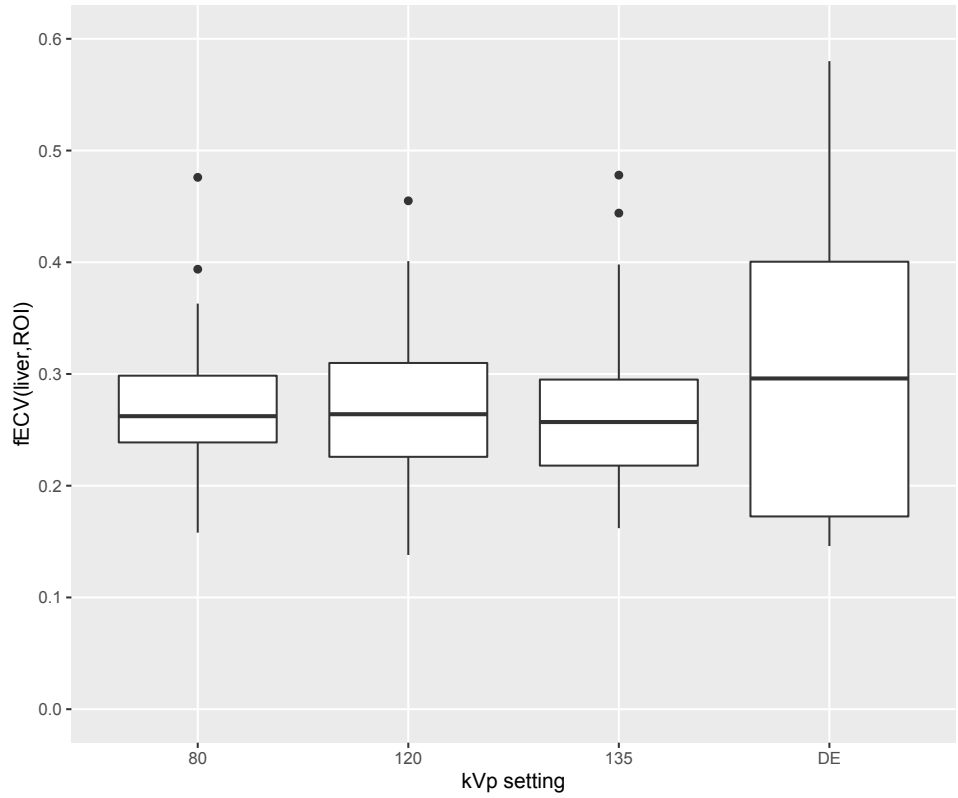

Figure 3 *A boxplot of fECV(liver,ROI) data for each kVp setting, grouped for all patients at visits 1 and 2; the central line of each box represents the data median, the lower and upper limits of the box represent the interquartile range (IQR), the lines extend from the 25th percentile minus 1.5 times the IQR to the 75th percentile plus 1.5 times the IQR and the points represent outliers from this range; DE = dual energy iodine density mode.*

fECV type	Median	Interquartile range	Median ENR
fECV(liver,ROI)	0.26	0.09	1.21
fECV(liver,VOI)	0.26	0.07	1.19

Table 4 *fECV(liver,ROI) and fECV(liver,VOI) results grouped for all patients, all kVps and visits 1 and 2 combined; ENR = enhancement to noise ratio.*

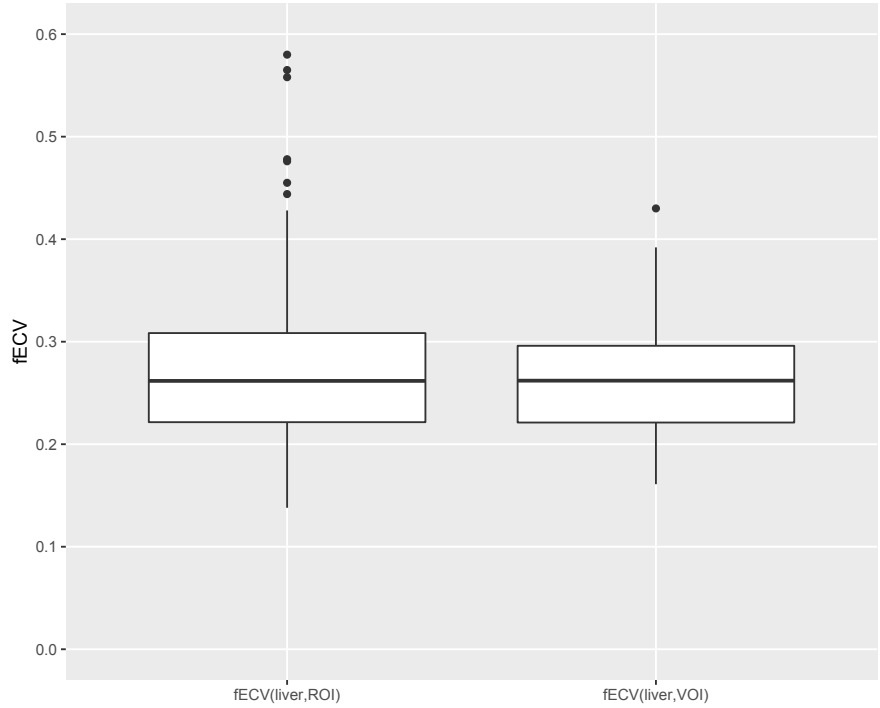

Figure 4 *A boxplot of fECV(liver,ROI) and fECV(liver,VOI) for all patients and kVp settings at visits 1 and 2 combined; the central line of each box represents the data median, the lower and upper limits of the box represent the interquartile range (IQR), the lines extend from the 25th percentile minus 1.5 times the IQR to the 75th percentile plus 1.5 times the IQR and the points represent outliers from this range.*

Patient	fECV(liver,VOI)		fECV(tumour)		Difference
	Mean [95% CI]	ENR	Mean [95% CI]	ENR	
A	0.25 [0.23, 0.26]	1.40	0.21 [0.19, 0.22]	1.08	0.04
B	0.27 [0.25, 0.29]	1.69	0.20 [0.18, 0.21]	1.34	0.08
C	0.23 [0.19, 0.27]	0.92	0.31 [0.26, 0.36]	0.86	-0.08
D	0.34 [0.32, 0.36]	1.15	0.27 [0.26, 0.29]	1.07	0.06
E	0.22 [0.21, 0.24]	1.46	0.25 [0.23, 0.26]	1.41	-0.03
F	0.27 [0.25, 0.28]	1.01	0.30 [0.28, 0.32]	1.07	-0.03

Table 5 *fECV(liver,VOI) and fECV(tumour) results for each trial patient at visit 1 for all kVp settings combined; CI = confidence interval; ENR = enhancement to noise ratio; Difference = mean fECV(liver,VOI) minus mean fECV(tumour).*

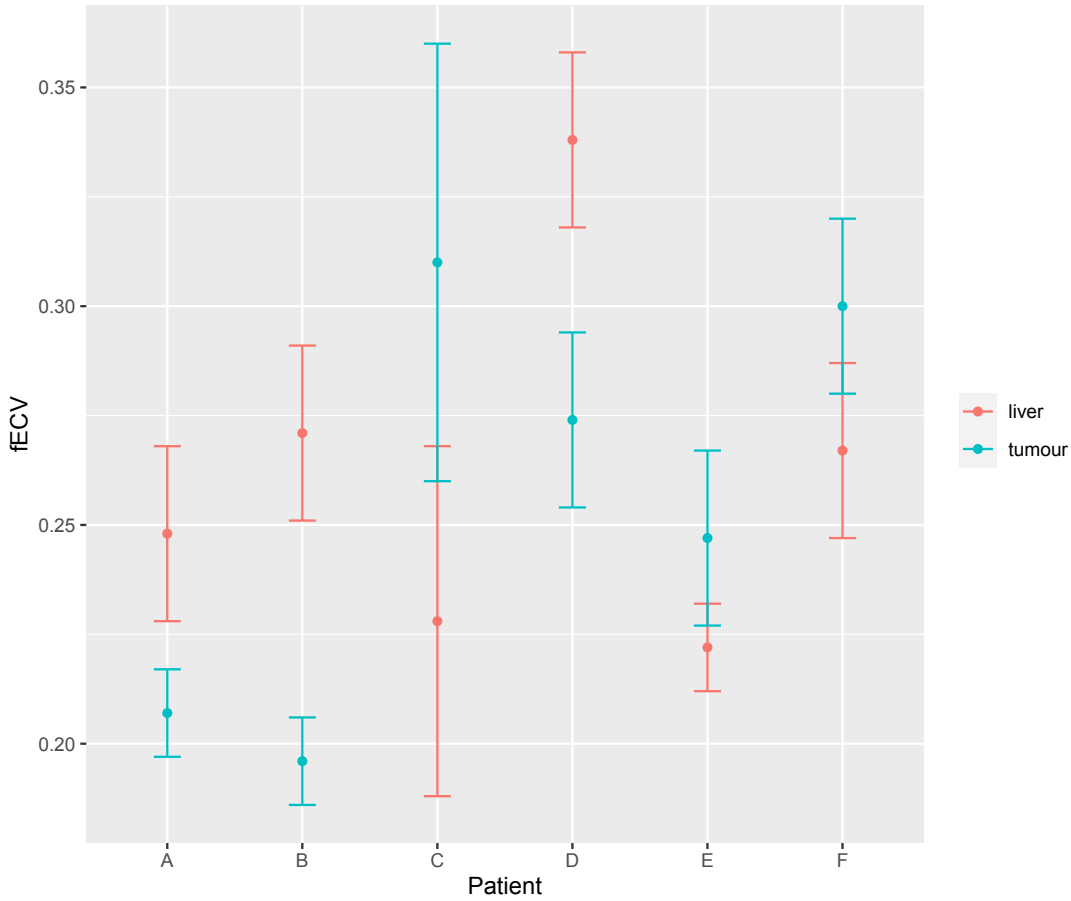

Figure 5 *fECV(liver,VOI) and fECV(tumour) results for all patients at visit 1, each point represents the mean result from all kVp settings (note no iodine density mode results were included due to inadequate enhancement for all of these images); error bars represent the 95% confidence interval for fECV measurements based on associated ENR value, note large error bars associated with patient C due to ENR < 1 for fECV(liver,VOI) and fECV(tumour) for this patient.*

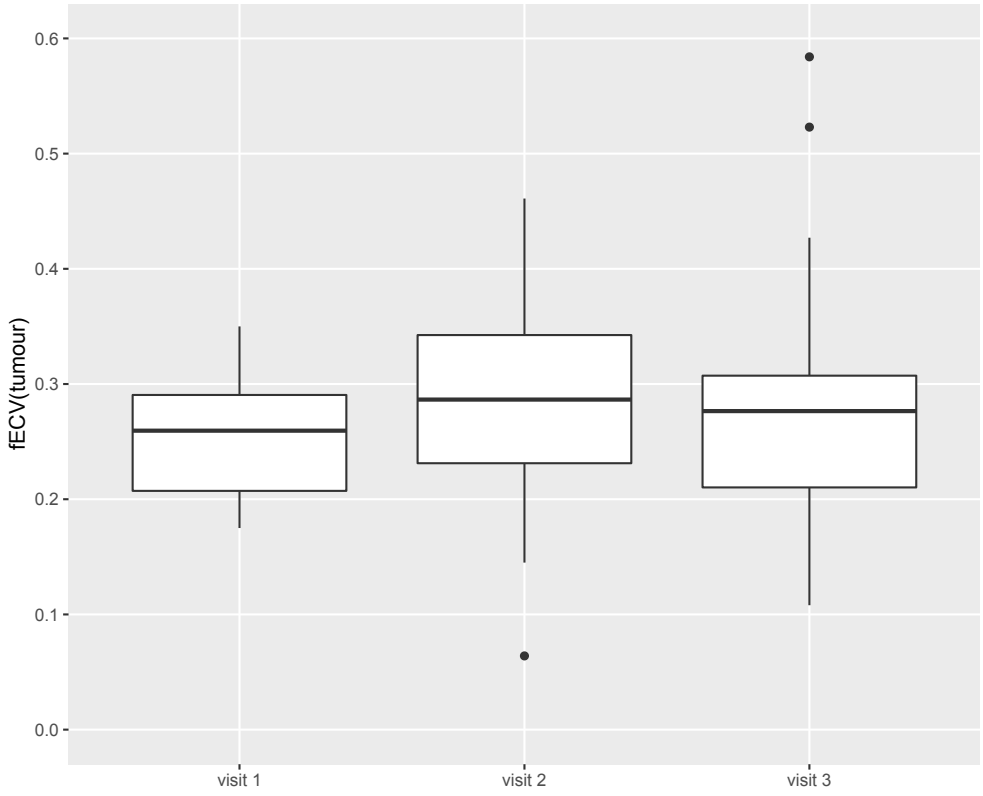

Figure 6 *Boxplot of fECV(tumour) results at each visit for all patients and kVp settings combined; the central line of each box represents the data median, the lower and upper limits of the box represent the interquartile range (IQR), the lines extend from the 25th percentile minus 1.5 times the IQR to the 75th percentile plus 1.5 times the IQR and the points represent outliers from this range.*

4. Discussion

In this study hepatic fECV was successfully measured using an EQ-CT technique in a cohort of patients with primary and secondary liver cancers, before and after TACE therapy. The linear mixed effects model demonstrated that fECV results in apparently disease-free sections of liver were reproducible in the same patient at two visits separated by up to seven days. As far as the authors are aware, this is the first time this has been established and it can give the clinical user increased confidence in the technique. However, as demonstrated by Figure 2, this may not necessarily true for all individuals included in this study and caution must be used when generalising the results from these patients to a wider population.

The median ENR for all results was 1.21, with the vast majority of ENR values reported being between 1 and 2. Previous work demonstrating the correlation between ENR value and fECV measurement accuracy in a phantom has shown that the 95% confidence interval of the measured fECV result is approximately ± 17% for an ENR of this magnitude using conventional SE modes.[21] Taking the example of patient A at visit 1, the median fECV(liver,ROI) was 0.25 with an ENR value of 1.40, which would give a 95% confidence interval of approximately 0.21 – 0.29 for the fECV(liver,ROI) result. This seems to be broadly in line with the range of data seen (Figure 2), giving an indication that the accuracy of the measurement in the clinical setting is similar to that previously established in a phantom. It is also important to note that the size of this error will dominate over the error associated with haematocrit measurement, reported as 1.8% and 1.2% for accuracy and precision respectively.[26]

The linear mixed effects model demonstrated that fECV(liver,ROI) measurements are robust to changes in kVp, giving the user some freedom to optimise this scan parameter without affecting the absolute result. However, whilst the use of DE CT iodine density mode did not have a significant effect on the absolute fECV(liver,ROI), the variation in results seen was much larger than those for 80, 120 and 135 kVp settings. This is likely to be due to the low measured enhancement values in DE CT iodine density mode, contributing to the lower ENR values seen. The low enhancement values were also responsible for the majority (77.8%) of data in this mode being excluded from analysis, due to the requirement imposed of only including enhancement values greater than a previously established limit of quantification for iodine on this scanner type.

This is in contradiction to several studies who have successfully reported hepatic fECV results using iodine density maps. However, none of these studies considered the effect of the limit of quantification of iodine on their results or validated iodine density derived fECV results to conventional HU value calculated fECV.[12–14] These alternative studies also used larger volumes of contrast materials and shorter time delays for their equilibrium imaging (all between three and four minutes) which would both result in higher iodine concentrations and

therefore improved enhancement values compared to this study. Based on the findings reported here, and in agreement with a phantom study, DE imaging resulted in lower accuracy, a higher technical failure rate and a higher radiation dose when compared to conventional CT imaging with a single x-ray spectrum. The use of DE iodine density images is therefore not recommended as part of the EQ-CT scan protocol.

When considering the conventional kVp settings used in this study (80, 120 and 135 kVp), it is tempting to recommend the use of a low kVp, namely 80 kVp. The potential advantage of using a low kVp is an increase in radiological contrast of iodine due to an increase in the cross section of the photoelectric effect as photon energies decrease.[20] The results presented here reflect this theory: 80 kVp shows the highest ENR and lowest IQR in fECV(liver,ROI) results. However, due to the relatively low absolute enhancement values, these gains are marginal and must be considered in the context of the potential disadvantages of using lower kVp, namely the introduction of image artefacts such as beam hardening and photon starvation, examples of which were seen in this study (Figure 7). A relatively high kVp is therefore recommended for the EQ-CT technique.

Several previous studies have noted that beam hardening artefacts from the highly attenuating vertebral bodies have caused issues with obtaining blood enhancement values in the aorta.[12,13,22] Similar issues were found in this study as enhancement values were seen to vary along the length of the abdominal aorta, as demonstrated by Figure 8: a 10 HU difference in blood enhancement in the context of a liver enhancement value of approximately 7 HU would have a large effect of fECV result. In an effort to overcome this issue, an average enhancement value was obtained along a 10 cm section of the abdominal aorta (VOI_{blood}). This was combined with VOI_{liver} in an attempt to further reduce the effect of inter-slice variation on fECV results.

Overall, fECV(liver,VOI) results were not found to be significantly different to fECV(liver,ROI) results. This, again, is a reassuring result and indicates that even though there were some beam hardening artefacts visualised in the study images, it was possible to adequately avoid these when placing the ROIs and VOIs. Importantly, there was a lower range of results with fewer outliers for fECV(liver,VOI). This observation, and the real possibility of beam hardening artefacts being unavoidably included in ROIs (particularly in the aorta), leads to the fECV(liver,VOI) technique being recommended for routine use. A possible disadvantage of using this technique is the increased analysis time involved in placing multiple ROIs to create the VOIs.

This study demonstrated that half the patients saw an increase in fECV(tumour) when compared to fECV(liver, VOI) and half saw a decrease. However, the uncertainty associated with the fECV values means that the differences are unlikely to be significant for all patients,

as demonstrated by the overlapping error bars in Figure 5. The large errors associated with low ENR values,[21] as demonstrated by patient C in this study, only serves to increase the uncertainty in being able to differentiate fECV values between tumour lesions and uninvolved liver tissue.

Relating these findings to the clinical situation, fECV is likely to be lower in tumour tissue due to the hypercellular nature of tumour lesions, however, the competing action of increased vascularity and fibrosis associated with some tumours could potentially offset or even reverse this reduction in fECV.[27,28] Due to the method used in this study of outlining the entire tumour volume for the measurement for fECV(tumour), it is likely that both these effects are seen in the end fECV measurement. The variation in the difference between liver and tumour fECV for different trial patients shown here means that it is possible that these tumours are characterised by different degrees of cellularity, vascularity and fibrosis. As it is likely that these characteristics are associated with different outcomes,[4,27,29] fECV(tumour) measurements could potentially provide the clinician with vital prognostic information from a relatively simple and easy procedure that could easily be built into the diagnostic pathway. This study has demonstrated that different fECV results are obtained in tumour lesions compared to unaffected liver in some trial patients, although unfortunately the small patient cohort, relatively large errors associated with fECV measurements at the ENR levels seen in this study and the potential for multiple processes occurring within the tumour microenvironment prevent any definitive conclusions being drawn based on the data presented. Future research into the relationship between fECV measurements and histopathologic analysis in liver cancer lesions is indicated.

Clinically realistic fECV(tumour) results were successfully obtained in the presence of radiopaque TACE beads at visit 3, where the highly attenuating TACE beads were segmented out of VOI_{tumour} using a threshold of 100 HU and replaced with an average background liver value. This technique is considered to be necessary to prevent the radiopaque beads having undue influence on enhancement values, particularly in the cases of tumour motion between pre-contrast and equilibrium phase images that could not be corrected for.

In terms of the effect of treatment on fECV(tumour), it is hypothesised that treatment could result in the reduction of cell density in the tumour resulting in an increased fECV, however, treatment related inflammation or oedema could mask or reverse this effect. It is also possible that embolised blood vessels could result in the trapping of iodine contrast in the areas surrounding the tumour volume, potentially leading to a higher enhancement measurement and higher fECV(tumour) values. In this study, there was no significant difference seen in fECV(tumour) results between the first two visits and visit three, suggesting that either these effects did not occur, or that the relatively short time frame

between visits did not leave sufficient time for these effects manifest in fECV results. Again, the results of histopathological analysis would be needed to correlate these radiological findings to true tissue characteristics and subsequent patient outcomes, however, the fact that seemingly realistic fECV measurements were obtained in the presence of the TACE beads serves as a proof of concept that EQ-CT could be a useful technique to monitor response to treatment over time in patients unfit for surgery.

The results presented here need to be considered in the context of the limitations associated with this study. One of the main limitations was that image data sets were only available for six trial patients. This is a relatively small number and more would be needed to confirm the findings are valid in the wider population, however the proof of concept has been demonstrated. The effect of patient size on fECV results has been reported in the literature, however, there were not enough subjects to investigate that phenomenon here.[14] Another major limitation was that there was no gold standard to establish the true fECV for each patient, therefore all comparisons between different acquisition kVp and techniques are relative to each other and there is no method for identifying systematic errors in fECV results, either globally or on a per-patient basis.

ROIs were drawn to avoid gross vessels and lesions (where appropriate), however the relatively low contrast appearance of some tumour lesions made this challenging in some cases. MRI guidance was necessary for some patients, which may not always be available during routine clinical implementation. Additionally, image registration was identified as an issue during image analysis due to the requirement to position the ROIs in the same place in pre-contrast and equilibrium phase images. As the liver is a soft organ whose shape and position will change during inspiration, there is much opportunity for organ and patient movement in the 7 minutes between image phases, an example of which is shown in Figure **9**. Without careful image registration there is strong potential for ROIs from the two phases to be misaligned, therefore generating misleading enhancement and fECV values. This issue was particularly noticed in VOI_{tumour} at visit three, where the relatively high contrast TACE beads included in the ROI resulted in high HU values. A slight change in ROI position would include or exclude a different number of beads and therefore have a strong influence on the overall mean HU value for the ROI. This problem was successfully overcome as described above, however if there is a large volume bead in one VOI this has the potential to affect overall fECV results.

The issue with image registration was investigated by a previous group studying fECV in the liver, who established that the use of a novel non-linear, non-rigid image registration algorithm provided a better method for registration of pre-contrast and equilibrium phase images.[11] Unfortunately this technology was not available to be used in this study, but its use would be recommended. It is also suggested that the use of DE generated ‘virtual non

contrast' images, where the iodine signal is subtracted from the equilibrium phase image to create a synthetic pre-contrast image from the same projection data, could be used to overcome this problem. The existing literature on this type of technology in EQ-CT is inconclusive and therefore warrants further investigation.[30] However, the issue with low signal from iodine quantification at concentrations encountered in this study would still remain, potentially causing issues in the generation of virtual non contrast images.

Another limitation is the relatively low ENR values obtained in this study due to the imaging protocol used, which led to the exclusion of many data points as previously discussed. The use of different image reconstruction technique to reduce noise and therefore improve ENR were not investigated but should be considered in future studies. Other approaches to improving ENR, such as a reduced equilibrium time delay or administering an increased volume of contrast material were also not included.

Finally, the results presented here are based on acquisitions and reconstructions performed on a single CT scanner make and model. The literature demonstrates CT quantification, particularly in dual energy modes, is often technology dependent, so the fact this study used a relatively unusual wide-detector configuration and dual energy technique means that the results would require additional validation on other CT technologies.[31,32]

In conclusion, this study has shown that hepatic fECV as measured with an EQ-CT technique in a cohort of patients with primary and secondary liver cancers is a reproducible technique, best performed in conventional CT mode with a relatively high kVp using a 10 cm length of the aorta to measure blood enhancement. It was not possible to establish a definitive difference between fECV values measured in tumour lesions and apparently unaffected liver, however, fECV measurement in the presence of TACE beads has been shown to be possible. It is therefore feasible that fECV measurements with EQ-CT can be confidently used as a tool to measure and monitor fECV in the management and treatment of patients with liver cancer.

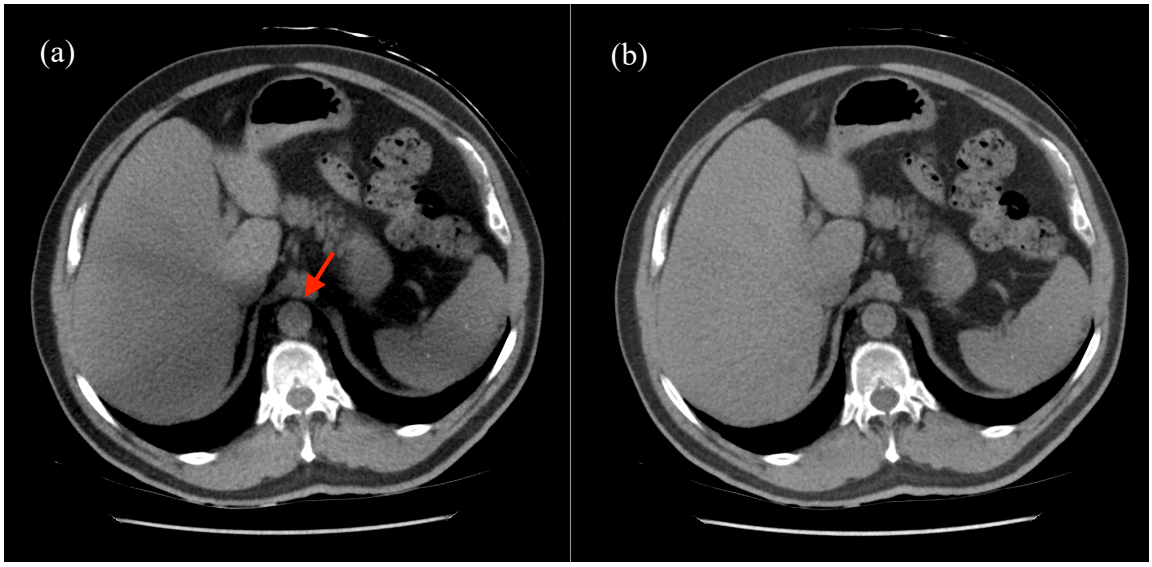

Figure 7 *Example of image artefact seen in pre-contrast images: (a) 80 kVp with beam hardening artefact (red arrow); (b) the equivalent image acquired at 135 kVp with no artefact. The mean HU in the aorta in image (a) and (b) were -19 HU and 20 HU respectively.*

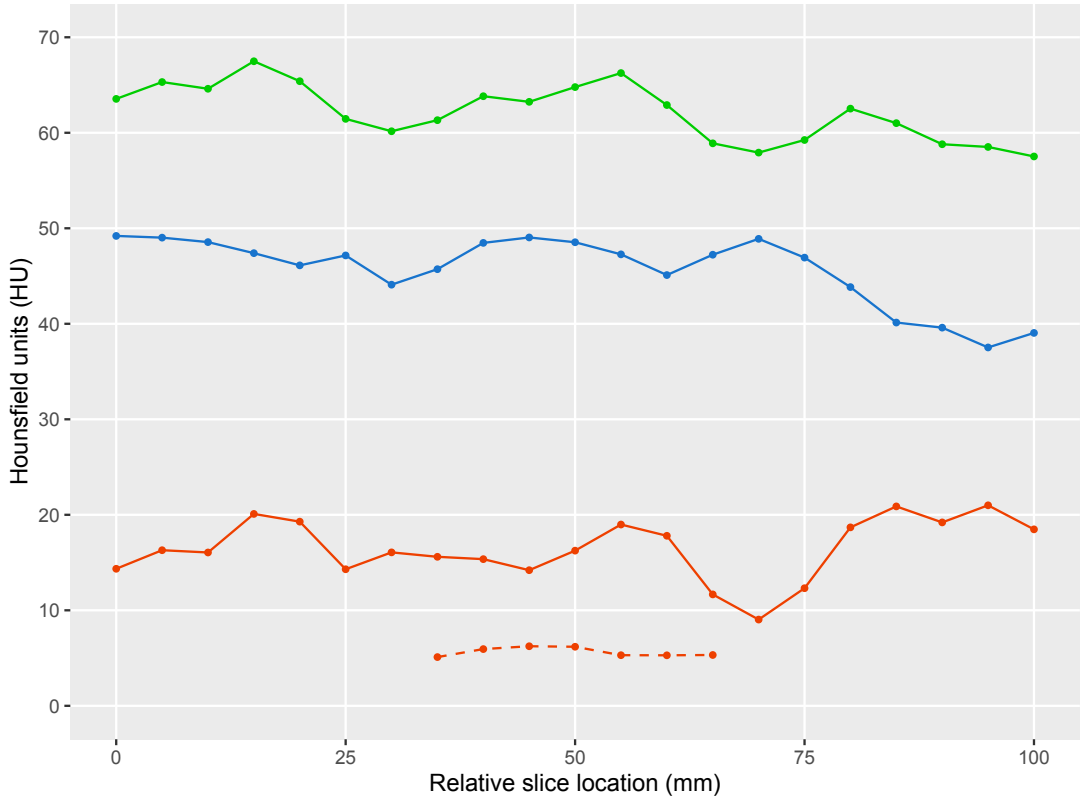

Figure 8 *An example of a plot of measured HU and enhancement values relative to slice location from one patient along a 10 cm length of the aorta. Solid lines represent the aorta; the dashed line represents liver: blue is pre-contrast aorta; green is equilibrium phase aorta; red line is enhancement (equilibrium minus pre-contrast).*

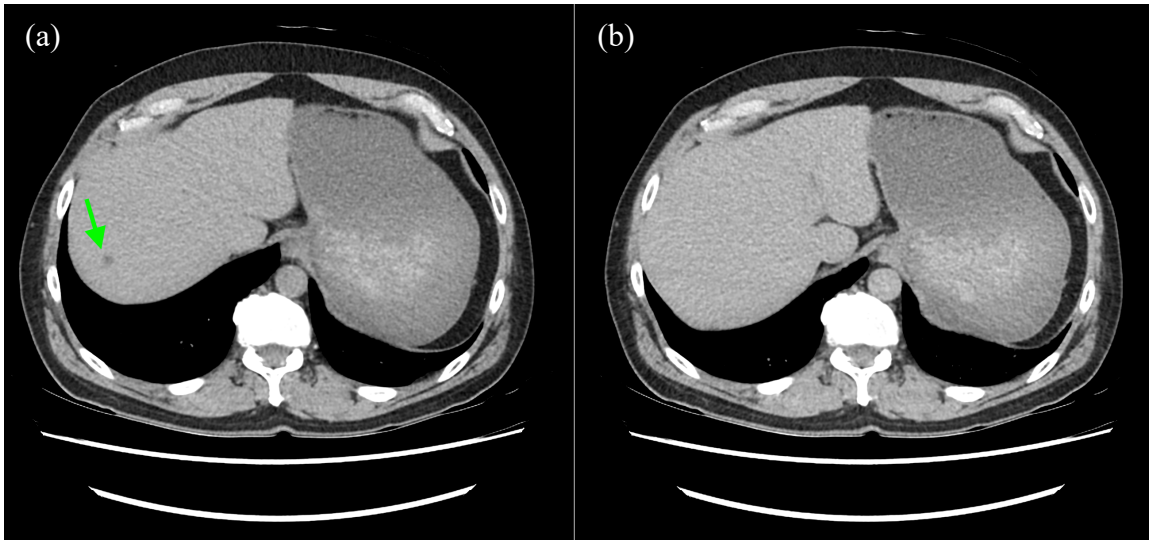

Figure 9 *An example of misregistration in the same patient at the same slice location between pre-contrast (a) and equilibrium phase images (b). The difference in inspiration is clear to see in the different sized lung fields and the hypoattenuating lesion visible on the pre-contrast scan is no longer visible at the same slice location in the equilibrium images: it appears on a slice approximately 1.5 cm superior to the displayed image.*

References

1. Bray F, Ferlay J, Soerjomataram I, Siegel RL, Torre LA, Jemal A. Global cancer statistics 2018: GLOBOCAN estimates of incidence and mortality worldwide for 36 cancers in 185 countries. *CA Cancer J Clin*. 2018;68(6):394-424. doi:10.3322/caac.21492
2. Ananthakrishnan L, Rajiah P, Ahn R, et al. Spectral detector CT-derived virtual non-contrast images: comparison of attenuation values with unenhanced CT. *Abdom Radiol*. 2017;42(3):702-709. doi:10.1007/s00261-016-1036-9
3. Afdhal NH, Nunes D. Evaluation of Liver Fibrosis: A Concise Review. *Am J Gastroenterol*. 2004;99(6):1160-1174. doi:10.1111/j.1572-0241.2004.30110.x
4. Iguchi T, Aishima S, Sanefuji K, et al. Both Fibrous Capsule Formation and Extracapsular Penetration Are Powerful Predictors of Poor Survival in Human Hepatocellular Carcinoma: A Histological Assessment of 365 Patients in Japan. *Ann Surg Oncol*. 2009;16(9):2539-2546. doi:10.1245/s10434-009-0453-1
5. Vogel A, Cervantes A, Chau I, et al. Hepatocellular carcinoma: ESMO Clinical Practice Guidelines for diagnosis, treatment and follow-up. *Ann Oncol*. 2018;29:iv238-iv255. doi:10.1093/annonc/mdy308
6. Horowitz JM, Venkatesh SK, Ehman RL, et al. Evaluation of hepatic fibrosis: a review from the society of abdominal radiology disease focus panel. *Abdom Radiol*. 2017;42(8):2037-2053. doi:10.1007/s00261-017-1211-7
7. Bandula S, Punwani S, Rosenberg WM, et al. Equilibrium Contrast-enhanced CT Imaging to Evaluate Hepatic Fibrosis: Initial Validation by Comparison with Histopathologic Sampling. *Radiology*. 2015;275(1):136-143. doi:10.1148/radiol.14141435
8. Yoon JH, Lee JM, Klotz E, et al. Estimation of Hepatic Extracellular Volume Fraction Using Multiphasic Liver Computed Tomography for Hepatic Fibrosis Grading. *Invest Radiol*. 2015;50(4):290-296. doi:10.1097/RLI.0000000000000123
9. Guo SL, Su LN, Zhai YN, et al. The clinical value of hepatic extracellular volume fraction using routine multiphasic contrast-enhanced liver CT for staging liver fibrosis. *Clin Radiol*. 2017;72(3):242-246. doi:10.1016/j.crad.2016.10.003
10. Yeung J, Sivarajan S, Treibel TA, et al. Measurement of liver and spleen interstitial volume in patients with systemic amyloid light-chain amyloidosis using equilibrium contrast CT. *Abdom Radiol*. 2017;42(11):2646-2651. doi:10.1007/s00261-017-1194-4
11. Shinagawa Y, Sakamoto K, Sato K, Ito E, Urakawa H, Yoshimitsu K. Usefulness of new subtraction algorithm in estimating degree of liver fibrosis by calculating extracellular volume fraction obtained from routine liver CT protocol equilibrium phase data: Preliminary experience. *Eur J Radiol*. 2018;103:99-104. doi:10.1016/j.ejrad.2018.04.012

12. Ito E, Sato K, Yamamoto R, Sakamoto K, Urakawa H, Yoshimitsu K. Usefulness of iodine-blood material density images in estimating degree of liver fibrosis by calculating extracellular volume fraction obtained from routine dual-energy liver CT protocol equilibrium phase data: preliminary experience. *Jpn J Radiol*. 2020;38(4):365-373. doi:10.1007/s11604-019-00918-z
13. Bak S, Kim JE, Bae K, et al. Quantification of liver extracellular volume using dual-energy CT: utility for prediction of liver-related events in cirrhosis. *Eur Radiol*. 2020;30(10):5317-5326. doi:10.1007/s00330-020-06876-9
14. Sofue K, Tsurusaki M, Mileto A, et al. Dual-energy computed tomography for non-invasive staging of liver fibrosis: Accuracy of iodine density measurements from contrast-enhanced data. *Hepatol Res*. 2018;0(0). doi:10.1111/hepr.13205
15. Yoshimitsu K, Shinagawa Y, Morita A, Urakawa H, Sakamoto K, Fujimitsu R. Comparison of extracellular volume fraction calculated from the three data sets of the equilibrium phase of dual-energy CT as surrogate markers for liver fibrosis: preliminary report. ECR 2016 EPOS. Published March 2, 2016. Accessed December 7, 2020. https://epos.myesr.org/poster/esr/ecr2016/C-0874
16. Zissen MH, Wang ZJ, Yee J, Aslam R, Monto A, Yeh BM. Contrast-Enhanced CT Quantification of the Hepatic Fractional Extracellular Space: Correlation With Diffuse Liver Disease Severity. *Am J Roentgenol*. 2013;201(6):1204-1210. doi:10.2214/AJR.12.10039
17. Bandula S, Banypersad SM, Sado D, et al. Measurement of Tissue interstitial volume in healthy patients and those with amyloidosis with equilibrium contrast-enhanced MR imaging. *Radiology*. 2013;268(3):858-864. doi:10.1148/radiol.13121889
18. Sadigh G, Applegate KE, Saindane AM. Prevalence of Unanticipated Events Associated With MRI Examinations: A Benchmark for MRI Quality, Safety, and Patient Experience. *J Am Coll Radiol*. 2017;14(6):765-772. doi:10.1016/j.jacr.2017.01.043
19. Dean PB, Kivisaari L, Kormano M. The Diagnostic Potential of Contrast Enhancement Pharmacokinetics. *Invest Radiol*. 1978;13(6):533.
20. Seeram E. Computed Tomography: A Technical Review. *Radiol Technol*. 2018;89(3):279CT-302CT.
21. Baker CD. Optimisation of extracellular volume measurement in equilibrium CT: a phantom study. *Manuscript in preparation.*
22. Bandula S, White SK, Flett AS, et al. Measurement of Myocardial Extracellular Volume Fraction by Using Equilibrium Contrast-enhanced CT: Validation against Histologic Findings. *Radiology*. 2013;269(2):396-403. doi:10.1148/radiol.13130130
23. Beaton L, Tregidgo HFJ, Znati SA, et al. VEROnA Protocol: A Pilot, Open-Label, Single-Arm, Phase 0, Window-of-Opportunity Study of Vandetanib-Eluting Radiopaque Embolic Beads (BTG-002814) in Patients With Resectable Liver Malignancies. *JMIR Res Protoc*. 2019;8(10). doi:10.2196/13696

24. Winter B. Linear models and linear mixed effects models in R with linguistic applications. *ArXiv13085499 Cs*. Published online August 26, 2013. Accessed October 13, 2021. http://arxiv.org/abs/1308.5499
25. Shrimpton PC, Jansen JTM, Harrison JD. Updated estimates of typical effective doses for common CT examinations in the UK following the 2011 national review. *Br J Radiol*. 2016;89(1057). doi:10.1259/bjr.20150346
26. Vis JY, Huisman A. Verification and quality control of routine hematology analyzers. *Int J Lab Hematol*. 2016;38(S1):100-109. doi:https://doi.org/10.1111/ijlh.12503
27. Martin J, Petrillo A, Smyth EC, et al. Colorectal liver metastases: Current management and future perspectives. *World J Clin Oncol*. 2020;11(10):761-808. doi:10.5306/wjco.v11.i10.761
28. Conrad R, Castelino-Prabhu S, Cobb C, Raza A. Cytopathologic diagnosis of liver mass lesions. *J Gastrointest Oncol*. 2013;4(1):53-61. doi:10.3978/j.issn.2078-6891.2012.020
29. Kim B, Lee JH, Kim JK, Kim HJ, Kim YB, Lee D. The capsule appearance of hepatocellular carcinoma in gadoxetic acid-enhanced MR imaging. *Medicine (Baltimore)*. 2018;97(25). doi:10.1097/MD.0000000000011142
30. van Assen M, De Cecco CN, Sahbaee P, et al. Feasibility of extracellular volume quantification using dual-energy CT. *J Cardiovasc Comput Tomogr*. 2019;13:81-84. doi:10.1016/j.jcct.2018.10.011
31. Jacobsen MC, Cressman ENK, Tamm EP, et al. Dual-Energy CT: Lower Limits of Iodine Detection and Quantification. *Radiology*. 2019;292(2):414-419. doi:10.1148/radiol.2019182870
32. Taylor RE, Mager P, Yu NC, Katz DP, Brady JR, Gupta N. Iodine quantification and detectability thresholds among major dual-energy CT platforms. *Br J Radiol*. 2019;92(1104):20190530. doi:10.1259/bjr.20190530

Section 4

Discussion and conclusions

1 Introduction

This body of work was focused on the optimisation of equilibrium CT (EQ-CT) as a tool for measuring fractional extracellular volume (fECV) and the investigation of this technique in a cohort of patients with liver cancer. A phantom study was performed to establish the initial accuracy and precision optimisation strategy for fECV measurements. This was followed by a clinical study to establish how the phantom results could be applied to patients with liver cancer undergoing treatment with a novel transarterial chemoembolization (TACE) therapy using images acquired as part of the VEROnA trial: *'*a window of opportunity study of vandetanib-eluting radiopaque beads (BTG-002814) in patients with resectable liver malignancies*'* (Beaton et al., 2019).

The initial literature review demonstrated that the existing body of evidence regarding hepatic fECV measurement with EQ-CT is overwhelmingly focussed on the correlation of fECV to fibrosis grade established with histopathologic assessment and other clinical measures of fibrosis. The literature highlighted the practicability of the EQ-CT technique by the fact that most studies were performed with otherwise clinically indicated imaging. Many authors have established cut off values for EQ-CT measured fECV for the diagnosis of cirrhosis, however, none have studied fECV in the setting of liver cancer. It is proposed that tumour fECV values could act as an imaging biomarker to provide useful additional quantitative information that could be related to disease aggressiveness, metastatic potential or be predictive of response to treatment. Pancreatic fECV has been shown to act as a predictor of survival in patients with stage IV pancreatic ductal adenoma (Fukukura et al., 2020) demonstrating the proof of concept, however, as far as the author is aware, this has not been studied in the setting of liver cancer.

Early evidence for the EQ-CT technique was reported from the use of conventional 'single energy' (SE) CT, followed by several studies utilising the opportunities available as dual energy (DE) became more widely available. The literature demonstrates that there has been little effort to establish the absolute accuracy or precision of the technique, which is considered vital to enable clinical users to interpret fECV results in the context of the limitations of the technique. There has also been little investigation of different acquisition parameters or analysis techniques, potentially a result of most of the published studies being clinically driven and retrospective in nature. Optimisation of the technique is also crucial to ensure the most accurate diagnostic information can be obtained whilst using the lowest practicable dose of ionising radiation (Ionising Radiation (Medical Exposure) Regulations 2017).

The following sections focus on different factors that were highlighted in both the phantom and clinical studies as important to the measurement of fECV with EQ-CT.

2 Measured attenuation values

2.1 HU and fECV accuracy in single energy CT

As the EQ-CT technique is dependent on the measurement of Hounsfield Unit (HU) enhancement, it is clear that accuracy of HU is central to the accuracy of measured fECV values. Surprisingly however, none of the papers listed in the literature review mention HU accuracy as an important factor. As EQ-CT is a subtraction technique, the underlying attenuation of materials within the body shouldn't have a significant effect on measurements of iodine enhancement as long as there are no major changes in underlying tissues within the seven minute delay between scan phases and the image noise is kept at a reasonable level. The initial focus of the phantom study was therefore to confirm the linear relationship, or calibration curve, between iodine concentration and HU value for different acquisition modes (SE kVp and DE iodine density mode). This also allowed the limits of detection (LOD) and limit of quantification (LOQ) of iodine to be established with the wide-beam mode on the Canon Aquilion ONE (Canon Medical Systems, Ōtawara, Tochigi, Japan). It is believed that this has not been reported in the literature previously.

As expected, a linear linear relationship between iodine concentration and HU value was demonstrated at all conventional kVp settings tested, giving reassurance that the simple subtraction of HU values from pre-contrast and equilibrium method would represent true iodine enhancement without the need for extensive absolute calibrations. This is a considerable advantage of EQ-CT over the equivalent technique using magnetic resonance imaging (MRI) as signal from gadolinium contrast in MRI is potentially not linear with contrast concentration, adding additional complexity to the technique (Coelho-Filho et al., 2013).

Although kVp setting was not shown to have a significant effect on fECV measurement accuracy in the phantom study, 80 and 100 kVp were established as the settings that resulted in the best measurement precision. 100 kVp appears to be the best compromise between an increase in iodine contrast and reduced potential for image artefacts, both of which are seen as kVp is decreased. It is unfortunate that 100 kVp was not available in the clinical study as the clinical imaging was bound by the trial protocol. This is considered to be a limitation of this body of work and 100 kVp would be recommended for use in future studies.

Enhancement to noise ratio (ENR) was found to be a good predictor of measurement precision. It follows that reducing image noise by using a relatively thick slice width and high radiation dose would logically increase the ENR. A slice width of 5 mm was used in the clinical study as a realistic 'thick' clinical slice width to reduce noise whilst being wary of the need to avoid partial volume errors, particularly in the non-linear course of the aorta and the potentially heterogeneous diseased hepatic tissue.

Increasing the radiation dose to the patient is something that clinical users would conventionally be cautious of. However, the improvement in measurement precision associated with this approach is considered to be optimisation of the EQ-CT technique and is therefore recommended here, particularly in the clinical context of cohort of patients included in this study. The data included in Section 2, Figure 5 indicates an ENR of 2 (using SE mode) would be a good target to aim for as a compromise between measurement accuracy and radiation dose: the error with ENR values below 2 are much higher, but there is only a modest decrease in error associated with ENR values in excess of 2. This however, would require justification by the practitioner who takes legal responsibility for such decisions, which would assume other options for increasing ENR have been exhausted (as discussed in the proceeding sections), as well as the future proven utility, or otherwise, of the fECV measurement in patient diagnosis and management (Ionising Radiation (Medical Exposure) Regulations 2017).

In terms of establishing the link between precision in the phantom and clinical studies, the interquartile range (IQR) of all SE kVp settings in the clinical study was approximately 7%, with associated ENRs between 1 and 2. The equivalent IQR in the phantom study for the same ENR bin (1-1.9) was 9%. This indicates the spread of results was similar between the two studies and therefore the precision ranges quoted in the phantom study have the potential to be applied clinically. This will give the clinician vital additional information about measurements obtained with this technique and bring some context to the cut off ranges for cirrhosis quoted by some authors in the literature review: a cut off values quoted to 0.01% by Yoon et al. (2015) is probably not realistic based on these findings. Additionally the accuracy of fECV cut off values of 32.0% and 32.8% reported by Guo et al. (2017) for the diagnosis of significant/advanced fibrosis and cirrhosis respectively are simply not realistic in the context of the overall accuracy or precision reported in either study here.

2.2 HU and fECV accuracy using dual energy CT

The HU signal from DE iodine density modes was lower than all conventional kVp modes tested. This led to a much higher rejection rate for iodine density patient images (based on the applied 4 HU enhancement threshold) and the lower signal was responsible for reduced ENR which was associated with lower precision in the phantom study. This is in agreement with Baerends et al. (2018) who found iodine density mode provided a lower contrast to noise ratio (analogous to ENR) compared to a subtraction technique and associated lower iodine discrimination thresholds from quantitative assessment in a phantom study.

As accurate signal quantification for DE iodine density mode was an important aspect of this body of work, previously published evidence from the literature was sought to ascertain what factors influenced absolute accuracy for future work. Unfortunately, this provided much conflicting evidence, for example:

- Chandarana et al. (2011) and Pelgrim et al. (2017) reported no significant difference in quantification for different phantom sizes, however, Papadakis and Damilakis (2017) and Marin et al. (2015) both report the opposite;
- Lu et al. (2019) found iterative reconstruction techniques did not influence quantification results but Marin et al. (2015) did;
- Jacobsen et al. (2018) concluded there were differences in iodine quantification between different DE-CT technologies, but Kim et al. (2018) did not.

Iodine quantification clearly presents new opportunities for EQ-CT fECV measurement which could be an alternative to using conventional HU values. However, in the studies presented here, DE iodine density mode was not found to offer any advantages over conventional imaging. In fact, results with this mode proved to provide a lower ENR giving less precise measurements of fECV. This led to a high rate of rejected image data at the same time as using a higher dose of ionising radiation compared to 120 kVp only image acquisition in the patient study: mean $CTDI_{vol}$ 16.1 mGy (DE) versus 7.7 mGy (120 kVp). It is therefore not recommended for use in future EQ-CT studies.

2.3 Limits of detection and limits of quantification

The LOD, LOQ and system calibration curves established in the phantom study provided the means to calculate the HU threshold values used in the patient study, which was considered to be vital information for the reliable clinical measurement of iodine enhancement. The threshold HU values were calculated as described below.

The calibration curves (Section 2, Figure 3) gave the relationship between measured HU (*HU*) and known iodine concentration (*iod*) for a specific kVp (Equation 1).

$$HU = m.iod - c$$

Equation 1

where *m* is the gradient of the calibration curve and *c* is the y-intercept. The LOQ for the iodine enhancement ($LOQ_{\Delta iod}$) is the minimum difference between the equilibrium phase image (*equ*) and the pre contrast image (*pre*) that can be accurately measured (Equation 2).

$$LOQ_{\Delta iod} = (iod_{equ} - iod_{pre})_{min}$$

Equation 2

Rearranging Equation 1 for *iod* and substituting into Equation 2 and simplifying gives Equation 3 (note how the y-intercept, *c*, cancels out).

$$LOQ_{\Delta iod} = \frac{(HU_{equ} - HU_{pre})_{min}}{m}$$

Equation 3

Equation 3 gives a simple way of calculating the minimum HU enhancement, $(HU_{equ} - HU_{pre})_{min}$, based on the established LOQ, which will be kVp, slice width and $CTDI_{vol}$ dependent, and the gradient of the calibration curve, which will also be kVp dependent. For the patient study, for 80 kVp, 5 mm slice width, 10 mGy $CTDI_{vol}$ (as an approximate match to the true clinical settings), LOQ = 0.06 mgI/mL; for the 80 kVp calibration curve, m = 46.2, therefore $(HU_{equ} - HU_{pre})_{min}$ = 2.8 HU. This was rounded to 3 HU and the same threshold applied to all kVp values to aid simplicity for routine clinical implementation. Similarly for DE iodine density mode, 5 mm slice width, 10 mGy $CTDI_{vol}$, LOQ = 0.22 mgI/mL; for the DE iodine density mode calibration curve, m = 16.7, therefore $(HU_{equ} - HU_{pre})_{min}$ = 3.7 HU. This was rounded to 4 HU.

Although the 3 HU (SE mode) and 4 HU (DE iodine density mode) enhancement thresholds used in the patient study resulted in the exclusion of much data, particularly for DE iodine density mode, it was regarded as being important to ensure the accuracy of the technique and the integrity of the results. The significance of this is demonstrated via re-analysis of the patient fECV(liver,ROI) data: fECV measurements using regions of interest (ROIs) taken in apparently disease-free regions of the liver (ROI_{liver}) and aorta (ROI_{blood}) on 5 consecutive single 5 mm images slices. Figure 1 shows two boxplots of the fECV(liver,ROI) results using 120 kVp and DE iodine density mode without the HU thresholds applied (note the y-axis has been matched across plots for comparison). The 120 kVp plot does not look that different to those in the patient paper as only 1 out of 30 results at 120 kVp was excluded. However, in the iodine density mode plot where only 2 out of the 30 enhancement values were above the 4 HU threshold, it is clear there is a large variance in results, with many fECV results greater than one and a couple are less than zero. Such fECV results are physically not possible, and clearly very different to those achieved at 120 kVp. This highlights the need to apply the enhancement threshold to ensure the integrity of the results.

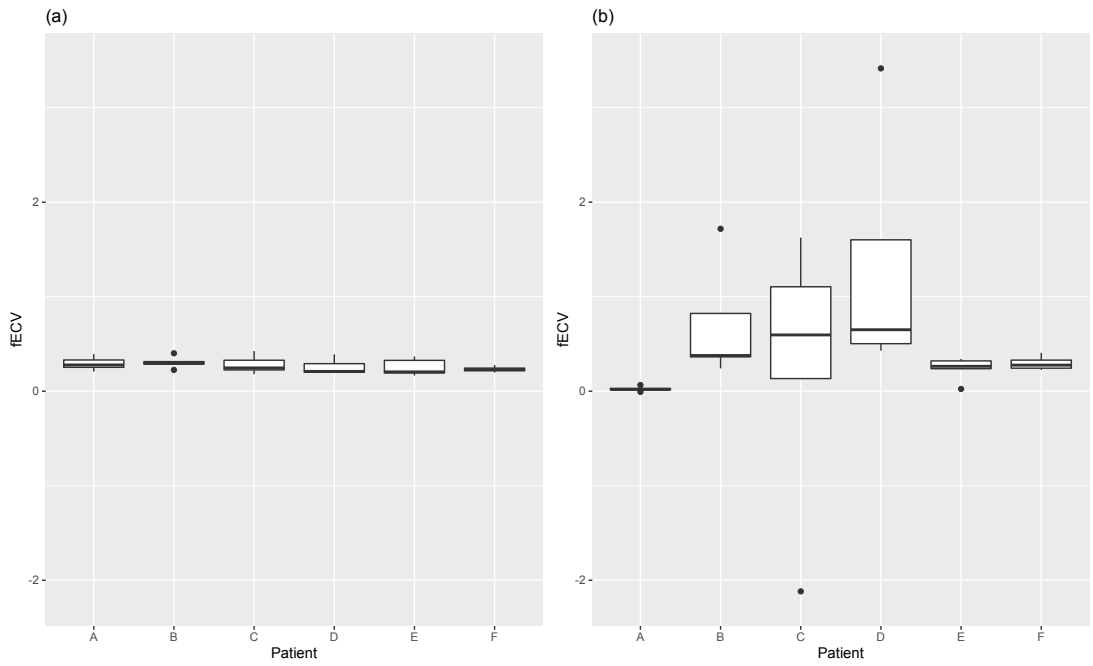

Figure 1 *Boxplots of fECV(liver,ROI) results for each patient at visit 1 with the HU thresholds removed: (a) 120 kVp; (b) for DE iodine density mode (scales equalised for comparison); the central line of each box represents the data median, the lower and upper limits of the box represent the interquartile range (IQR), the lines extend from the 25th percentile minus 1.5 times the IQR to the 75th percentile plus 1.5 times the IQR and the points represent outliers from this range.*

The HU thresholds were chosen based on the established LOQ values for all settings tested on the particular scanner with the concentrations of iodine prepared for the phantom study. Unfortunately the measured enhancement values in many of the patient images were lower than the limited evidence suggested by Bak et al. (2020) and Yoon et al. (2015) and therefore the phantom inserts did not cover the whole range of clinically encountered concentrations. In the absence of inserts at the very low iodine concentrations encountered clinically, coefficient of variation results from the available phantom inserts were extrapolated to lower concentration levels to establish the point at which measurement precision would become acceptable. However, if the phantom study was to be repeated, it is suggested lower concentrations of iodine insert are used to eliminate the uncertainty associated with extrapolation of data.

Notwithstanding these issues, the literature provides evidence that the LOD and LOQ established here are similar to those found by other authors on the subject, although the caveat that findings will be CT scanner make, model and software dependent is frequently stated (Ehn et al., 2017; Kim et al., 2018; Jacobsen et al., 2019; Taylor et al., 2019). The LOD and LOQ results in the literature must also be treated with caution as they are frequently ascertained using relatively high radiation doses: the American College of Radiology reference $CTDI_{vol}$ for abdominal scans is 25 mGy and is a commonly used

standard. Radiation doses in the UK tend to be lower, with the national diagnostic reference level for an abdominal scan being 14 mGy (Public Health England, 2019). The results presented in this phantom study show that dose and noise have a direct effect on LOD and LOQ which is in agreement with findings from Lu et al. (2019) and Papadakis and Damilakis (2017), both of whom reported that iodine quantification accuracy was reduced below a $CTDI_{vol}$ of approximately 10 mGy.

2.4 Beam hardening artefacts

Beam hardening is known to affect HU values (Seeram, 2018). As related to clinical EQ-CT measurements of fECV, Bandula et al. (2013) cite beam hardening artefacts from the vertebral endplates as an issue when measuring HU in the aorta for calculation of fECV in the myocardium. They resorted to measuring enhancement in the left ventricular blood pool. Similarly Ito et al. (2020) found a better correlation of EQ-CT measured fECV to pathological findings when the inferior vena cava was used in place of the aorta to measure blood attenuation due to its location further away from spine. Unfortunately, these approaches may not be an option when considering routine EQ-CT of targeted sections of the liver as the scan length may not extend that far, therefore an alternative method was proposed and investigated in the clinical study. Using an average value of enhancement from a 10 cm section of the abdominal aorta was found to produce fECV results that were equivalent to using values from individual slices, but with less variation and fewer outliers. This would require at least a 10 cm section of the aorta to be imaged, but it is proposed as an improved to the standard technique that could increase precision and repeatability of measured fECV values. This technique could also mitigate against potentially erroneous measurements due to localised artefacts from calcified deposits in the aorta, although this particular issue was not seen with the patients included in the clinical study.

An alternative approach to reducing the effects of beam hardening could be to use different reconstruction methods designed for this purpose. Emoto et al. (2020) successfully used model based iterative reconstruction to reduce the effects beam hardening on fECV results in the myocardium. The reconstruction was also successful in reducing image noise, which would increase ENR and therefore fECV precision. Unfortunately, this technology was not available for use in this study, but this approach would clearly warrant further investigation in future studies.

DE imaging also theoretically provides the potential for the removal of beam hardening artefacts with the use of monoenergetic images (Mileto et al., 2015). Again, unfortunately this technology was not available for use for the phantom study or for the majority of patient imaging so it was not included in the previous papers. However, monoenergetic reconstructions at 66 keV were available for analysis in two out of the six patients in the clinical study.

2.5 Monoenergetic images

The study of monoenergetic images in terms of absolute HU accuracy has been considered in the literature by many authors. Ehn et al. (2017) and Goodsitt et al. (2011) both established the best performance of monoenergetic images was at energies no less than 60 keV. Absolute errors of up to 14 HU at 40 keV were seen by Goodsitt et al. (2011), compared to 5 HU above 60 keV. Theoretically, lower energies would provide improved iodine enhancement measurements due to an increased cross-section of the photoelectric effect, however the potential for increased errors of this magnitude (14 HU) would counteract this benefit in fECV measurements. The selection of 66 keV for the patient images in this study, which was chosen due to being closest to the mean energy of a 120 kVp spectrum, therefore appears to be a fortunate choice. Goodsitt et al. (2011) also studied the effect of phantom size on HU accuracy in monochromatic energy scanning. They found that HU values were affected by phantom size, which was more pronounced at lower keVs, indicating that some beam hardening is still present and therefore reconstructions are not truly monoenergetic and the benefit may not be as great as initially hoped. This is similar to the findings of several other authors, for example Wu et al. (2018) and Mileto et al. (2014), however Michalak et al. (2016) report that the effect of patient size on HU is smaller with monoenergetic reconstructions in comparison to conventional imaging with polyenergetic x-ray spectra. Ueguchi et al. (2018) also carried out a similar study but compared different scanner technologies (dual source versus single source) and, as with other aspects of quantitative CT imaging, they found significant differences between them.

To investigate the effect of monoenergetic reconstructions for the patient images available in this study, the 66 keV images were used. 66 keV images were generated using the DE data set (80 and 135 kVp) and the default reconstruction parameters with the manufacturer's proprietary software, 'Dual-Energy Raw Data Analysis' (Canon Medical Systems, Ōtawara, Tochigi, Japan). fECV measurements were made using ROI_{liver} and ROI_{blood} copied from the SE 80 kVp images of the same patient at the same visit and scan phases. This resulted in a set of fECV(liver,ROI) values for two patients at visits 1 and 2. The same 3 HU enhancement threshold was applied to ensure enhancement measurements were above the LOQ for iodine, although it is recognised that this LOQ threshold would require separate validation for monoenergetic images. Interestingly no images were excluded due to inadequate enhancement. Figure 2 shows how the fECV(liver,ROI) calculated from the monoenergetic images compare to the equivalent data from other kVp stations. The Wilcoxon signed rank test showed no significant difference to 80, 120 or 135 kVp data when both patients and visits were grouped together (p = 0.55, p = 0.34, and p = 0.48 respectively). There was also no statistical difference in the variance of results from the monoenergetic data compared to SE kVp results (Brown-Forsythe equality of variance test, p = 0.78). Unfortunately, there is little data for any solid conclusions to be drawn. However, from these initial findings, it appears that monoenergetic reconstructions at 66 keV provide little benefit to fECV

measurements for the two patients for which data was available. Notwithstanding this, if there was a patient in which beam hardening artefact resulted in difficulties positioning ROIs, monoenergetic images could provide a useful alternative. The availability of such images would be dependent on a dual energy image acquisition being speculatively performed for this purpose, which would require justification based on the increased radiation dose associated with the dual energy acquisition.

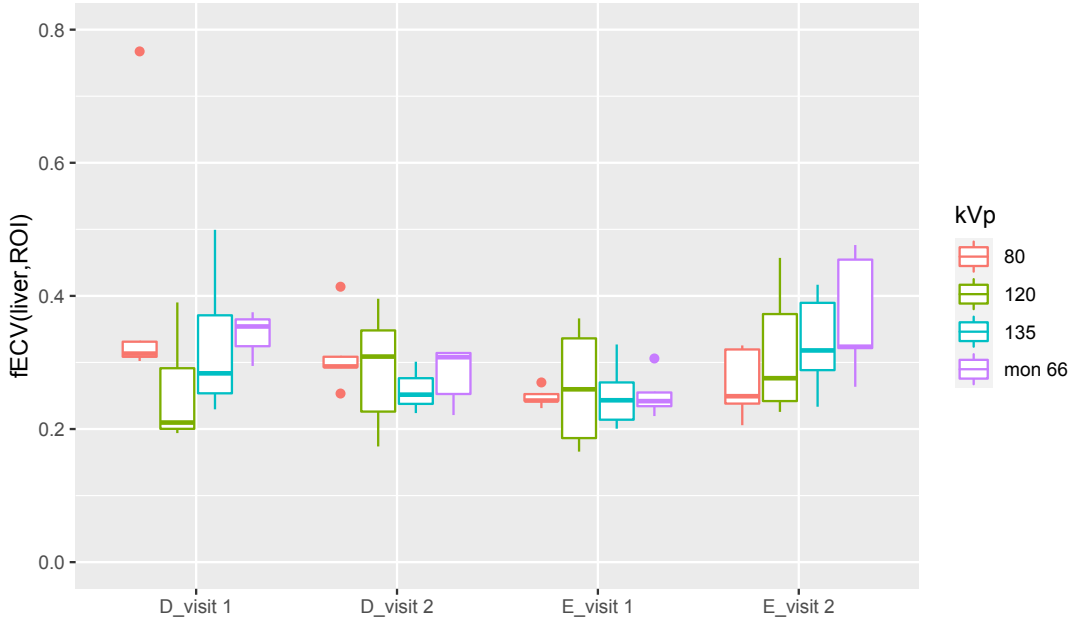

Figure 2 *Boxplot of fECV(liver,ROI) results for the two patients (D and E) with monoenergetic image reconstructions available at visits 1 and 2, compared to conventional SE CT images at 80,120 and 135 kVp; 'mon 66' = monoenergetic reconstruction at 66 keV; the central line of each box represents the data median, the lower and upper limits of the box represent the interquartile range (IQR), the lines extend from the 25th percentile minus 1.5 times the IQR to the 75th percentile plus 1.5 times the IQR and the points represent outliers from this range.*

2.6 Image registration

One of the main issues that was highlighted with the analysis of patient images was problems with image registration between the pre-contrast and equilibrium phase images. This is an unsurprising problem due to the relatively long time delay between the two phases and the fact the liver changes position and shape with patient breathing. Even with good patient compliance it is unlikely exactly the same degree of patient inspiration will be achieved at the two scan timepoints.

This misregistration issue was even seen during the 1.5 seconds it took to acquire the DE data, as shown in Figure 3. As DE data was acquired using two sequential rotations of 0.5

seconds, separated by 0.5 seconds, there is time for the liver to move during the acquisition. This not only causes issues when trying to register the two data sets to ensure the ROIs are in the same position, but the DE specific image processing, such as the generation of iodine density maps, also unavoidably uses misregistered data and therefore will not represent the true iodine concentrations, as demonstrated in Figure 3. This is a limiting factor associated with the CT technology used by this manufacturer and could be another contributing effect to the large variance seen with iodine density images in the clinical study. Other approaches to dual energy imaging hardware used by alternate equipment vendors such as rapidly switching kVp during tube rotation, two orthogonally mounted x-ray tubes operating at different tube voltages, split filter x-ray beams and dual layer detectors mitigate these issues to some effect (Goo and Goo, 2017). However, most of these technologies lose the advantage of acquiring the entire organ in one rotation.

In this study, simple manual rigid image registration was used to overcome patient motion between scan phases which was noted to be time consuming. Recognising similar difficulties, Shinagawa et al. (2018) used a novel non-rigid, non-linear image registration software to improve fECV measurement in the liver, however, this was not available at the time of the current study. Alternatively, a promising technique to mitigate the requirement to perform image registration that was not explored in this study was the use of virtual non contrast (VNC) images.

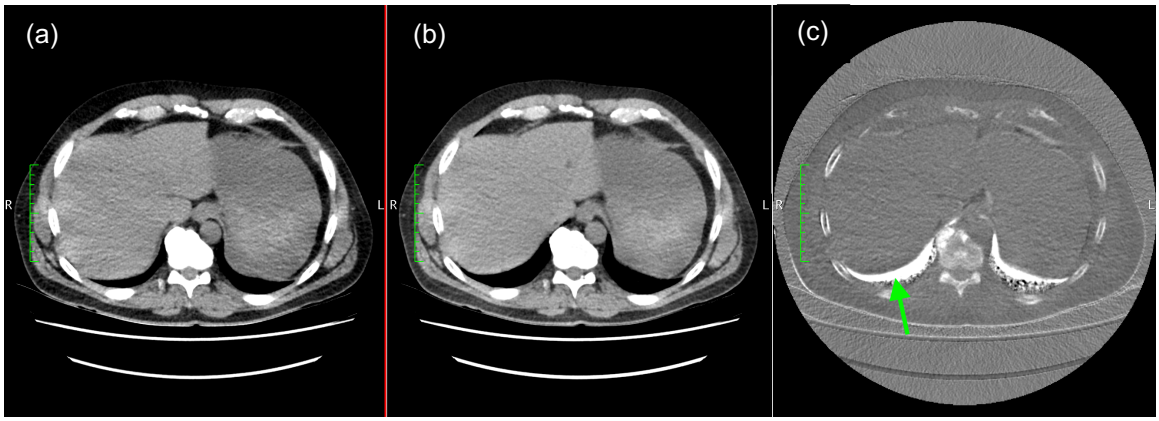

Figure 3 *Example of misregistration of images during a dual energy acquisition. All images taken from the same slice location: 80 kVp (a), 135 kVp (b) and DE iodine density image (c). The green arrow represents the area of misregistration at the periphery of the liver, which has been incorrectly assigned a high iodine content.*

2.7 Virtual non contrast and equilibrium phase only imaging

Virtual removal of iodine signal from the equilibrium images to deliver a virtual pre-contrast, or VNC, image would eradicate image registration issues as both the pre-contrast and equilibrium phase images would be generated from the same set of projection data. This is

possible with DE imaging, where iodine-based materials are identified and then subtracted from the equilibrium phase image. This would also have the great advantage of only requiring one image acquisition phase, thereby halving the radiation dose from the EQ-CT protocol.

As with conventional CT, it is important to consider the accuracy of HU values presented in VNC images if they are to be used for quantitative measurements. Once again, the literature shows conflicting evidence regarding the equivalence of VNC and 'true non contrast' (TNC) HU values. In a range of studies based on patient images, Graser et al. (2009) and Ananthakrishnan et al. (2017) found no significant difference between the HU values obtained from VNC and TNC images, however, Sahni et al. (2013) and Connolly et al. (2017) did find differences in some cases. In the clinical arm of their study, Toepker et al. (2012) found agreement between HU values for VNC and TNC within 15 HU for 92% of measurements and 10 HU for 75% of measurements. Interestingly there was better agreement in the liver compared to the aorta with decreased accuracy in the aorta being attributed to beam hardening by the vertebral bodies (Toepker et al., 2012). Whilst these differences may be acceptable for quantitative image quality, when measuring small differences in attenuation in EQ-CT of the order of 10-30 HU, as found in this clinical study, a 15 HU error due to VNC inaccuracy would become unacceptably large.

The differences reported above have been attributed to different DE-CT acquisition and reconstruction techniques available from different manufacturers, different delayed phase timings, patient size and variable iodine concentrations. The inconclusive evidence warrants further investigation on local equipment and software. Unfortunately, VNC software was not available for the current study.

In the phantom study it was recognised that measuring the iodine content of the insert that contained only water in iodine density mode could lead to misleading fECV results due to the LOD and LOQ findings. Assuming this insert had zero iodine content gave sensible results, although less precise compare to SE subtraction methods. The same logic could follow in the clinical study: using the assumption that the iodine content of the liver and aorta was zero in the pre-contrast scan (a valid clinical assumption), the pre-contrast iodine measurements could be assumed to also be zero and therefore the measured iodine density on the equilibrium scan could be used in isolation to calculate fECV. This was the approach used by Yoshimitsu et al. (2016) and Bak et al. (2020) in their studies.

Although not reported in the patient study, this technique was trialled. The results of the fECV(liver,ROI) using only the iodine density as measured on the equilibrium phase images are shown in Figure 4. This shows that the calculations where the pre-contrast phase has not been used are very different to results from the originally used subtraction technique,

and the majority of results are negative. This clearly indicates the absolute calibration of iodine quantification is not correct as either the liver or aorta ROI have been attributed a negative value of iodine. It should be noted that the 4 HU enhancement threshold was not used for these images as it would have resulted in all the data being excluded. The only conclusions that can be drawn from this is that using only the iodine quantification on the equilibrium scan in isolation is not a feasible method for fECV measurement using EQ-CT with the technology and reconstruction settings used in this study. This is in agreement with Sofue et al. (2018) who tried the same approach but found the non-zero iodine values in the pre-contrast scan resulted in misleading fECV values.

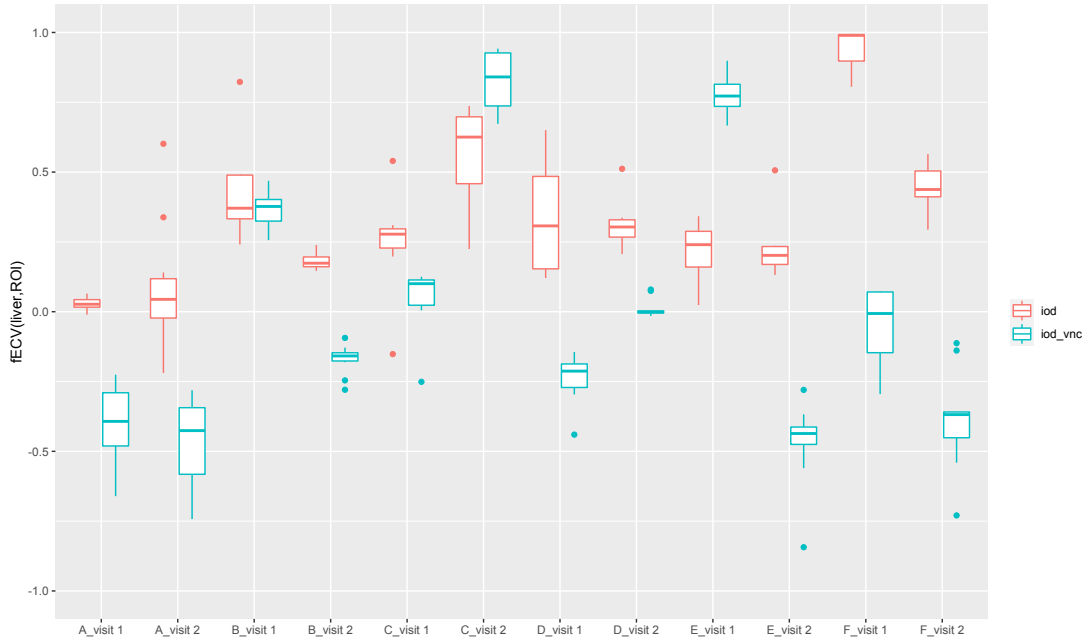

Figure 4 *Boxplot of fECV(liver,ROI) results for all patients at visits 1 and 2, calculated with both pre-contrast and equilibrium iodine density ('iod', red) and with equilibrium only iodine density ('iod_vnc', aqua). Note no 4 HU threshold has been applied to enhancement values; the central line of each box represents the data median, the lower and upper limits of the box represent the interquartile range (IQR), the lines extend from the 25th percentile minus 1.5 times the IQR to the 75th percentile plus 1.5 times the IQR and the points represent outliers from this range.*

A possible avenue for future work could be to investigate the effect of different iodine reconstruction settings to improve the absolute accuracy of the iodine quantification to enable an equilibrium only acquisition for fECV calculation. This approach has been used by Ito et al. (2020) who reported superior fECV results when iodine and blood were used as basis pairs in place of iodine and water. However, this may require frequent calibration and verification to ensure ongoing accuracy of iodine density measurements, adding unnecessary complexity to the existing simple EQ-CT subtraction technique. The acquisition

of a pre-contrast phase may also provide additional qualitative diagnostic information that would not be available if the 'equilibrium only' approach was used.

2.8 Additional factors affecting HU values

It must be recognised that the accuracy and precision of CT numbers will also be dependent on other factors that have so far not been considered in these studies. Patient centring can significantly affect CT number and image noise due to the shape of the bowtie filter used in CT resulting in different beam qualities being incident on different parts of the patient (Szczykutowicz et al., 2017). Fortunately, it is unlikely that the patient will be moved by the operator between the pre-contrast and equilibrium phase images, so changes in HU values due to changes in patient position are not thought to be an issue in isolated EQ-CT measurements. However, this may become important if serial measurements are being made on the same patient at different visits (as in this study). Clinically realistic patient centring errors, typically of 4 cm can have been shown to increase image noise (Szczykutowicz et al., 2017). This effect is particularly seen in areas where there are lots of dense tissues (bone), so the posterior of the abdomen could be affected, which would be of interest in hepatic fECV measurements. This effect is likely to be patient dependent, however, good operator technique and a reproducible set up between visits has the potential to reduce this source of error.

Data acquisition technique, for example axial versus helical, has also been shown to affect CT numbers. Of particular interest in this study are the findings from Ohno et al. (2019) which is one of only a few studies that could be found where the investigators used the Canon Aquilion ONE wide-beam technology used in the current studies. The wide x-ray beam (16 cm) will produce more scatter compared to a conventional beam (typically 4 cm). Additional scatter would theoretically produce lower contrast and increased noise in images thereby reducing image quality and potentially HU accuracy. However, Ohno et al. (2019) found HU values measured with wide beam acquisitions were more accurate than helically acquired HU values with a 4 cm total collimation. The reconstruction software and detector collimation used by Canon is therefore considered to be effective at mitigating the effects of additional scatter with a wide x-ray beam.

The results from the patient study demonstrate that there was no significant difference in median measured fECV or variance in results between wide-beam axial and helical scanning (based on comparing results from 120 kVp and 135 kVp data sets). This indicates any difference in HU accuracy between the two modes are small in the context of measured enhancement in EQ-CT or are mitigated against due to the subtraction technique. The findings of Ohno et al. (2019) that the reproducibility of CT number was within 0.7 HU for all acquisitions, are also reassuring for the EQ-CT subtraction technique.

Whilst so far in this study noise has been considered as a predicator of accuracy of HU values, Zhang et al. (2018) has shown both theoretically and experimentally that the HU value accuracy of a lesion depends on both dose (noise) and the contrast of the lesion compared to the background. As related to fECV measurement with EQ-CT, this has the potential to affect measured enhancement, particularly in the aorta where the contrast compared to surrounding tissue can be large. This could potentially disrupt the linear relationship between HU value and iodine contrast and effect fECV measurements. This has not been considered in this patient study but would be an avenue of investigation in future studies. A phantom with a highly attenuating material next to the iodine insert, or an anthropomorphic phantom with the ability to place iodine inserts next to the spine could be useful for this purpose. This could also be used to further investigate beam hardening reduction techniques.

3 Timing of equilibrium phase

One important factor of the EQ-CT technique that has been highlighted but not specifically investigated in these studies was the time delay between the administration of contrast and the equilibrium phase scan. In this particular patient protocol, a seven minute delay was used to be in no doubt that the state of equilibrium had been achieved. However, the penalty of using a long time delay is reduced overall concentration of iodine due to renal excretion. This was demonstrated empirically by, Treibel et al. (2015) who measured fECV in the myocardium in patients with cardiac amyloid at 5 and 15 minutes post contrast administration and found the 5 minute measurement gave better correlation with MR measured fECV due to a globally reduced signal at 15 minutes.

A theoretical approach to establishing the time of equilibrium in hepatic imaging demonstrates it is predicted to begin at 120 seconds post contrast administration (Dawson and Morgan, 1999). Clearly any time delay shorter than this would not be recommended for EQ-CT, as proven by Zissen et al. (2013) who concluded images acquired in the portal venous phase (90 seconds) were not useful for fECV measurement.

The optimal time point for EQ-CT is clearly not obvious, as demonstrated by the fact that most of the studies included in the literature review have used different time delays for their equilibrium phase. These range from 3 to 10 minutes. It is noted Yoon et al. (2015) published a technical success rate of 96% at achieving the equilibrium phase with a time delay of 3 minutes and Shinagawa et al. (2018) had 100% success rate using 4 mintues, both using a comparison of HU measured in the aorta and portal vein to establish true equilibrium. This suggests a minimum time delay of 4 minutes is indicated, which is longer than that predicted by Dawson and Morgan (1999), possibly due to the reduction in diffusion in fibrotic tissue which could slow the onset of the equilibrium phase (Aubé et al., 2004). Ito et al. (2020) clearly states the need for a study dedicated to establishing the optimum time delay for liver-based EQ-CT, however this would involve scanning the same patient at multiple time points in quick succession and would incur a relatively high radiation dose. It is suggested here that previously acquired CT liver perfusion studies could provide a useful retrospective data source for such a study and would be a suggestion for future work. There is the additional caveat that contrast dynamics could also be affected by other factors such as bolus volume and delivery rate and clinical conditions such as ascites (Mitsuzaki et al., 1996; Dawson and Morgan, 1999).

Due to the relatively high technical failure rate in the clinical study presented here, where measured enhancement was lower than the established LOD and LOQ for this scanner make and model, it is suggested that a seven minute delay for EQ-CT is on the limits of what is technically feasible. Every effort should be made to increase the ENR in EQ-CT images

and reducing the time delay would be recommended for future studies. Based on the evidence available in the literature, a delay of 4 minutes is suggested.

4 Haematocrit

Accuracy of haematocrit will also unavoidably have an effect on the accuracy of the fECV measurement, however it was beyond the scope of this study to investigate this. As reported in Section 1, a basic literature search found requirements for the limits of accuracy and repeatability (coefficient of variation) for measurements of haematocrit to be 1.8% and 1.2% respectively for 'state of the art' haematology analysers (Vis and Huisman, 2016). These figures compare to a 95% confidence interval of approximately ±17% for single fECV measurements, as measured in the phantom for clinically observed ENR values, and an average coefficient of variation of 8.4% across all phantom measurements at 120 kVp. Even if the average of five measurements are taken ($fECV_{avg}$ in the phantom study), the 95% confidence intervals are approximately ±7%. From these values, it appears that the accuracy and precision of haematocrit measurements are likely to be far in excess of measured enhancement values, particularly when you consider that uncertainty errors are usually added in quadrature. This validates the approach of a focus on measured enhancement values in this study to establish the uncertainties associated with EQ-CT derived fECV.

5 Further work

There have been many recommendations for further work throughout this study. In addition to these, there are several more suggestions that would add to the impact of the findings already presented.

Ideally the clinical study would be greatly expanded to include more patients. This would enable additional statistical certainty in the conclusions drawn and would possibly enable further avenues of investigation such as how patient size affects fECV precision and reproducibility. The use of other measures of fECV (for example pathology) has also previously been mentioned to add certainty to the assessment of clinical accuracy of the technique.

A long term follow up of patients with liver cancer, including those being treated with TACE therapy, to include repeat fECV(tumour) measurements over time would enable the prognostic use of fECV to be established. If proven to be an indicator of disease aggressiveness, metastatic potential or responsiveness to treatment fECV measurements using EQ-CT could become an important and widely used diagnostic tool in liver cancer. The follow up of fECV measurement in the presence of TACE beads could also potentially provide information regarding the effectiveness of the treatment over time by monitoring the rate of change of fECV. The response, or lack of response, of individuals to certain forms of TACE treatment could be useful in future patient management decisions.

Finally, ideally these studies would be repeated on a wide range of makes and models of CT scanners to establish if the findings are vendor and technology specific. This may particularly affect the conclusions drawn about dual energy iodine density modes due to the different approaches to dual energy acquisitions from different vendors.

6 Conclusion

This body of work set out to address several research questions which have been the focus of the two papers presented in the preceeding sections of this thesis.

What is the expected accuracy of EQ-CT derived fECV measurements in the liver?

The median error of fECV measurements in a phantom is reported as 0.1%, indicating excellent accuracy of the technique under controlled conditions. Precision has been shown to be dependent on ENR. At ENR levels seen in the clinical study, the 95% confidence interval for measurement error was found to be approximately fECV ±17% when a single fECV measurement was made using was conventional SE imaging. Confidence intervals decreased with increasing ENR.

What are the optimum acquisition and reconstruction settings for EQ-CT to measure fECV in the liver, using conventional and dual energy CT?

The accuracy of EQ-CT fECV measurements was robust to changes in the acquisition and reconstruction settings tested. 100 kVp combined with the highest justifiable $CTDI_{vol}$ and a slice width of 5 mm are considered to the be optimum parameters. Dual energy CT is not recommended for routine EQ-CT fECV measurements. A time delay of 7 minutes between iodine contrast administration and acquisition of equilibrium phase images has been shown to be viable, however, a reduced time delay of 4 minutes would result in higher iodine enhancement measurements leading to a lower technical failure rate and increased measurement precision.

Are clinical EQ-CT derived hepatic fECV measurements reproducible?

Clinical EQ-CT derived fECV measurements in disease free regions of the liver have been shown to be reproducible in the same patient at visits separated by approximately 7 days.

Does measured fECV change in liver cancer lesions?

The difference in fECV results in apparently disease-free liver and liver cancer lesions varied between the 6 patients included in the study: both increases and decreases in fECV were seen. However, the errors associated with fECV measurements, the small patient cohort and the possibility of multiple conflicting processes occurring within the tumour volume prevent any definitive conclusions being drawn in answer to this research question. A future study of the relationship between tumour fECV measurement and histological analysis is recommended.

Is fECV measurement possible in the presence of TACE beads?

fECV measurements were successfully made in the presence of TACE beads, which showed no significant difference to the results obtained prior to treatment. This is therefore a potentially viable tool for monitoring response to treatment.

These questions have been answered with the combination of a phantom and clinical studies. fECV measurement using EQ-CT is a technique that shows promise in both the assessment of liver fibrosis and liver cancer. It is a relatively simple technique that would be widely available and easy to implement in existing clinical pathways, however, it is important the established accuracy and precision of fECV results are acknowledged by clinical users of the technique. It is clear that further research is indicated, particularly in establishing the prognostic value of fECV in liver cancer and how fECV changes in the long term follow up of patients undergoing TACE therapy. Ongoing publication of studies relating to EQ-CT to measure fECV in the liver should further increase clinical interest in the technique as a useful diagnostic tool for the diagnosis and management of patients.

References

Ananthakrishnan, L., Rajiah, P., Ahn, R., Rassouli, N., Xi, Y., Soesbe, T. C., Lewis, M. A., Lenkinski, R. E., Leyendecker, J. R. and Abbara, S. (2017) 'Spectral detector CT-derived virtual non-contrast images: comparison of attenuation values with unenhanced CT.' *Abdominal Radiology*, 42(3) pp. 702–709.

Aubé, C., Racineux, P. X., Lebigot, J., Oberti, F., Croquet, V., Argaud, C., Calès, P. and Caron, C. (2004) '[Diagnosis and quantification of hepatic fibrosis with diffusion weighted MR imaging: preliminary results].' *Journal De Radiologie*, 85(3) pp. 301–306.

Baerends, E., Oostveen, L. J., Smit, C. T., Das, M., Sechopoulos, I., Brink, M., de Lange, F. and Prokop, M. (2018) 'Comparing dual energy CT and subtraction CT on a phantom: which one provides the best contrast in iodine maps for sub-centimetre details?' *European Radiology*, 28(12) pp. 5051–5059.

Bak, S., Kim, J. E., Bae, K., Cho, J. M., Choi, H. C., Park, M. J., Choi, H. Y., Shin, H. S., Lee, S. M. and Kim, H. O. (2020) 'Quantification of liver extracellular volume using dual-energy CT: utility for prediction of liver-related events in cirrhosis.' *European Radiology*, 30(10) pp. 5317–5326.

Bandula, S., White, S. K., Flett, A. S., Lawrence, D., Pugliese, F., Ashworth, M. T., Punwani, S., Taylor, S. A. and Moon, J. C. (2013) 'Measurement of Myocardial Extracellular Volume Fraction by Using Equilibrium Contrast-enhanced CT: Validation against Histologic Findings.' *Radiology*, 269(2) pp. 396–403.

Beaton, L., Tregidgo, H. F. J., Znati, S. A., Forsyth, S., Clarkson, M. J., Bandula, S., Chouhan, M., Lowe, H. L., Zaw Thin, M., Hague, J., Sharma, D., Pollok, J.-M., Davidson, B. R., Raja, J., Munneke, G., Stuckey, D. J., Bascal, Z. A., Wilde, P. E., Cooper, S., Ryan, S., Czuczman, P., Boucher, E., Hartley, J. A., Lewis, A. L., Jansen, M., Meyer, T. and Sharma, R. A. (2019) 'VEROnA Protocol: A Pilot, Open-Label, Single-Arm, Phase 0, Window-of-Opportunity Study of Vandetanib-Eluting Radiopaque Embolic Beads (BTG-002814) in Patients With Resectable Liver Malignancies.' *JMIR Research Protocols*, 8(10).

Chandarana, H., Megibow, A. J., Cohen, B. A., Srinivasan, R., Kim, D., Leidecker, C. and Macari, M. (2011) 'Iodine Quantification With Dual-Energy CT: Phantom Study and Preliminary Experience With Renal Masses.' *American Journal of Roentgenology*, 196(6) pp. W693–W700.

Coelho-Filho, O. R., Mongeon, F.-P., Mitchell, R., Moreno, H., Nadruz, W., Kwong, R. and Jerosch-Herold, M. (2013) 'Role of transcytolemmal water-exchange in magnetic resonance measurements of diffuse myocardial fibrosis in hypertensive heart disease.' *Circulation. Cardiovascular Imaging*, 6(1) pp. 134–141.

Connolly, M. J., McInnes, M. D. F., El-Khodary, M., McGrath, T. A. and Schieda, N. (2017) 'Diagnostic accuracy of virtual non-contrast enhanced dual-energy CT for diagnosis of adrenal adenoma: A systematic review and meta-analysis.' *European Radiology*, 27(10) pp. 4324–4335.

Dawson, P. and Morgan, J. (1999) 'The meaning and significance of the equilibrium phase in enhanced computed tomography of the liver.' *The British Journal of Radiology*, 72(857) pp. 438–442.

Ehn, S., Sellerer, T., Muenzel, D., Fingerle, A. A., Kopp, F., Duda, M., Mei, K., Renger, B., Herzen, J., Dangelmaier, J., Schwaiger, B. J., Sauter, A., Riederer, I., Renz, M., Braren, R., Rummeny, E. J., Pfeiffer, F. and Noël, P. B. (2017) 'Assessment of quantification accuracy and image quality of a full-body dual-layer spectral CT system.' *Journal of Applied Clinical Medical Physics*, 19(1) pp. 204–217.

Emoto, T., Kidoh, M., Oda, S., Nakaura, T., Nagayama, Y., Sasao, A., Funama, Y., Araki, S., Takashio, S., Sakamoto, K., Yamamoto, E., Kaikita, K., Tsujita, K. and Yamashita, Y. (2020) 'Myocardial extracellular volume quantification in cardiac CT: comparison of the effects of two different iterative reconstruction algorithms with MRI as a reference standard.' *European Radiology*, 30(2) pp. 691–701.

Fukukura, Y., Kumagae, Y., Higashi, R., Hakamada, H., Nakajo, M., Maemura, K., Arima, S. and Yoshiura, T. (2020) 'Extracellular volume fraction determined by equilibrium contrast-enhanced dual-energy CT as a prognostic factor in patients with stage IV pancreatic ductal adenocarcinoma.' *European Radiology*, 30(3) pp. 1679–1689.

Goo, H. W. and Goo, J. M. (2017) 'Dual-Energy CT: New Horizon in Medical Imaging.' *Korean Journal of Radiology*, 18(4) pp. 555–569.

Goodsitt, M. M., Christodoulou, E. G. and Larson, S. C. (2011) 'Accuracies of the synthesized monochromatic CT numbers and effective atomic numbers obtained with a rapid kVp switching dual energy CT scanner.' *Medical Physics*, 38(4) pp. 2222–2232.

Graser, A., Johnson, T. R. C., Hecht, E. M., Becker, C. R., Leidecker, C., Staehler, M., Stief, C. G., Hildebrandt, H., Godoy, M. C. B., Finn, M. E., Stepansky, F., Reiser, M. F. and Macari, M. (2009) 'Dual-Energy CT in Patients Suspected of Having Renal Masses: Can Virtual Nonenhanced Images Replace True Nonenhanced Images?' *Radiology*, 252(2) pp. 433–440.

Guo, S. L., Su, L. N., Zhai, Y. N., Chirume, W. M., Lei, J. Q., Zhang, H., Yang, L., Shen, X. P., Wen, X. X. and Guo, Y. M. (2017) 'The clinical value of hepatic extracellular volume fraction using routine multiphasic contrast-enhanced liver CT for staging liver fibrosis.' *Clinical Radiology*, 72(3) pp. 242–246.

Ionising Radiation (Medical Exposure) Regulations 2017. Available at: https://www.legislation.gov.uk/uksi/2017/1322/pdfs/uksi_20171322_en.pdf (Accessed: 29 April 2019).

Ito, E., Sato, K., Yamamoto, R., Sakamoto, K., Urakawa, H. and Yoshimitsu, K. (2020) 'Usefulness of iodine-blood material density images in estimating degree of liver fibrosis by calculating extracellular volume fraction obtained from routine dual-energy liver CT protocol equilibrium phase data: preliminary experience.' *Japanese Journal of Radiology*, 38(4) pp. 365–373.

Jacobsen, M. C., Cressman, E. N. K., Tamm, E. P., Baluya, D. L., Duan, X., Cody, D. D., Schellingerhout, D. and Layman, R. R. (2019) 'Dual-Energy CT: Lower Limits of Iodine Detection and Quantification.' *Radiology*, 292(2) pp. 414–419.

Jacobsen, M. C., Schellingerhout, D., Wood, C. A., Tamm, E. P., Godoy, M. C., Sun, J. and Cody, D. D. (2018) 'Intermanufacturer Comparison of Dual-Energy CT Iodine Quantification and Monochromatic Attenuation:' *MEDICAL PHYSICS*, 287(1) p. 11.

Kim, H., Goo, J., Kang, C., Chae, K. and Park, C. (2018) 'Comparison of Iodine Density Measurement Among Dual-Energy Computed Tomography Scanners From 3 Vendors.' *Investigative Radiology*, 53(6) pp. 321–327.

Lu, X., Lu, Z., Yin, J., Gao, Y., Chen, X. and Guo, Q. (2019) 'Effects of radiation dose levels and spectral iterative reconstruction levels on the accuracy of iodine quantification and virtual monochromatic CT numbers in dual-layer spectral detector CT: an iodine phantom study.' *Quantitative Imaging in Medicine and Surgery*, 9(2) pp. 188–200.

Marin, D., Pratts-Emanuelli, J. J., Mileto, A., Husarik, D. B., Bashir, M. R., Nelson, R. C. and Boll, D. T. (2015) 'Interdependencies of acquisition, detection, and reconstruction techniques on the accuracy of iodine quantification in varying patient sizes employing dual-energy CT.' *European Radiology*, 25(3) pp. 679–686.

Michalak, G., Grimes, J., Fletcher, J., Halaweish, A., Yu, L., Leng, S. and McCollough, C. (2016) 'Technical Note: Improved CT number stability across patient size using dual-energy CT virtual monoenergetic imaging.' *Medical Physics*, 43(1) p. 513.

Mileto, A., Barina, A., Marin, D., Stinnett, S. S., Roy Choudhury, K., Wilson, J. M. and Nelson, R. C. (2015) 'Virtual Monochromatic Images from Dual-Energy Multidetector CT: Variance in CT Numbers from the Same Lesion between Single-Source Projection-based and Dual-Source Image-based Implementations.' *Radiology*, 279(1) pp. 269–277.

Mileto, A., Nelson, R. C., Samei, E., Choudhury, K. R., Jaffe, T. A., Wilson, J. M. and Marin, D. (2014) 'Dual-Energy MDCT in Hypervascular Liver Tumors: Effect of Body Size on Selection of the Optimal Monochromatic Energy Level.' *American Journal of Roentgenology*, 203(6) pp. 1257–1264.

Mitsuzaki, K., Yamashita, Y., Ogata, I., Nishiharu, T., Urata, J. and Takahashi, M. (1996) 'Multiple-phase helical CT of the liver for detecting small hepatomas in patients with liver cirrhosis: contrast-injection protocol and optimal timing.' *American Journal of Roentgenology*, 167(3) pp. 753–757.

Ohno, Y., Fujisawa, Y., Fujii, K., Sugihara, N., Kishida, Y., Seki, S. and Yoshikawa, T. (2019) 'Effects of acquisition method and reconstruction algorithm for CT number measurement on standard-dose CT and reduced-dose CT: a QIBA phantom study.' *Japanese Journal of Radiology*, 37(5) pp. 399–411.

Papadakis, A. E. and Damilakis, J. (2017) 'Fast kVp-switching dual energy contrast-enhanced thorax and cardiac CT: A phantom study on the accuracy of iodine concentration and effective atomic number measurement.' *Medical Physics*, 44(9) pp. 4724–4735.

Pelgrim, G. J., van Hamersvelt, R. W., Willemink, M. J., Schmidt, B. T., Flohr, T., Schilham, A., Milles, J., Oudkerk, M., Leiner, T. and Vliegenthart, R. (2017) 'Accuracy of iodine quantification using dual energy CT in latest generation dual source and dual layer CT.' *European Radiology*, 27(9) pp. 3904–3912.

Public Health England (2019) *National Diagnostic Reference Levels (NDRLs) from 19 August 2019*. GOV.UK. [Online]. Available at: https://www.gov.uk/government/publications/diagnostic-radiology-national-diagnostic-reference-levels-ndrls/ndrl. (Accessed: 30 November 2020).

Sahni, V. A., Shinagare, A. B. and Silverman, S. G. (2013) 'Virtual unenhanced CT images acquired from dual-energy CT urography: Accuracy of attenuation values and variation with contrast material phase.' *Clinical Radiology*, 68(3) pp. 264–271.

Seeram, E. (2018) 'Computed Tomography: A Technical Review.' *Radiologic Technology*, 89(3) pp. 279CT-302CT.

Shinagawa, Y., Sakamoto, K., Sato, K., Ito, E., Urakawa, H. and Yoshimitsu, K. (2018) 'Usefulness of new subtraction algorithm in estimating degree of liver fibrosis by calculating extracellular volume fraction obtained from routine liver CT protocol equilibrium phase data: Preliminary experience.' *European Journal of Radiology*, 103, June, pp. 99–104.

Sofue, K., Tsurusaki, M., Mileto, A., Hyodo, T., Sasaki, K., Nishii, T., Chikugo, T., Yada, N., Kudo, M., Sugimura, K. and Murakami, T. (2018) 'Dual-energy computed tomography for non-invasive staging of liver fibrosis: Accuracy of iodine density measurements from contrast-enhanced data.' *Hepatology Research*, 0(0).

Szczykutowicz, T. P., DuPlissis, A. and Pickhardt, P. J. (2017) 'Variation in CT Number and Image Noise Uniformity According to Patient Positioning in MDCT.' *American Journal of Roentgenology*. American Roentgen Ray Society, 208(5) pp. 1064–1072.

Taylor, R. E., Mager, P., Yu, N. C., Katz, D. P., Brady, J. R. and Gupta, N. (2019) 'Iodine quantification and detectability thresholds among major dual-energy CT platforms.' *The British Journal of Radiology*. The British Institute of Radiology, 92(1104) p. 20190530.

Toepker, M., Moritz, T., Krauss, B., Weber, M., Euller, G., Mang, T., Wolf, F., Herold, C. J. and Ringl, H. (2012) 'Virtual non-contrast in second-generation, dual-energy computed tomography: Reliability of attenuation values.' *European Journal of Radiology*, 81(3) pp. e398–e405.

Treibel, T. A., Bandula, S., Fontana, M., White, S. K., Gilbertson, J. A., Herrey, A. S., Gillmore, J. D., Punwani, S., Hawkins, P. N., Taylor, S. A. and Moon, J. C. (2015) 'Extracellular volume quantification by dynamic equilibrium cardiac computed tomography in cardiac amyloidosis.' *Journal of Cardiovascular Computed Tomography*, 9(6) pp. 585–592.

Ueguchi, T., Ogihara, R. and Yamada, S. (2018) 'Accuracy of Dual-Energy Virtual Monochromatic CT Numbers: Comparison between the Single-Source Projection-Based and Dual-Source Image-Based Methods.' *Academic Radiology*, 25(12) pp. 1632–1639.

Vis, J. Y. and Huisman, A. (2016) 'Verification and quality control of routine hematology analyzers.' *International Journal of Laboratory Hematology*, 38(S1) pp. 100–109.

Wu, R., Watanabe, Y., Satoh, K., Liao, Y.-P., Takahashi, H., Tanaka, H. and Tomiyama, N. (2018) 'Quantitative Comparison of Virtual Monochromatic Images of Dual Energy Computed Tomography Systems.' *Journal of Computer Assisted Tomography*, 42(4) pp. 648–654.

Yoon, J. H., Lee, J. M., Klotz, E., Jeon, J. H., Lee, K., Han, J. K. and Choi, B. I. (2015) 'Estimation of Hepatic Extracellular Volume Fraction Using Multiphasic Liver Computed Tomography for Hepatic Fibrosis Grading.' *Investigative Radiology*, 50(4) pp. 290–296.

Yoshimitsu, K., Shinagawa, Y., Morita, A., Urakawa, H., Sakamoto, K. and Fujimitsu, R. (2016) *Comparison of extracellular volume fraction calculated from the three data sets of the equilibrium phase of dual-energy CT as surrogate markers for liver fibrosis: preliminary report*. ECR 2016 EPOS. European Congress of Radiology - ECR 2016. [Online]. Available at: https://epos.myesr.org/poster/esr/ecr2016/C-0874 (Accessed: 7 December 2020).

Zhang, R., Cruz-Bastida, J. P., Gomez-Cardona, D., Hayes, J. W., Li, K. and Chen, G.-H. (2018) ‘Quantitative accuracy of CT numbers: Theoretical analyses and experimental studies.’ *Medical Physics*, 45(10) pp. 4519–4528.

Zissen, M. H., Wang, Z. J., Yee, J., Aslam, R., Monto, A. and Yeh, B. M. (2013) ‘Contrast-Enhanced CT Quantification of the Hepatic Fractional Extracellular Space: Correlation With Diffuse Liver Disease Severity.’ *American Journal of Roentgenology*, 201(6) pp. 1204–1210.

Appendix 1

List of previously completed DClinSci units: list of Alliance Manchester Business School (AMBS) A units, Medical Physics B units and section C credits together with assignment details

DClinSci Appendix – List of AMBS A units and Medical Physics B units together with assignments – Chris Baker

AMBS – A Units		
Unit title	**Credits**	**Assignment word count**
A1: Professionalism and professional development in the healthcare environment	30	Practice paper – 2000 words A1 – assignment 1 – 1500 words A1 – assignment 2 – 4000 words
A2: Theoretical foundations of leadership	20	A2 – assignment 1 – 3000 words A2 – assignment 2 – 3000 words
A3: Personal and professional development to enhance performance	30	A3 – assignment 1 – 1500 words A3 – assignment 2 – 4000 words
A4: Leadership and quality improvement in the clinical and scientific environment	20	A4 – assignment 1 – 3000 words A4 – assignment 2 – 3000 words
A5: Research and innovation in health and social care	20	A5 – assignment 1 – 3000 words A5 – assignment 2 – 3000 words

Medical Physics – B Units		
Unit title	**Credits**	**Assignment word count**
B1: Medical Equipment Management	10	2000 word assignment
B2: Clinical and Scientific Computing	10	2000 word assignment
B3: Dosimetry	10	Group presentation 1500 word assignment
B4: Optimisation in Radiotherapy and Imaging	10	Group presentation 1500 word assignment
B6: Medical statistics in medical physics	10	3000 word assignment
B8: Health technology assessment	10	3000 word assignment
B9: Clinical applications of medical imaging technologies in radiotherapy physics	20	Group presentation 2000 word assignment
B10b: Assessment of Image Quality	10	1500 word report
B10f: Radiation Protection Advice	10	1500 word report/piece of evidence for portfolio
B10i: Ionising Radiations Instrumentation Specialisation	10	1500 word report/piece of evidence for portfolio
Generic B Units		
B5: Contemporary issues in healthcare science	20	1500 word assignment + creative project
B7: Teaching Learning Assessment	20	20 minute group presentation
Section C		
C1: Innovation Project	70	Literature Review and a Lay presentation

Appendix 2

DClinSci section C: doctoral research and innovation in clinical science project

Innovation proposal: direct access to Rb-82 PET/CT myocardial perfusion imaging in the emergency department for diagnosis of acute coronary syndrome

Innovation proposal: direct access to Rb-82 PET/CT myocardial perfusion imaging in the emergency department for diagnosis of acute coronary syndrome

Lay summary

It is common for people to turn up to emergency departments (ED) suffering with chest pain. Chest pain can be associated with a heart attack and it is important that anyone having a heart attack is diagnosed, admitted to hospital and treated as quickly as possible. However, chest pain can also be associated with other conditions, many of which don't require admission to hospital. It is therefore important that doctors in ED are able to quickly tell which patients require admission for treatment and which patients can be safely sent home. Currently there are a series of tests that are recommended to try and achieve this; however NHS statistics show that there are still many patients with chest pain being admitted when they don't need to be. This costs the NHS a lot of money whilst also causing worry for patients and their families.

The innovation proposed here is that doctors have direct and immediate access to a specialised imaging test, cardiac positron emission tomography/computed tomography (PET/CT), which is able to rapidly and reliably tell if the patient is suffering from a dangerous heart condition when the other tests currently used in ED are inconclusive. If the patient has a normal cardiac PET/CT scan they can be safely discharged from ED within a short amount of time without the need for admission and possible unnecessary treatment. PET/CT imaging has many technical and logistical advantages over other potential methods for imaging the heart in this context and therefore it is suggested as the best currently available option. Unfortunately cardiac PET/CT is a relatively new and expensive technology that isn't yet in widespread use in the UK. This means there is very little evidence regarding its use in the ED setting. It remains to be seen if the innovation is practical and cost effective in an NHS ED setting and careful consideration would be needed before putting this innovation into practice. However, there is potential for reducing the number of unnecessary admissions to hospital which could save the NHS a significant amount of money and create a better experience for patients.

The innovation

Rapid and accurate diagnosis of acute coronary syndrome (ACS, which includes myocardial infarction and unstable angina) in ED is essential to ensure the correct care is delivered to patients presenting with chest pain whilst ensuring the most effective use of available healthcare resources. NICE (2016, 2014) currently recommend clinical evaluation alongside high-sensitivity cardiac troponin (hs-cTn) testing to try and achieve this. In the right clinical context, hs-cTn results below the limit of detection

or above the 99th percentile reference limit for the general population can effectively rule out or rule in myocardial infarction respectively. However, the high sensitivity of the test has resulted in low specificity (Al-Saleh *et al*., 2014): many patients present with non-negative cTn results which may require further investigation before ACS can be confirmed or excluded. Additionally cTn may not rise with unstable angina and there is potential for a missed diagnosis of ACS in the subset of patients with this condition (Reichlin *et al*., 2009).

It is therefore proposed that patients presenting with chest pain can be subdivided into three categories: 'rule out ACS', 'rule in ACS' or 'other'. Commonly used risk scores based on initial ECG findings, history and clinical examinations, for example the TIMI risk score (Antman *et al*., 2000), combined with hs-cTn results can be used to classify patients into these groups:

- Rule out ACS: low risk scores combined with a hs-cTn result below the limit of detection would effectively rule out ACS and the patient can be discharged, following recommendations from NICE (2016).
- Rule in ACS: high risk scores with markedly elevated hs-cTn results above the 99th percentile would require admission and immediate treatment.
- Other: alternative combinations of risk score and hs-cTn results and/or the ED physician is unsure of what management would be best for the patient is where the innovation of immediate access to Rb-82 PET/CT myocardial perfusion imaging (MPI) is suggested to provide the additional information required to accurately diagnose the patient to ensure the most appropriate care can be delivered. It is the patients in this group who would currently be admitted to hospital at great expense to the healthcare organisation, many of whom would be discharged at a later date without a definitive diagnosis, as proven by the statistics from the Department of Health (2016).

This proposal is innovate as there is no published evidence that the use of Rb-82 PET/CT MPI alongside hs-cTn in the ED has been previously implemented in the NHS. The use of CT coronary angiography is this setting is currently subject to a large randomised controlled trial by Gray *et al.* (2016), which validates the concept of access to imaging directly from ED. However, the diagnostic ability of Rb-82 PET/CT MPI along with the technical and practical aspects of imaging patients with this technology could result in it being more effective than alternative imaging modalities at identifying patients who can be safely discharged from ED. This innovation proposal uses a relatively new imaging technology alongside recently improved biochemical marker tests in an innovative patient pathway with the prospect of improving patient care whilst reducing overall costs to the healthcare system.

Stakeholder engagement

Throughout the development of this innovation proposal there has been consultation with a wide range of stakeholders including consultant ED physicians, consultant nuclear medicine physicians, consultant radiologists, cardiology registrars, nuclear medicine radiographers/technologists and clinical scientists. Due to various limitations it has not been possible to engage with patients or members of the public at the time of writing this proposal, but it is recognised that this would be vital if the project was to be taken forward. This would be done by approaching the trust 'patient experience group', which ideally would contain patients who had previously attended ED with chest pain so they could share their thoughts and feelings on the proposed innovation. Although it might seem logical that a patient would want to receive a quick diagnosis and avoid being admitted if possible, it is feasible that some patients might like the reassurance of being in the hospital environment at a time when they are in pain or would prefer not to undergo an examination that uses radioactive materials. This is why patient engagement would be critical.

General feedback from the majority of staff groups was that they supported the innovation. Nuclear medicine and radiology consultants were particularly positive about the prospect of the innovation, possibly as it would promote the role of their speciality in the diagnosis of these patients. Importantly, ED consultants were similarly supportive as it would give them definitive and clear information for this often difficult group of patients. In contrast, cardiology staff were less enthusiastic as they felt that using their specialist knowledge they could perform more appropriate diagnostic tests based on each individual's symptoms and test results. However, the rationale behind the innovation is that this doesn't currently happen and unless a cardiologist is in the ED at all times to provide this specialist advice (which perhaps could be an alternative to the proposed innovation) the use of Rb-82 PET/CT MPI is designed to give a rapid and definitive answer to the non-specialist. There were also reservations from the radiographer/technologist groups about the practicalities of staffing the proposed emergency service outside of standard working hours.

Business case

The business case of this innovation is centred on the fact that it should ultimately reduce the number of patients being unnecessarily admitted to hospital. NHS reference costs for England show the average cost per patient admitted for 'unspecified chest pain' is either £370 or £1,172 for short (less than two days) or long stays respectively (Department of Health, 2016). The reference data also shows the average cost of 'myocardial PET' as £224, although it is noted there is no national tariff for this examination- prices are to be negotiated locally (NHS Improvement, 2017). Therefore, in a very simple model, if a patient presented with chest pain which was ultimately shown to be of non-

cardiac origin, a trust could save £948 if the patient was sent for Rb-82 PET/CT MPI which enabled them to be safely discharged as opposed to being admitted for a long stay. For a short stay patient this figure is reduced to a saving of £146. Based on the number of non-elective short and long stay admissions included in the NHS reference costs there is potential for a total saving of £57.7 million for the NHS every year. Cost savings for individual trusts would depend on many factors including different patient populations and existing patient pathways, but a saving of £700,000 has been calculated for a local trust based on audit results of 1,300 patients admitted with chest pain and later discharged with no diagnosis of ACS over one year.

It is assumed that the figure of £224 quoted above for providing the Rb-82 PET/CT MPI examination includes all the costs associated with the test to include drugs, radiopharmaceuticals, consumables, staff time and reporting time. The Sr-82/Rb-82 generator required for the examination is expensive with an estimate of approximately £10,000 per generator (G Keramida 2017, personal communication, 7 December), although this can be used for up to 6 weeks with virtually no limit of the number of patients being imaged using it. A trust would therefore have to be confident that enough patients would undergo the test to justify this high cost and make the service cost effective. It is likely that an organisation with an existing Rb-82 PET/CT MPI service will be performing regular outpatient lists and therefore by running an emergency service and using the generator when it would otherwise be unused (including overnight) would make financial sense.

The figures for costs and cost savings quoted above are very simplistic as they assume that all patients undergoing PET imaging will receive a negative result (which is unlikely), it doesn't consider any further downstream diagnostic tests or treatments that patients might undergo and there is no consideration of how much it would cost to start the service (discussed further below). Careful consideration of all the possible outcomes and patient pathways will be required to establish if the innovation is cost effective, as will some measure of how the innovation will improve the experience for patients. The commonly used quality adjusted life years (QALY) metric could be calculated after follow up of patients who have undergone the proposed pathway and an incremental cost-effectiveness ratio (ICER) calculated. This could be especially powerful if the Rb-82 PET/CT MPI identified significant numbers of patients who would have otherwise been misdiagnosed.

Barriers to implementation

The major barrier to the implementation of this innovation will be the position of NHS England commissioners: they currently only commission two centres in the country to perform Rb-82 PET/CT MPI (NHS England, 2016). Initial implementation of the innovation may therefore have to be restricted to these centres and getting the service set up elsewhere may not be possible until there is

evidence that the innovation is effective, enabling the commissioners to change their position. Additionally, the majority of PET/CT services in the country (with the exception of some major cities) are run by a third party company, Alliance Medical, in conjunction with the NHS (Alliance Medical, 2017). Introducing a new service like the one proposed here would need the agreement and support from this company which may involve contract renegotiation and likely further charges.

Even if it was possible to secure funding for Sr-82/Rb-82 generators, PET/CT is currently primarily commissioned for oncology imaging with the expectation that approximately 90% of the work is oncology related (NHS England, 2016). A potentially high throughput of patients from ED requiring cardiac scans would probably have a disruptive impact on the oncology service and the two might not be able to run in tandem on the same camera. The solution to this would be a dedicated ED PET/CT camera, but the cost of this may prove to be prohibitive: based on conversations with staff at a local centre, this could be in anywhere between £2 million and £4.5 million (which includes design and planning costs, building materials, engineering work and significant equipment and IT infrastructure costs). Staff costs associated with a new service would also be significant: radiographers, medical staff, scientific staff and administration staff would all require substantial levels of training. All these costs may be hard to justify with a predicted saving of up to £700,000 a year- it could take up to seven years to see a return on the investment for a site that requires a new PET/CT installation. Providing an emergency service would also need adequately trained staff available 24/7 which would be a major change to working patterns for nuclear medicine staff which may face resistance and incur additional costs. A further barrier may be the lack of appropriate physical space required for a PET/CT unit.

Summary

Direct access to Rb-82 PET/CT MPI in the ED has been proposed as an innovation to facilitate rapid and accurate diagnosis of suspected ACS with the aim of improving patient care and reducing overall costs to the NHS. Whilst there is the potential to generate considerable savings by reducing the number of patients being admitted to hospital, the cost of establishing the service may be prohibitive in centres that do not currently offer Rb-82 PET/CT MPI. The mixed feedback received from professional groups would also need addressing prior to implementation, with further dialogue between ED and cardiology specialists seen as essential to ensure the most appropriate set up of the innovation. A pilot study at an existing Rb-82 PET/CT MPI centre with detailed analysis of costings and patient follow up is suggested which may, or may not, provide the evidence required to enable the innovation to be implemented more widely.

References

Alliance Medical (2017). *National PET/CT contract* [Online]. Available at: https://www.alliance medical.co.uk/what-we-do/patient-services/national-petct-contract (Accessed: 26 February 2018).

Al-Saleh, A., Alazzoni, A., Al Shalash, S., Ye, C., Mbuagbaw, L., Thabane, L. and Jolly, S.S. (2014). 'Performance of the high-sensitivity troponin assay in diagnosing acute myocardial infarction: systematic review and meta-analysis', *CMAJ Open*, 2(3), pp. E199-207.

Antman, E. M., Cohen, M., Bernink, P. J., McCabe, C. H., Horacek, T., Papuchis, G., Mautner, B., Corbalan, R., Radley, D. and Braunwald, E. (2000). 'The TIMI risk score for unstable angina/non-ST elevation MI: A method for prognostication and therapeutic decision making', *JAMA*, 284(7), pp. 835-842.

Department of Health (2016). *NHS reference costs 2015 to 2016* [Online]. Available at: https://www.gov.uk/government/publications/nhs-reference-costs-2015-to-2016 (Accessed: 18 September 2017).

Gray, A.J., Roobottom, C., Smith, J.E., Goodacre, S., Oatey, K., O'Brien, R., Storey, R.F., Na, L., Lewis, S.C., Thokala, P. and Newby, D.E. (2016). 'The RAPID-CTCA trial (Rapid Assessment of Potential Ischaemic Heart Disease with CTCA) — a multicentre parallel-group randomised trial to compare early computerised tomography coronary angiography versus standard care in patients presenting with suspected or confirmed acute coronary syndrome: study protocol for a randomised controlled trial', *Trials,* 17(579).

NHS England (2015). *Clinical commissioning policy statement: positron emission computed tomography–computed tomography (PET-CT) guidelines (all ages)* [Online]. Available at: https://www.england.nhs.uk/commissioning/wp-content/uploads/sites/12/2015/10/b02psa-emssn-tomogrphy-guids-oct15.pdf (Accessed: 26 February 2018).

NHS Improvement (2017). *2017-19 non-mandatory price model* [Online]. Available at: https:// improvement.nhs.uk/uploads/documents/2017-2019_Non-mandatory_price_model.xlsx (Accessed: 26 February 2018).

NICE (National Institute for Health and Care Excellence) (2016). *Chest pain of recent onset: assessment and diagnosis; Clinical guideline 95* [Online]. Available at: https://www.nice.org.uk/ guidance/cg95/ chapter/Recommendations (Accessed: 19 February 2018).

NICE (National Institute for Health and Care Excellence) (2014). *Myocardial infarction (acute): Early rule out using high-sensitivity troponin tests (Elecsys Troponin T high-sensitive, ARCHITECT STAT High Sensitive Troponin-I and AccuTnI+3 assays); Diagnostics Guidance 15* [Online]. Available at: https://www.nice.org.uk/guidance/dg15 (Accessed: 19 February 2018).

Reichlin, T., Hochholzer, W., Bassetti, S., Steuer, S., Stelzig, C., Hartwiger, S., Biedert, S., Schaub, N., Buerge, C., Potocki, M., Noveanu, M., Breidthardt, T., Twerenbold, R., Winkler, K., Bingisser, R. and Mueller, C. (2009). 'Early diagnosis of myocardial infarction with sensitive cardiac troponin assays', *New England Journal of Medicine*, 361(9), pp. 858–867.